EVAPORATION FROM BARE SOIL

FOLLOWING RAINFALL

A Thesis

Submitted to the College of Graduate Studies and Research

in Partial Fulfillment of the Requirements

for the Degree of

Master of Science

in the

Department of Agricultural and Bioresource Engineering

University of Saskatchewan

Saskatoon, Saskatchewan, Canada

by

Brenda Margaret Toth

Fall 1999

PERMISSION TO USE

In presenting this thesis in partial fulfillment of the requirements for a postgraduate degree from the University of Saskatchewan, I agree that the Libraries of this University may make it freely available for inspection. I further agree that permission for copying this thesis in any manner, in whole or in part, for scholarly purposes may be granted by the professor or professors who supervised my thesis work or, in their absence, by the Head of the Department or the Dean of the College in which my thesis work was done. It is understood that any copying or publication or use of this thesis or parts thereof for financial gain shall not be allowed without my written permission. It is also understood that due recognition shall be given to me and to the University of Saskatchewan in any scholarly use which may be made of any material in my thesis.

Requests for permission to copy or to make other use of material in this thesis in whole or in part should be addressed to:

Head of the Department of Agricultural and Bioresource Engineering

University of Saskatchewan

57 Campus Drive

Saskatoon, Saskatchewan S7N 5A9

ABSTRACT

The semi-arid environment experiences a potential for evaporation that exceeds the supply of precipitation. In addition a significant portion of precipitation falls in small daily amounts that might not be sufficient to counter evaporative demands of the following day. The objective of this project was to establish the relationship between daily rainfall amounts and that portion of the rainfall lost to evaporation in the subsequent 24-hour period.

Evaporation is the link between the hydrological cycle and the surface energy budget, therefore the evaporation evaluation techniques were based on both the soil water balance and the energy balance. The energy balance methods included the Bowen ratio, and the Penman-Monteith and G-D equations. The soil water balance was evaluated with precipitation measurements as well as replicates of two different types of microlysimeters that allowed evaluation of the drainage component. The dataset consisted of daily soil moisture changes from microlysimeters, soil moisture measurements, and daily rainfall; additional measurements included net radiation, ground heat flux, air temperatures, relative humidities, and windspeed. This dataset spanned 36 days in August and early September 1994.

The microlysimeters that permitted drainage were deemed to be more representative of field conditions, as they allowed the drainage during rainfall to

be quantified, but the drainage component after rainfall was difficult to isolate. The replicated microlysimeters produced a spatially averaged estimate of evaporation.

Microlysimetric and energy balance methods gave evaporation estimates of 43.1 to 64.4 mm during a time when the precipitation received was 59.9 mm. The two methods deemed to most accurately reflect actual evaporative losses were the G-D and cotton-capped (corrected for drainage) microlysimetric methods which produced evaporative loss estimates of 43.1 and 47.1 mm, respectively. Estimates of subsequent 24-hour evaporation by the two methods indicate 20.1 and 22.2 mm, respectively, of the 59.9 mm of precipitation was lost on the day following rainfall. The dataset was limited and no rigorous regression techniques could be used to establish a quantifiable relationship between daily rainfall amounts and subsequent 24-hour evaporative loss, but the portion of daily rainfall that could be viewed as effective precipitation decreased with decreasing daily depths of rainfall.

ACKNOWLEDGEMENTS

I would like to gratefully acknowledge the support, encouragement and patience of my supervisor, Dr. Charles Maulé. His guidance through both my undergraduate and graduate training has been invaluable and this task could not have been completed without his assistance.

My committee members have also been very instrumental in the formation of this work. Dr. Ernie Barber is thanked for his involvement as chair of my committee. I was also fortunate in having Dr. Eeltje de Jong and Dr. Don Gray both insist that I question my answers.

The field project could not have been accomplished without assistance from the Division of Hydrology, both in equipment and personnel. Tom Brown is acknowledged for building and maintaining the oscillating motor driven device used for the temperature and humidity sensor as well as collecting the data from the Bowen ratio mast system. Dell Bayne is very sincerely thanked for his assistance with the installation of the microlysimeters, his camaraderie and cheerful field spirit is appreciated. Assistance for the post-season lab work was provided by M. Sandano and R. Spewak.

The formation of this thesis was completed with help of further discussion with Dr. Raoul Granger and Dr. Kevin Shook as well as the donation of facilities and time from Dr. John Pomeroy and Dr. Don Gray. I am very fortunate to work with these individuals and am grateful for their significant contribution to this task and my professional development.

The National Sciences and Engineering Research Council was responsible for the funding of this project. The University of Saskatchewan Teaching Fellowship program supported my graduate work. I am also extremely grateful to the Saskatchewan Wheat Pool, who make very generous scholarships available to those pursuing research in the agricultural sector, they are to be commended.

To my friend and mentor, Don Norum, who has proven that academic assistance takes a range of forms; from proofreading many documents, critiquing the presentation of graphical material, through to the practical task of donning rubber boots, trudging out in a field of wet clay, and performing site measurements.

DEDICATION

I would like to thank the members of my family; Mom, Carolyn, Joanne, and Greg, who never questioned my ability to finish this task or my sanity for starting it in the first place. I am also grateful to Joel, Amy, and Emily, who help me to look at things as if I've never seen them before.

To Ken, without whom I couldn't have completed something that was so important to me, and without whom it wouldn't matter anyway.

This thesis is dedicated to Jim McCoy and Eric Toth.

TABLE OF CONTENTS

LIST OF FIGURES

LIST OF TABLES

LIST OF SYMBOLS

A	unit cross sectional area (m^2)
C_p	specific heat of air at constant pressure (J kg^{-1} $°C^{-1}$)
d_o	zero plane displacement height (m) for surface roughness
dS	change in soil water stored
E	evaporation
E_a	drying power of the air (mm d^{-1})
e	vapour pressure (kPa)
e^*_a	saturated vapour pressure evaluated the air temperature (kPa)
$f(u)$	wind function (mm d^{-1} kPa^{-1})
G	relative evaporation (the ratio of actual to potential evaporation)
g	gravitational constant (9.81 m s^{-2})
h	crop or roughness height (m)
h_v	latent heat of vaporization (kJ kg^{-1})
K	hydraulic conductivity or the soil's ability to transfer (m s^{-1})
K_h	coefficient of heat transfer (m^2 s^{-1})
K_e	coefficient of vapor transfer (m^2 s^{-1})
κ_e	molecular diffusion coefficient for vapor transfer (m^2 s^{-1})
κ_h	molecular diffusion coefficient for heat transfer (m^2 s^{-1})
κ_m	molecular diffusion coefficient for momentum (m^2 s^{-1})

k von Karman constant (0.41)

P precipitation

P_a atmospheric air pressure (equal to 95.395 kPa at 511.8 m ASL)

p the matric pressure or suction (N m^{-2} or Pa)

Q daily total net energy available for evaporation ($Q_n - Q_g$) expressed as an equivalent depth of water (mm d^{-1})

Q_e latent heat flux (W m^{-2})

Q_g ground heat flux (W m^{-2})

Q_h sensible heat flux (W m^{-2})

Q_n net radiation (W m^{-2})

Q_p energy used in photosynthesis (W m^{-2})

Q_s storage of energy in vegetative biomass (W m^{-2})

R radiant flux density emitted (W m^{-2})

R_i run on and/or groundwater inflow

R_o runoff and/or groundwater outflow

r_a aerodynamic resistance to vapour transfer by turbulence (s m^{-1})

r_s the surface or soil resistance to vapour flow (s m^{-1})

T temperature (°C)

u horizontal windspeed (m s^{-1})

u_z mean wind speed at level z (m s^{-1})

u^* friction velocity (m s^{-1})

V volume of flux (m^3 s^{-1})

z elevation above the reference plane (m)

z_o aerodynamic roughness height (m)

ε emissivity of a the body ($\varepsilon = 1$ for a blackbody)

ρ density of water (kg m^{-3})

ρ_a air density (kg m^{-3})

$\phi_{1,2}$ hydraulic potential at points 1 and 2 where $\phi_2 > \phi_1$ (m)

l_{12} path length parallel to soil water flow (m)

τ dynamic viscosity, shearing stress per unit area (kg m^{-1} s^{-2})

σ Stefan-Boltzmann constant (5.67 x 10^8 W m^{-2} K^{-4})

γ psychrometric constant (kPa $°C^{-1}$)

λ peak wavelength (μm) of emitted radiation by a body

Δ slope of saturated vapour pressure vs air temperature curve (kPa $°C^{-1}$)

θ measured volumetric moisture (%)

1.0 INTRODUCTION

The agricultural industry is an important element of the western Canadian economy. However, the semi-arid environment of the region experiences periodic soil moisture deficits that reduce optimum yields. These moisture deficits are a product of a temperate climate in which precipitation is often exceeded by atmospheric demand due to high summer insolation, high summer temperatures, low relative humidity, and strong winds. These meteorological conditions contribute to the physical process of evaporation from the reserves of soil water necessary for plant growth.

Successful crop production requires diligent management of the supply of moisture for crop production. Investigation of soil moisture deficits and water use is a critical area of research in the Prairie environment. The knowledge of soil moisture deficits has direct applications in irrigation scheduling, crop yield predictions, and crop management decisions.

Much research is based on simple assumptions that plant growth is related either directly to spring soil water content, growing season rainfall, total water use, irrigation amount, potential evaporation or a combination of these. Crop yields are generally expressed as a function of these variables (Doorenbos et al. 1986). These correlation-based equations are widely used on the Canadian Prairies with the understanding that care must be exercised in their applications due to their simplification (Department of

Agricultural Engineering 1989). There is a need to further examine the physical processes that contribute to moisture deficits and the lack of soil water availability for plant growth. Primary amongst these processes is evaporation.

Evaporation from soils in arid environments is also significant in the areas of soil conservation, climate modeling, and surface and groundwater hydrology. The study of soil salinization, the effect of climate change, and the dependency of surface and groundwater stores on soil moisture status all require the examination of the process of evaporation.

1.1 Evaporation

Evaporation is one of the main phases of the hydrological cycle and is the link between the energy budget and water budget. The hydrological cycle involves a release of energy and the transfer of mass as condensation of atmospheric water vapor results in precipitation to the earth's surface. The transfer of water continues as surface and subsurface flows, seepage and groundwater recharge. The cycle closes as an input of energy produces evaporation and water vapor returns to the atmosphere from both the surface of the soil and the free water surfaces of streams, rivers, lakes and oceans. Unfortunately, evaporation from soil and vegetative surfaces is one of the least understood aspects of the hydrological cycle (Brutsaert 1982).

Evaporation occurs when liquid water changes phase to water vapor. There are three conditions necessary for evaporation from a soil surface to occur. There must first be a supply of energy that drives the change in state from water to vapor. The second requirement is that there must be a vapor pressure gradient within the atmosphere which

produces a demand for the water vapor that is produced. These two conditions, the supply of energy and the vapor pressure gradient, are external to the soil and are influenced by meteorological conditions such as air temperature, windspeed, humidity and radiation. These conditions define the atmospheric evaporativity. The third requirement is a supply of water from the soil surface or through the body of soil beneath the evaporation site. This supply of water to the soil surface is affected by the moisture status of the soil surface and the conductive properties of the soil profile.

Stated in terms of soil moisture availability for plant growth, the change in soil water storage is a function of the amount of precipitation as well as the subsequent atmospheric demand. However, this change in soil water storage is not only dependent upon atmospheric conditions but also the surface and profile moisture characteristics of the soil as the atmospheric demand will produce an evaporative flux that is dependent on the soil moisture status. The relation of evaporation to water application and the storage of water for plant use has been investigated by many researchers (Staple and Lehane 1944, Gardner and Gardner 1969). Gardner and Gardner (1969) concluded that soil evaporation was greater for small and frequent additions of precipitation versus the same amount applied in a single event. Lesser daily rainfall amounts that do not penetrate deeply into the soil profile may be more susceptible to the ensuing evaporation, and should not be considered as effective precipitation. Prairie rainfall occurring in daily amounts of 5 mm or less comprises approximately 25% of the summer rainfall and daily amounts of 10 mm and less contribute about 46% of rainfall totals (Saskatoon Airport data). The evaluation of that portion of smaller daily rainfall amounts which is effective in contributing to a storage of moisture for plant utilization is a major consideration.

1.2 Objective

The objective of this project is to establish a relationship between daily rainfall and that portion of the rainfall lost to evaporation in the following 24-hour period. The hypothesis is that lighter intensity rainfall amounts cannot be held within the soil against evaporative demand and do not increase the storage of soil water in the root zone. The scope of the project is limited to the daily examination of the top 30 cm of a bare, fallow plot during the growing season.

1.3 Methods of Evaluating Evaporation

In this thesis effective precipitation is defined as the portion of precipitation that contributes to an increase in soil moisture storage within the root zone for longer than a 24-hour period. To determine effective precipitation, the components of the hydrological cycle must be evaluated. Precipitation can be measured directly. Runoff and drainage are physical processes that lend themselves to operational monitoring which yields reasonable estimates. However evaporative flux is determined indirectly from the measurement of other parameters and through the use of known, inferred or derived relationships (Brutsaert 1982).

As evaporation is a component of both the water and energy budgets, consideration of both mass and energy conservation can be employed to estimate evaporative flux.

2.0 LITERATURE SURVEY AND THEORY

2.1 Evaporation and Effective Precipitation

Effective precipitation has been defined by some researchers (Blaney and Criddle 1950, Pierce 1960) as the total amount of precipitation received less surface runoff and deep percolation, implying that the remainder of the rainfall will be available for evapotranspiration or be "effective". However, other researchers, primarily those involved in irrigation (Gardner and Gardner 1969, Heermann and Shull 1976), determined that seasonal evapotranspiration requirements was a function of the depth and frequency distribution of the total water received, and increased for smaller and more frequent applications. Gardner and Gardner (1969) used artificial columns of soil and added water at various rates ranging from 2.5 mm per day to 102 mm once in 20 days. They found that the water lost to evaporation varied from 100% for the smaller and more frequent additions, to 31.2% of the greater application depths. Heerman and Shull (1976) examined seasonal, daily, and hourly evaporation occurring from different precipitation depths in a natural growing environment. They found that daily evapotranspiration increased immediately after a rainfall and that total seasonal evapotranspirative was also higher when smaller application depths were involved. Heerman and Shull also questioned whether an increase in evapotranspiration

immediately following rainfall might be offset by a decrease in potential evapotranspiration with the decrease of solar radiation, air cooling and higher relative humidity associated with the precipitation event.

Findings of this type of research have led to the redefinition of effective precipitation as that fraction of rainfall or irrigation that is held in the root zone after runoff, deep drainage, and evaporation during a specific time period (Bos et al. 1996). It is a function of many variables (Bos et al. 1996), the major influences being: amount and frequency of precipitation, time of occurrence of precipitation, rainfall intensity, soil characteristics (infiltration capacity, water holding capacity, soil water movement), and landscape characteristics (field slope, land surface condition, depth to groundwater).

Crop scientists and irrigation planners investigate the portion of precipitation that is retained and utilized within the root zone after subsequent evapotranspirative depletion. The efficiency of applied water depths is assessed in terms of crop yield (Heerman and Shull 1976, Doorenbos et al. 1986, Patwardhan et al. 1987).

2.2 Physical Principles

Evaporation, and thus effective precipitation, are functions of the transfer of vapour, heat and momentum at the earth's surface. Conservation of mass, energy, and momentum forms the basis for the evaluation of evapotranspiration. A key to applying the conservation of mass, energy, and momentum is the quantification of control volumes.

In the atmosphere, gradients in humidity, temperature and wind speed are found in the vertical direction and immediately above the surface. For this reason the air near

the surface is critical and termed the boundary layer. In the boundary layer the horizontal scales of most properties are much larger than the vertical, so that horizontal gradients are negligible compared to vertical gradients. The same is true for the soil system near the earth's surface; soil water and temperature gradients are strongest in the vertical direction.

It is appropriate to divide the soil-atmosphere system into a series of layers aligned parallel to the evaporating surface. In the layer closest to the surface the exchange processes take place at a molecular level. Random molecular motion or diffusion is the predominant transfer mechanism and is key in two layers pertinent to this work; the soil layer immediate to the surface, and the laminar boundary layer of the atmosphere. The laminar layer is only a few millimeters deep and the flowlines (planes of constant temperature, water vapour and momentum) are parallel with no mixing. The depth of this laminar boundary is defined by a critical combination of speed of flow, distance, fluid viscosity, and surface roughness. A transition layer exists above this laminar sublayer and the parallel flowlines begin to break down. Beyond this transition zone is a fully turbulent zone, where heat, vapour and momentum are transferred by eddies. Turbulence is the most effective transfer mechanism not only for energy (heat) and mass (vapour) transfer, but momentum transfer as well.

2.2.1 The Soil-Atmosphere Continuum

The removal of water from the soil involves the net upward transport of water from the soil matrix to liquid/air interfaces within the porous soil. Once evaporation has occurred at this interface, water vapour is transferred to the bulk air by molecular

diffusion and turbulent eddy movement. The upward movement of liquid water within the soil matrix is by flow in response to negative soil moisture pressure and capillary rise. Vapour transport within the soil, near the surface and at the surface, is by molecular movement or diffusion across a thin boundary layer. Beyond the boundary layer there is a transitional region in which both molecular diffusion and turbulent eddy movement are involved. While diffusive transfer is by random molecular movement, turbulent transfer is by eddies or moving parcels of fluid, primarily air or water. Subsequently, the transitional region merges into the fully turbulent zone where turbulent (eddy) transport is the primary mechanism (Slayter 1967).

Mass, energy and momentum must be conserved. The exchange of these entities is governed by a general transport equation, written in a flux-gradient form:

Flux of an Entity	=	Ability to Transfer	x	Gradient of a Relevant Property

In a one-dimensional system, the flux density of an entity is directly related to the gradient multiplied by an ability to transfer, called a transfer coefficient.

Solar radiation drives the energy and mass exchange at the surface of the earth. This includes the transfers between the atmosphere and the earth's surface as well as between the earth's surface and the underlying soil.

A more compete discussion based on soil physical properties and processes may be found in Hillel (1982) as well as Marshall and Holmes (1988) while the atmospheric principles are described more fully in Slayter (1967), Fleagle and Businger (1980), Brutsaert (1982), Jones (1992), and Oke (1993).

The Soil Matrix

Water moves upward in the soil in response to a potential energy gradient. The potential energy in an unsaturated soil is due to the interaction of water with the solid particles, solutes, and air voids that comprise the soil matrix (Marshall and Holmes 1988). Water added to unsaturated soil is subject to gravitational, osmotic, and capillary forces (which includes surface adsorption to the particles) within the pore volumes. Thus the potential energy of a soil is made up of gravitational, osmotic, and matric (due to surface adsorption and capillary forces) potentials. Energy is needed to withdraw water against these forces hence the potential energy is negative. Osmotic forces are significant in soils where solutes play a key role (such as saline soils or tailing piles in mining), but are outside the scope of this work.

The gravitational potential is defined as the amount of work that is required to move water from one elevation to another and represents the work done against the gravitational field. If a volume of water (V) is moved from zero height at the reference plane to a height (z), the amount of work done is $V\rho\, g\, z$. The gravitational potential (Z) per unit volume, mass (equal to $\rho\, V$) and weight (equal to $g\, \rho\, V$) of water are given by:

$$Z_v = \rho g z$$
$$Z_m = g z \qquad [2.1\ a, b, c]$$
$$Z_w = z$$

where:

ρ = density of water (kg m^{-3}),
g = gravitational constant (9.81 m s^{-2}),
z = elevation above the reference plane (m),

and the subscripts v, m, w refer to the volume, mass and weight basis. The height z is also termed the elevation head.

The matric potential arises from the interactive forces of water within the matrix of solid particles. These forces are attractive. The amount of work that would have to be done to remove a volume of water against matric forces is $V\rho\, g\, h$. The matric potential (Ψ) per unit volume, mass (equal to $\rho\, V$) and weight (equal to $g\, \rho\, V$) of water are given by:

$$\begin{aligned} \psi_v &= \rho\, g\, h \\ \psi_m &= g\, h \\ \psi_w &= h \end{aligned} \qquad [2.2\text{ a, b, c}]$$

where h is the matric pressure (m). Matric pressure is the matric force per unit area of soil matrix (N m^{-2} or Pa) and can be expressed as a height, h, of water in an open column of water:

$$h = \frac{p}{\rho\, g} \qquad [2.3]$$

where:

p = the matric pressure or suction (N m^{-2} or Pa).

The hydraulic potential is the total of the matric and gravitational heads:

$$\phi = h + z \qquad [2.4]$$

The flux of soil water per unit area of saturated soil is governed by Darcy's Law:

$$v = \frac{V}{A} = K\frac{\phi_2 - \phi_1}{l_{12}} \qquad [2.5]$$

where:

V = volume of flux ($m^3\ s^{-1}$),
A = unit cross sectional area (m^2),
K = hydraulic conductivity or the soil's ability to transfer (m s^{-1}),
$\phi_{1,2}$ = hydraulic potential at points 1 and 2 where $\phi_2 > \phi_1$ (m), and
l_{12} = path length parallel to soil water flow (m).

The difference in potential over the pathlength provides the gradient that drives flow and the soil's ability to transfer, or the hydraulic conductivity, is constant in saturated flow.

In unsaturated soils, the hydraulic conductivity is not constant and decreases as the soil dries.

The Near-surface Soil Layer

Evaporation from a non-vegetated surface can be considered to occur in three stages (Hillel 1982). In the first stage the soil is saturated and water is freely available to the evaporative demand. In this stage the rate of evaporation is controlled by atmospheric conditions and the molecular exchange process is driven by the vapour concentration gradient in the boundary layer. The duration of this first stage depends on the rate of evaporation and the ability of the soil profile to supply the necessary vapour flux. The movement of the water to meet this evaporative demand is primarily in the liquid phase, is in response to energy gradients, and is calculated on the basis of atmospheric measurements as it is the atmosphere which controls evaporation. For constant atmospheric conditions, the rate of drying does not vary and thus the first stage of evaporation is often called the constant-rate stage and may last from few hours to a day or two (Brutsaert and Chen 1995).

As evaporation continues, the ability of the soil to supply water to the surface falls below the atmospheric demand. In this second or falling-rate stage, the soil is not saturated, movement of water vapour through the soil matrix is by liquid conduction and by vapour diffusion, and there is a resistance to liquid and vapour movement supplied by a combination of soil factors that include surface adsorption of water. In this stage the

rate of vapour flux is restricted by the soil's inability to release water vapour from soil particle surface. The water retained in large soil pores vaporizes earlier than that in the small pores due to the weaker capillary force on the water in the larger pores. The falling rate stage is also called the soil-profile controlled stage and lasts much longer than the constant-rate stage.

As the soil dries a residual slow-rate stage is eventually established. During this stage the soil surface is too dry to support liquid water conduction. Evaporation is controlled by vapour diffusion, is affected by the vapour diffusivity of the surface soil, and the adsorptive forces between the surface of the soil particles and pore water. This slow-rate stage is also called the vapour diffusion stage.

In both the second and third stages of drying the vapour flux is sensitive to temperature gradients in the soil. When considering heat exchange and temperature, heat flows from an area of higher temperature to one of low temperature and the magnitude of the flux is proportional to the temperature gradient. Vapour flux in the water and air filled voids of the soil profile is from areas of higher to lower vapour pressure.

Temperature affects soil water movement in the liquid phase by its effect on surface tension. A decrease in temperature causes a decrease in the surface tension and a smaller matric potential (suction) of the soil water. Thus a temperature gradient in soils of uniform water content gives rise to a gradient in suction that induces movement in the liquid phase from regions of high to low temperature.

Vapour flux in response to temperature gradients is not very well understood. In theory a decrease in soil temperature will cause a corresponding decrease in the vapour pressure. This results in a water vapour movement in response to a vapour pressure from

a warm temperature (and thus high vapour pressure) area of the soil to the low temperature (and correspondingly the lower vapour pressure) area of the soil (Slayter 1967, Marshall and Holmes 1988). Nevertheless Menenti (1984) has shown that thermal convection of soil air carries vapour in the direction of increasing soil temperature. Additionally Feddes et al. (1988) postulate that heat and vapour flow, in very dry soils, can be in opposite directions due to density gradients induced by vapour production. However, it should be noted that when the soil is very dry, the rate of evaporation is usually negligible and of little hydrological significance (Brutsaert 1982).

In this near-surface layer water vapor is transported by molecular diffusion from the water surface in the soil pore to the surface. This water vapour is then subject to atmospheric demand within the laminar boundary layer.

Laminar Layer Transport

In the laminar layer there is no convection, and transfer is by molecular diffusion. The flux of water vapour through this layer is expressed by Fick's Law (Oke 1993):

$$Q_e = - \frac{\rho_a C_p}{\gamma} \kappa_e \frac{\partial e}{\partial z} \qquad [2.6]$$

heat conduction is by Fourier's:

$$Q_h = - \rho_a C_p \kappa_h \frac{\partial T}{\partial z} \qquad [2.7]$$

and momentum flux is described by Newton's Law of Viscosity:

$$\tau = \rho_a \kappa_m \frac{\partial u}{\partial z} \qquad [2.8]$$

where:

Q_e = latent heat flux, energy per unit surface area (W m^{-2}),
Q_h = sensible heat flux, energy per unit surface area (W m^{-2}),
τ = dynamic viscosity, shearing stress per unit area (kg m^{-1} s^{-2}),
ρ_a = air density (kg m^{-3}),
C_p = specific heat of air at constant pressure (J kg^{-1} $°C^{-1}$),
γ = psychrometric constant (kPa $°C^{-1}$),
κ_e = molecular diffusion coefficient for vapor transfer (m^2 s^{-1}),
κ_h = molecular diffusion coefficient for heat transfer (m^2 s^{-1}),
κ_m = molecular diffusion coefficient for momentum (m^2 s^{-1}),
e = vapour pressure (kPa),
T = air temperature (°C),
u = horizontal windspeed (m s^{-1}), and
z = elevation (m).

The negative sign in the vapour and heat transport equations indicate that the direction of flux is opposite to that of the gradient, or that the flow is in the direction of decreasing concentration or temperature. In the laminar layer, the diffusion coefficients are constant with elevation above the surface and very small (in the order of 10^{-5} m^2 s^{-1}).

Turbulent Layer Transport

Turbulent transfer is much more efficient than that due to molecular activity. However there is a similarity in the role played by eddies and that of the molecules in diffusion. Hence the flux gradient transfer equations for vapour, heat and momentum are extended to fluxes in the turbulent zone and the molecular diffusion coefficients are replaced with eddy diffusivities (K_v, K_h and K_m, all with units m^2 s^{-1}). These diffusivities are not constant, are larger than molecular diffusion constants, and increase with elevation (10^{-5} m^2 s^{-1} to 10^2 m^2 s^{-1}). Figure 2.1 illustrates the development of the turbulent layer as well as the flux, diffusion coefficient and gradient profiles with elevation.

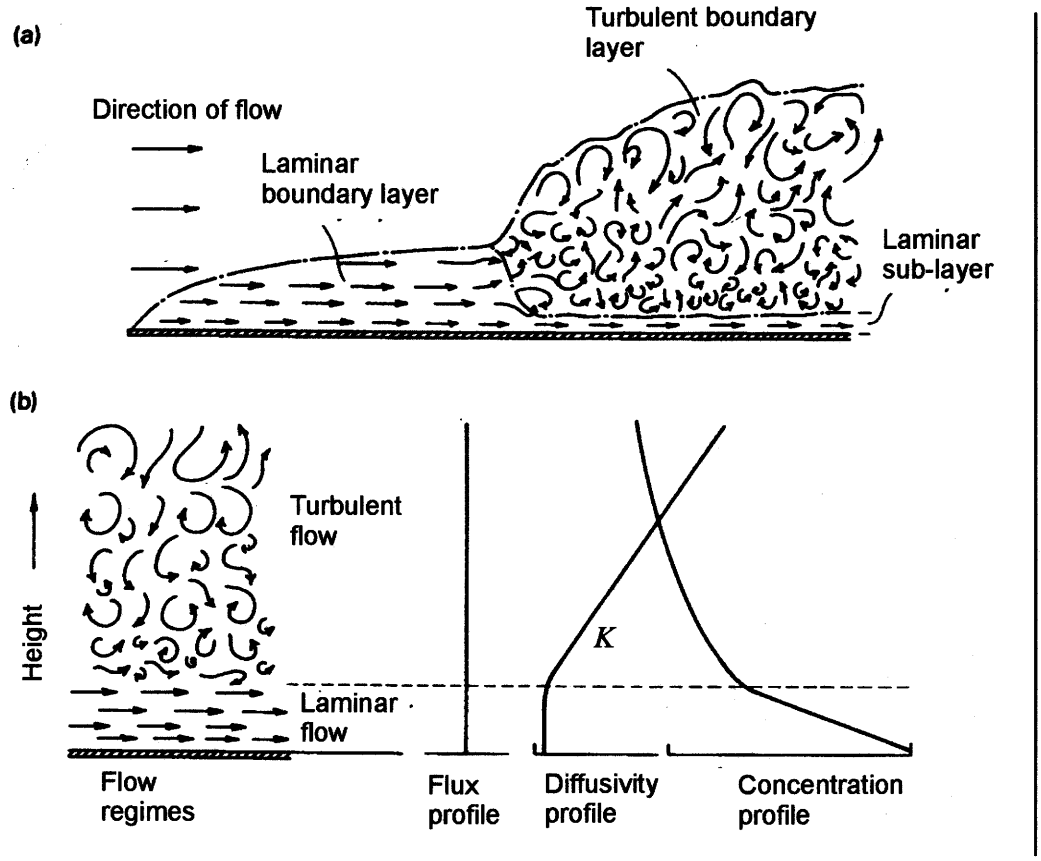

Figure 2.1 The development of (a) laminar boundary layer as well as the transition to turbulent flow, and (b) the vertical variation of the flux of any entity and the associated diffusion and the concentration of any property (adapted from Oke 1993).

Logarithmic Wind Profile

The influence of wind, a purely mechanical turbulence, and its role in the removal of water vapour in the turbulent zone defines a need to examine the wind speed profile. Unlike temperature and water vapour profiles, wind speed has a zero boundary condition at the surface. This allows the calculation of the transfer of momentum if the wind speed

above the surface in known. The transfers of heat and water vapour are then related to the transfer of momentum.

Wind speed increases logarithmically with height above the surface. The logarithmic wind profile equation is (Brutsaert 1982):

$$u_z = \frac{u^*}{k} ln \frac{z}{z_0} \quad [2.9]$$

where:

u_z = mean wind speed at level z (m s^{-1}),
z = elevation above surface (m),
u^* = friction velocity (m s^{-1}),
k = von Karman constant (0.41), and
z_0 = roughness length (m).

The roughness length, z_0, is a measure of the aerodynamic roughness of the surface and is related to the height, shape and density of the roughness elements. It is defined as the height at which the wind profile extrapolates to zero wind speed.

The friction velocity, u^*, characterizes a turbulent regime and increases with wind speed and roughness at a given height. The friction or shear velocity is related to the shearing stress by:

$$(u^*)^2 = \frac{\tau}{\rho_a} \quad [2.10]$$

where:

u^* = friction velocity (m s^{-1}),
τ = dynamic viscosity, shearing stress per unit area (kg m^{-1} s^{-2}), and
ρ_a = atmospheric density (kg m^{-3}).

The friction velocity can be calculated from the wind profile measurements. It is the slope of the logarithmic windspeed with elevation plot. Thus for wind speed measurements within the boundary layer (Brutsaert 1982):

$$u^* = \frac{k(u_2 - u_1)}{\left[ln\left(\frac{z_2 - d_0}{z_0}\right) - ln\left(\frac{z_1 - d_o}{z_0}\right)\right]} \quad [2.11]$$

where:

k = von Karman constant (0.41),
u_1, u_2 = wind speed measurements taken at height z_1, z_2 (m s^{-1}),
z_1, z_2 = elevation above surface (m),
d_o = zero plane displacement height (m) for surface roughness ($d_o = 0.67\ h$),
z_o = aerodynamic roughness height (m) ($z_o = 0.13\ h$), and
h = crop or roughness height (m).

2.2.2 The Radiation Balance

Radiation is the transfer of energy by electromagnetic waves and it is solar radiation which provides the energy to drive the earth's energy balance and hydrological cycle. The emission of radiation is governed by radiation laws.

Wien's Law states that the peak wavelength of emitted radiation by a body is inversely proportional to the absolute temperature of that body:

$$\lambda = \frac{2897}{T} \quad [2.12]$$

where:

λ = peak wavelength (μm) of emitted radiation by a body,
T = temperature (K) of the body.

The sun, at a temperature of about 6000 K (Fleagle and Businger 1980, Jones 1983), emits radiation primarily in the wavelengths of 0.2 to 3 μm (shortwave radiation) with a wavelengths peaking at approximately 0.48 μm. The earth, at a considerably cooler temperature of about 300 K, emits terrestrial radiation in wavelengths of between 4 and 100 μm (longwave radiation).

The amount of energy emission of a body may be expressed as the rate of flow of radiation energy, or flux, (J s^{-1}, or W) from a unit area (m^{-2}) of a plane surface into the overlying hemisphere. The flux per unit area is its flux density (W m^{-2}). The Stefan-Boltzmann Law defines the radiant flux density emitted by a body to be a function of the fourth power of absolute temperature of that body,

$$R = \varepsilon \sigma T^4 \qquad [2.13]$$

where:

R = radiant flux density emitted (W m^{-2}),
ε = emissivity of a the body ($\varepsilon = 1$ for a blackbody),
σ = Stefan-Boltzmann constant (5.67×10^8 W m^{-2} K^{-4}), and
T = absolute temperature of the body (K).

The sun's energy is radiated more or less uniformly in all directions, but the earth intercepts only a fraction of the output of the sun. The flux of solar radiation per unit horizontal area at the top of the atmosphere depends strongly on the zenith angle of the sun and much less strongly on the variable distance of the sun to the earth. The radiant flux density of solar energy received at the top of the earth's atmosphere normal to the direction of the solar beam at the mean sun to earth distance of 149.5×10^6 km is known as the solar constant (I_o). The magnitude of the I_o, averaged over the year, is 1367 W m^{-2} (Oke 1993). This is an upper limit for the short-wave radiation as the solar constant assumes an ideal orientation (i.e., the solar beam is always normal to the intercepting plane, the atmosphere). When averaged over the year, the mean daily solar radiation flux density over the top of the atmosphere is exactly $I_o/4 = 342$ W m^{-2}, and for 50° N latitude varies from 80 W m^{-2} to slightly over 450 W m^{-2} (Fleagle and Businger 1980). The

daytime partitioning of this solar radiation within the atmosphere and at the earth's surface is given in Figure 2.2.

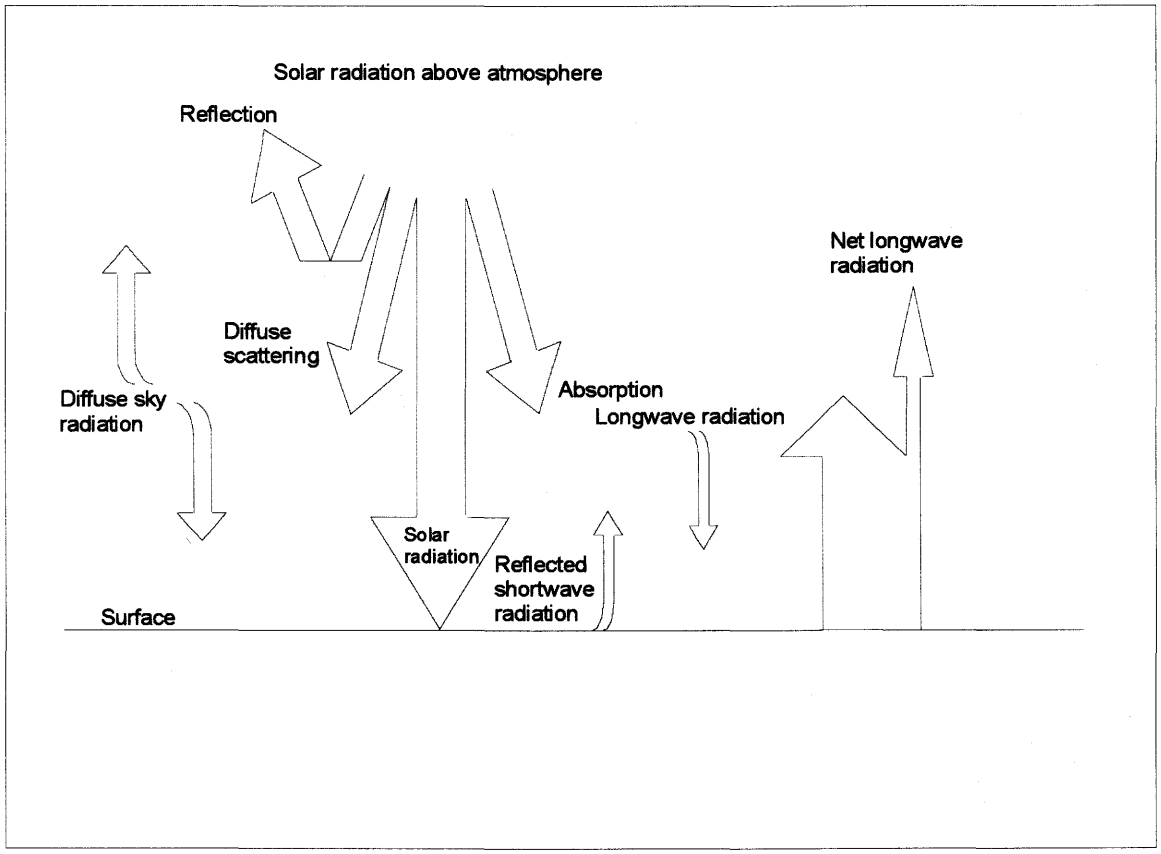

Figure 2.2 The daytime radiation balance. The night time radiation balance is limited to the longwave exchange (adapted from Slayter 1967).

Solar radiation is attenuated by reflection, scattering and absorption as it passes through the atmosphere. Clouds within the atmosphere reflect about 19% of the solar radiative flux back to outer space while scattering and absorbing about 5% the solar radiation. The scattering of incoming solar radiation produces diffuse solar radiation while that which is absorbed is re-emitted as longwave radiation. Other atmospheric constituents (carbon dioxide, ozone, salts, dust and other aerosols) reflect a further 6% of the sun's radiation to space while scattering and absorbing about 20% of solar input,

again subsequently producing diffuse radiation as well as emitting longwave radiation. The remainder of the original solar beam is transmitted to the earth's surface where approximately 53% is reflected and the remaining approximately 47% of the solar radiative flux is absorbed and is partly consumed in the heating of the earth's surface (Oke 1993). Reflected solar (shortwave) radiative flux is highly variable, depending on the reflective properties (albedos) of the surface.

The atmospheric absorption of shortwave radiation and subsequent longwave emission of energy are complemented by the emission of longwave radiation by the earth's surface. It should be noted that while the earth continually emits longwave radiation it receives shortwave radiation only during daylight hours. Therefore at night the radiation balance is equivalent to the net longwave exchange. Net longwave radiation is the difference between the outgoing longwave radiation emitted from the earth's surface and incoming longwave from the atmosphere. Incoming longwave radiation from the atmosphere, in the absence of clouds, depends on atmospheric temperature and does not show significant diurnal variation. Outgoing longwave radiation is a function of surface temperature and shows a strong diurnal variation.

Net radiation received at the earth's surface is the sum of net shortwave and longwave radiative exchanges and can be described by:

$$Q_n = Q_{ns} + Q_{nl} \qquad [2.14]$$

where:

Q_n = net all wave radiation (W m^{-2}),
Q_{ns} = net shortwave radiation (W m^{-2}), and
Q_{nl} = net longwave radiation (W m^{-2}).

Net radiation is the source of energy at the earth's surface that is used for evaporation, heating the air and heating the underlying surface.

2.3 Energy Partitioning and Evaporation at the Earth's Surface

2.3.1 Surface Energy Balance

By defining a control volume that examines only vertical fluxes, the energy equation is:

$$Q_n = Q_g + Q_h + Q_e + Q_s + Q_p \qquad [2.15]$$

where:

Q_n = net radiation (W m^{-2}),
Q_g = ground heat flux (W m^{-2}),
Q_h = sensible heat flux (W m^{-2}),
Q_e = latent heat flux (W m^{-2}),
Q_s = storage of energy in vegetative biomass (W m^{-2}), and
Q_p = energy used in photosynthesis (W m^{-2}).

For the non-vegetated surface typical of a prairie agricultural fallow environment, Q_s and Q_p, can be considered negligible. The energy balance then reduces to:

$$Q_n = Q_g + Q_h + Q_e \qquad [2.16]$$

The sign convention followed is the energy source that drives energy and mass exchange (net radiation) is positive to the earth's surface. Latent, sensible and ground heat are positive when directed away from the surface. Examples of typical flux directions for daylight and night are presented in Figure 2.3. As net radiation follows a diurnal cycle, the processes that depend on net radiation: ground heat, and turbulent (latent and sensible heat) fluxes also exhibit a diurnal trend.

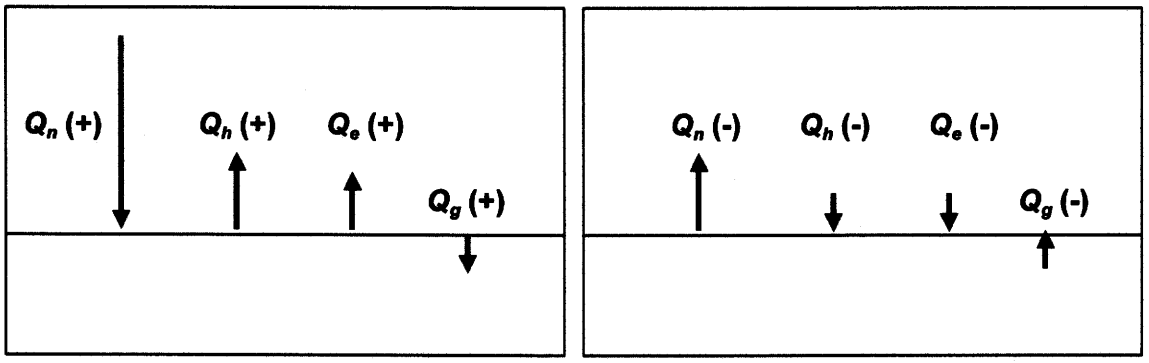

Figure 2.3 Sign conventions and typical flux directions for typical daylight and night conditions.

2.3.2 The Bowen Ratio Energy Method

Net radiation is disposed of in the form of latent and sensible atmospheric as well as ground heat fluxes. The transfer mechanism for sensible heat is the same as that of latent transfer; both take place within the turbulent zone. As well, the energy consumed in latent transfer is often supplied by the sensible energy component. This has led to the development (Appendix E.1) of the Bowen ratio energy balance method for the evaluation of evaporation (Bowen 1926).

The Bowen ratio (B) is the ratio of sensible heat to latent flux. Combining this definition with the energy balance equation (Equation 2.16), yields an expression for evaporation (Equation E.4):

$$Q_e = \frac{Q_n - Q_g}{1 + B} \qquad [2.17]$$

where:

Q_n = net radiation (W m^{-2}), and
Q_g = ground heat flux (W m^{-2}).

The Bowen ratio approach yields latent and sensible heat flux calculations from measurements of vapor pressure and temperature at two levels. The measurements must

be made within the turbulent transfer layer and, to ensure that the vertical fluxes are adequately representative, an extensive fetch is required.

The Bowen ratio approach for estimating evaporation is the most accurate when B is small (Brutsaert 1982). It is only valid when the latent flux and sensible heat transfer are directed towards the lower concentration or decreasing temperature, consistent with the development of the equation (Angus and Watts 1984). It also should be noted that solving for evaporation is problematic when B equals -1 and Equation 2.17 becomes undefined. This usually occurs when the fluxes are low; at times around sunrise, sunset and occasionally at night. Indeed as B approaches -1, errors in the measurement of the temperature and humidity profiles may yield unrealistic evaporation estimates. Ohmura (1982) designed a set of criteria to test data for rejection for those times when instrument error becomes significant (near B = -1) or the direction of calculated fluxes render the Bowen ratio approach invalid. Section 3.2.2 outlines the rejection criteria equations and the protocol for evaporation estimation when the Bowen ratio method can not be used.

The above considerations notwithstanding, the Bowen ratio approach is widely used as it lends itself to continuous monitoring of latent and sensible heat fluxes (Rouse and Wilson 1971/1972, Malek and Bingham 1993). The approach simplifies instrumentation regimes as it does not require windspeed monitoring but only measurements of net radiation, ground heat flux, as well as temperature and vapour pressure at two levels. Under ideal conditions, and for homogeneous terrain, the Bowen ratio approach has a reported uncertainty in the estimation of latent flux of only 10% (Sinclair et al. 1975).

2.3.3 The Penman-Monteith Method

Penman (1948) developed an equation based on the energy balance to estimate evaporation from open water or a saturated surface (Appendix E.2). Monteith (1965) reformulated Penman's equation (1948) in terms of the adiabatic cooling and loss of moisture from the air in the diffusion process as well as incorporating an aerodynamic resistance term, r_a, to replace the wind function. Monteith also extended Penman's equation to non-saturated conditions. Two resistances to vapour flux, surface resistance of a drying soil and the aerodynamic resistance (r_s and r_a), are considered for a non-saturated evaporating surface in the Penman-Monteith equation (Appendix E.2).

The use of the Penman-Monteith equation requires measurement of temperature and vapour pressure at one height. Additional measurements needed are windspeed, net radiation, ground heat flux and an estimation of the resistance terms. The Penman-Monteith equation is a popular evaporation estimation technique and has been utilized by a large number of researchers (Wallace 1995).

While the role and physics of the aerodynamic resistance term seem to be well understood, the surface resistance term, r_s, (vegetative stomatal and/or soil resistance) is not and has been defined in terms of individual species of vegetation (Russell 1980) and for bare soil (Camillo and Gurney 1986). Others have considered fairly heterogeneous environments and have investigated r_s in terms of sparse canopies (Shuttleworth and Wallace 1985) or canopies comprised of more than one type of species (Blanken and Rouse 1995).

Bare soil resistance has been described as a function of volumetric soil moisture content. The near-surface soil layer is considered to be location of the evaporating

surface. Researchers have expressed r_s in terms of the soil moisture content in the top 0.5 cm (Shu Fen Sun 1982, Camillo and Gurney 1986), the top 1 cm (van de Griend and Owe 1994), the top 2 cm (Kondo et al. 1990), or the surface 2 or 5 cm (Daamen and Simmonds 1996). The dependence of r_s on soil surface moisture has been expressed in many forms, from a simple linear relationship (Camillo and Gurney 1986) to a power function (Shu Fen Sun 1982, Kondo et al. 1990). Additionally van de Griend and Owe (1994) showed a relationship for soil resistance that grows exponentially as the soil dries. The range of estimated values for the surface resistance is from 0 to over 4000 s m^{-1}.

Daamen and Simmonds (1996) compared the r_s values computed from moisture contents from different profile depths (0 to 2 cm as well as 0 to 5 cm). Interestingly, as the thickness of the surface layer decreased, the r_s estimation improved. However it is erroneous to conclude that an r_s model might be accurate if the thickness of the surface layer considered is reduced to some arbitrarily thin layer. Daamen and Simmonds (1996) demonstrated that parameterizing even very thin soil layers (i.e., 0 to 0.3 cm) can provide inaccurate r_s estimates. Daamen and Simmonds also showed that r_s is not a simple function of surface soil moisture, but also depends on evaporative demand. With soil moisture content held constant, as the potential evaporation increases, r_s increases.

2.3.4 The G-D Method

The G-D method (Granger and Gray 1989) is an extension of the Penman approach and makes use of the concept of relative evaporation, *G*, or the ratio of actual (non-saturated) to potential (saturated) evaporation (Appendix E.3). It employs a dimensionless relative drying power term, *D*, which is the ratio of the drying power of

the air (E_A) to the sum of the net energy available for turbulent transfer (Q_n - Q_g) and the drying power of the air (E_A).

Granger and Gray (1989) studied 158 evaporation periods in the semi-arid environment of western Canada and defined relative evaporation in terms of commonly measured parameters. Section 3.2.2 and equations 3.19 to 3.24 cover the estimation of evaporation by the G-D method. The measurements required are net radiation, air temperature, humidity, windspeed and ground heat flux. The G-D method offers the advantage of an estimation technique that does not require the estimation of a soil surface resistance factor as well as temperature, humidity and windspeed measurements at only one height.

While the G-D method was developed as a daily method within a prairie agricultural setting, it has been further utilized in other semi-arid environments including the boreal forest and the arctic tundra (Granger 1996, Pomeroy et al. 1997). The method is suitable for use with remote sensing (Granger 1997) and has also been modified to accommodate hourly or half hourly evapotranspiration estimates (Pomeroy et al. 1997, Elliott et al. 1998).

2.4 The Soil Profile and Evaporation at the Earth's Surface

The emphasis that has been placed on soil moisture availability (e.g., r_s in Penman-Monteith) is due to the fact that the process of evaporation, in most environments, occurs primarily in the falling-rate or slow-rate evaporation stages where the soil profile exerts control on evaporation. This is particularly true in semi-arid

climates. However, immediately following a rainfall event, evaporation may be close to the atmospheric demand (i.e., within the atmosphere limiting stage, or stage one drying).

Brutsaert and Chen (1995, 1996) found that second stage drying was reached quite quickly, often within one day, but that due to the diurnal fluctuations in net radiation, soil drying and moisture redistribution in the soil profile, soil evaporation might fluctuate during the day between stage one and two drying. For a bare soil all of these factors are exaggerated; after rainfall the progression to stage two drying is more rapid (more drying and no root uptake from deeper soil moisture stores) and the more extreme gradients within a bare soil lead to wider diurnal fluctuations.

The significance of the drying stage of the soil during evaporation is that it is soil properties that control evaporation and thus evaporative estimates, particularly by the water budget method, once the soil reaches the second stage of drying. With evaporation determined in the water budget as the precipitation less the change in soil moisture ($E = P - dS$), the spatial variability in soil properties such as soil water storage, total hydraulic gradient, hydraulic conductivity and soil water flux densities at depth influence the calculation of evaporation. The influence of the variability of these parameters has resulted in a 40% coefficient of variation for calculation of evaporation based on the water balance (Villegra et al. 1995). Using 25 experimental plots along a 25 m transect they found that while the variability in soil water storage was low, the hydraulic gradient and hydraulic conductivity both exhibited heightened variability. The variability in soil water flux density at the 150 cm depth was also high, but was only hydrologically significant during wet periods; during dry periods the values were small and had relatively little influence on the water balance calculations. Rouse and Wilson (1971/72)

indicated that the water budget approach presents a difficulty in assessing evaporation on a daily basis and that the accuracy of evaporation determination increases with an increasing estimation interval. However, these studies focussed on study periods that were dominated by stage two drying. Brutsaert and Chen (1996) showed that for those periods when soil moisture was above 27% (a value close to their field capacity) the spatial distribution of evaporation was uniform and they concluded that soil properties did not exert a control on evaporation or the variability of its estimation during the initial (i.e., stage one) drying stages.

2.4.1 The Water Budget and Lysimetry

The lysimetric method of determining evapotranspiration from soil has long been popular (van Bavel 1961, Robins 1965, Tanner 1967, Black et al. 1969). Its popularity stems from the appeal of a direct and independent measure of soil evaporation as well as its ease of use (Boast and Robertson 1982, Boast 1986). Lysimeters are isolated volumes of soil weighed to determine soil water loss. In some cases the confined volumes of soil are massive containments of both soil as well vegetation and continuous soil moisture loss or gain is measured by a pressure transducer. The installation, and subsequent monitoring, of these large lysimeters represents a formidable task. In other cases, smaller volumes of soil (microlysimeters), are removed periodically from the field and weighed. The isolation of the soil is usually accomplished by driving an open cylinder vertically into the soil, removing the cylinder and contained core of soil, and applying a barrier to the bottom of the cylinder yielding a barrier-capped microlysimeter. The cylinder and contained soil are returned to the site with the surface of the core flush with the

surrounding soil. Initial and subsequent weighing indicate the soil water lost to evaporation.

The validity of lysimetric methods for determining evaporation is contingent on how the evaporation from the isolated body of soil performs as an indicator of field soil water losses. Errors in this method of estimation may occur if the soil within a lysimeter is different from the field soil conditions in any of the properties important to vapour flux; namely the water content, the thermal regime, the density of the soil or the additional withdrawal due to transpirative demand. Additionally one-dimensional (vertical) flux of water and energy must be assumed to be true for the field. Therefore the main sources of error associated with lysimetric measurements are (Daamen et al. 1993):

1. the barrier to water flow imposed at the base of the lysimeter, which is assumed to be a zero flow boundary;
2. the conduction of heat through the lysimeter casing;
3. the disturbance of the soil in the driving, coring and extraction process;
4. the disturbance of roots at the perimeter of the soil core once it is isolated in the lysimeter; and
5. the prevention of net horizontal flow to or from the vertical soil column.

The magnitude of these errors depends on the depth of the lysimeter (point 1), the time since the soil core was hydrologically isolated (points 1, 2 and 4), the containment material (point 2), the diameter of the lysimeter (points 2 and 3), the significance of root extraction (point 4) and perhaps the positioning of the lysimeter within a sloping site (point 5).

The use of microlysimeters (smaller volumes of soils) has recently increased. Specifications of microlysimeters in use vary significantly (Table 2.1). Studies designed to test microlysimeter depth as a source of error (as an example the assumption of a zero flow boundary at the base of the microlysimeter) include a laboratory study of Boast and Robertson (1982), as well as a field study of Shawcroft and Gardner (1983). Daamen et al. (1993) considered appropriate diameters, depths and useable lifetimes for microlysimeters used in field studies on sandy soils and developed a protocol for the use of microlysimeters in water balance studies.

Daamen et al. (1993) investigated the effect of microlysimeter on heat conduction, on soil temperature, and subsequent evaporation. They concluded that diameter did not affect evaporation significantly. Microlysimeters, with their attendant barrier capping, were not useful for determining evaporative losses immediately following rainfall due to the water retention, higher soil moistures and higher evaporation. Outside rainfall events the depth of the microlysimeters has been investigated to test if the increasing the depth of capping (the assumed zero flux plane) would increase the effectiveness of microlysimeters. Payne et al. (1990) found that the zero flux boundary for bare soil plots in sandy soil was located between 0 and 250 mm during most of the growing season while Simmonds and Williams (1989) discovered that the zero flux plane reached 300 mm only after 36 days of drying.

Table 2.1 Dimensions and useable lifetime of microlysimeters in field and laboratory studies (adapted from Daamen et al. 1993).

Source	Internal Diameter (mm)	Depth (mm)	Useable Lifetime (days)
Boast and Robertson (1982)	76	146 106 70	n/a n/a 1 - 2
Walker (1983) (see also Boast 1986)	76	120	8 - 10
Shawcroft and Gardner (see also Boast 1986)	203	200 100 50	crop season (water added)
Martin et al. (1985)	150	200	crop season (water added)
Lascano and van Bavel (1986)	74	130	1 - 2
Matthias et al. (1986)	76	150	6
Villalobos and Fereres (1990)	200	300	1
Allen (1990)	100	150	2
Wallace et al. (1992)	150	300	1
Daamen et al. (1993)	214 152 51	100	3

Work by other researchers subsequent to the initiation of this project's field program in 1994 includes that of Evett et al. (1995), in which the effect of wall materials and barrier capping on the temperatures of the soils within the microlysimeters as well as the resultant evaporation was studied. They found that capping the bottom of the soil columns resulted in overestimation of the evaporation immediately following rainfall due to higher moisture contents. Additionally, the end capping caused a restriction in heat conduction and increased soil temperatures at the base of the microlysimeters. Heat conduction down the wall materials was found to be significant in steel microlyimeters and their contained soil warmed rapidly at depth leaving the soil surface cooler during

the day and warmer at night. They concluded by recommending that microlysimeters should be constructed of wall materials of low thermal conductivity, capping materials should maximize heat conduction from the bottom of the soil columns, and that 30 cm depth microlysimeters could be continuously used for a period of nine days.

3.0 EXPERIMENTAL SITE, EQUIPMENT, AND METHODS

3.1 Introduction

Conservation of mass and energy form the basis of the evaluation of evaporation, and thus assists in the determination of effective precipitation.

One of the physical bases of the hydrological cycle is the conservation of mass. Therefore to evaluate evaporation a water budget approach was used which states that, within any control volume over time:

$$dS = P - E + R_i - R_o \qquad [3.1]$$

where:

P = precipitation,
E = evaporation,
R_i = run on and/or groundwater inflow,
R_o = runoff and/or groundwater outflow, and
dS = change in moisture stored.

The evaporation term was determined as the unknown residual in this equation. Precipitation and changes in soil moisture were measured and the inflow/outflow were forced, or assumed, to be negligible. Precision in the measurement of precipitation and soil moisture was necessary, as the resolution of these measurements may introduce large errors in the estimation of evaporation. Additionally, in areas where variability in soil hydraulic characteristics is relevant, the water budget method yields a large coefficient of variation in evaporative estimates (Villagra et al. 1995). For these reasons an alternate

method of assessing evaporation was employed (Rouse and Wilson 1971/72, Malek and Bingham 1993).

Evaporation is the link between the conservation of mass and the conservation of energy in the hydrological cycle. An evaluation of the energy budget at the soil surface lead to evaluation of surface evaporation and an independent check of the water budget. In a simple vertical system (no advection), where photosynthesis and heat stored in vegetative mass are neglected, the energy budget is:

$$Q_n = Q_e + Q_h + Q_g \qquad [3.2]$$

where:

Q_n = net radiation flux,
Q_e = flux of energy involved in latent transfer,
Q_h = flux of heat into the atmosphere, and
Q_g = heat flux conducted into the earth.

The water budget and forms of the energy budget were employed to evaluate relationship between daily rainfall amounts, the ensuing 24-hour evaporative loss and the storage of soil moisture within the root zone.

Field measurements of soil and atmospheric conditions were were performed or evaluated at the same time each day to negate the effect of the diurnal cycling of soil temperature on soil moisture movement. Each measurement contributed to the calculation of evaporation as a term for either a water budget, an energy budget, or a combined energy budget-aerodynamic equation. These methods allowed quantification of the daily loss of soil moisture within a 30 cm control volume of the top of the soil profile. The 30 cm profile, for the purposes of this project was deemed to be the depth of active root growth and plant utilization.

The water budget equation was used to estimate evaporation as a residual term. Other water budget equation measurements included the use of precipitation gauges, gravimetric sampling, twin gamma probes, and weighing of microlysimeters. The evaluation of evaporation as a component of the energy balance required the examination of the energy partitioning at the soil surface. Net radiation and soil heat flux were measured. Latent heat flux and sensible heating were determined by monitoring humidity and temperature measurements. The assessment of evaporation using a combined energy-aerodynamic equation required the monitoring of these energy fluxes as well as the measurement of the wind speed. A summary of the evaporation estimation methods utilized and the physical measurements performed (Table 3.1) is provided to give the reader the framework for the field project.

Table 3.1 Summary of methods used and parameters measured.

Evaporation Estimation Method	Equation	Parameters Measured
Water balance method	3.1	precipitation differential weighing of microlysimeters twin gamma probe gravimetric sampling
Energy balance (EB) methods		
Bowen ratio equation	3.5	net radiation ground heat flux air temperature profile (two elevations)
Combined EB and aerodynamic methods		
Penman-Monteith equation	3.9	net radiation ground heat flux air temperature (one elevation) windspeed (one elevation)
G-D equation	3.19	net radiation ground heat flux air temperature (one elevation) windspeed (one elevation)

3.2 The Experimental Site and Field Measurements

Field data were collected at the University of Saskatchewan's Kernen Research Farm (Lat. 52° 9' N, Long. 106° 32' W, elevation 515 metres ASL) near Saskatoon, Saskatchewan. The farm is situated in the Chernozemic Dark Brown soil zone and its soil is defined as a Sutherland association (Rego and Orthic Dark Brown series). The experimental site had a slope of less than 3%. Management during 1991, 1992, and 1993 involved a wheat-fallow-wheat crop rotation. In 1994 the site was fallow, bare of residue, and was monitored daily from August 5th to September 9th for components of both the energy budget and the water budget.

3.2.1 Precipitation in the Study Region

Climate data collected at the Saskatoon airport from September 1922 to August 1990 is summarized in Table 3.2. Monthly rainfall depths during the growing season (May to September) range from 33.4 mm in September to 63.9 mm in June. The lowest coefficient of variation for these monthly average amounts is in July and the growing season month that experiences the most variability in total rainfall depth is August.

Daily rainfall less than 5 mm contribute approximately 25% of the total precipitation throughout the growing season (Table 3.3) while amounts of between 5 and 10 mm contribute a further 22%.

Table 3.2 Average of total precipitation depths received per month (Saskatoon Airport data, 1922-1990).

Month	Depth (mm)	Coefficient of Variation (%)
Jan	15.7	63.1
Feb	14.5	68.9
March	16.3	68.7
April	20.6	77.7
May	37.7	65.8
June	63.9	61.0
July	58.4	60.6
Aug	38.9	75.0
Sept	33.4	60.8
Oct	18.6	80.6
Nov	15.1	70.9
Dec	16.7	65.9
Yearly Total	349.8	

Table 3.3 The distribution of average daily rainfall amounts by depth interval and month for the growing season (Saskatoon Airport data, 1922-1990).

Month	Depth Interval (mm)					Monthly Total
	< 5	5 - 10	10 - 20	20 - 35	35 - 60	(mm)
May	9.7	8.3	12.0	6.6	1.1	37.7
June	13.3	12.8	14.5	13.4	9.9	63.9
July	13.4	12.0	15.9	9.6	7.5	58.4
August	10.1	10.0	11.2	5.3	2.3	38.9
September	10.4	6.9	8.4	5.9	1.8	33.4
Seasonal Depth						**Seasonal Total**
(mm)	56.9	50.0	62.0	40.8	22.6	232.3
Percentage of Seasonal Total	25	22	27	18	10	

3.2.2 The Evaluation of Field Soil Properties

In addition to meteorological conditions and soil moisture status, the soil moisture retention curve (SMRC), bulk density, and texture were examined. A set of undisturbed cores was hand-excavated for these purposes from the study site on June 10, 1994. The undisturbed soil cores were 8.5 cm in diameter and 3 cm deep near the surface or 5 cm

deep further into the soil profile. Three replicates were taken for the each of the depth intervals from 0.5 - 3.5 cm, 2.5 - 7.5 cm, 7.5 - 12.5 cm, 17.5 - 22.5 cm, and 27.5 - 32.5 cm. These intervals were chosen to evaluate soil properties for the nominal depths of 2, 5, 10, 20 and 30 cm.

Soil moisture retention was determined for the undisturbed field cores using a pressure plate apparatus (Klute 1986). The cores were placed in hydraulic contact with a known potential via a porous membrane. A ceramic plate was used to establish the potentials to 500 kPa. Soil samples obtained from the cores were ground, sieved and a cellulose membrane was employed with a high-pressure apparatus to yield the 1500 kPa potential. Hysteresis is a factor in soil water retention and the SMRC was determined for a drying regime.

After the moisture retentions had been determined, the undisturbed cores were dried to determine bulk density. Finally the cores were ground and sieved to allow a quantification of the sand and clay content. The modified pipette method described by Indorante (1990) was employed.

3.2.3 Water Budget Measurements

Several types of monitoring regimes were established to evaluate the water budget equation. The measurement device used, its resolution, and the replication and frequency of measurement are summarized in Table 3.4.

Precipitation was measured 150 metres from the site using an Atmospheric Environment Services (AES) tipping bucket rain gauge (TBRG) system. This involves the use of a tipping bucket mechanism coupled with a chart recorder, yielding both

precipitation amounts and intensities. Precipitation amounts were also measured with an AES Type B rain gauge both at the experimental site and at the TBRG system site.

Table 3.4 Field instrumentation for the determination of the components of the water balance.

Measurement Device/Replicates	Depth/Site Monitored	Resolution	Measurement Frequency	Comments
Microlysimeter -zero flux, barrier-capped, two sets of five replicates	0 - 30 cm on site	0.2 mm of water (5 g resolution)	daily first set weighed Aug 5 - Sept 9 second set Aug 20 - Sept 9	measured change in soil moisture in a control volume that does not allow drainage
Microlysimeter -contacting, cotton-capped five replicates	0 - 30 cm on site	0.2 mm of water	daily Aug 5 - Sept 9	measured change in moisture in a soil column that allowed drainage
Microlysimeter -unbroken, five replicates	0 - 30 cm on site	0.2 mm of water	installed Aug 5 weighed Sept 9	control microlysimeters represent field conditions
Twin gamma probe two replicates	0 - 60 cm on site	0.1 mm of water	daily	measured change in wet bulk density
Twin gamma probe two replicates	0 - 100 cm on site	0.1 mm of water	every second day	measured change in wet bulk density
Oakfield corer three replicates	0 - 40 cm on site		daily	measured mass moisture content of soil sample
Tipping bucket (TB) one replicate	150 m from site	0.254 mm	continuous chart recorder	measured rainfall intensity (rate) and depth
Standard rain gauge four replicates	three on site one at TB	0.254 mm	daily	measured rainfall depth

Gravimetric sampling to determine changes in soil moisture was performed with an Oakfield corer (2.0 cm inside diameter), taking three replicates at each sampling depth

interval. Samples were obtained to a depth of 40 cm to give a representation of the soil moisture within the 30 cm control volume as well as the moisture movement across the 30 cm boundary.

A twin gamma probe with a Cesium 137 source was utilized at two sets of dual access tubes within the site. One of the access tubes sets was arranged parallel to the slope while the other set monitored a transect orthogonal to the slope. The change in attenuation of gamma rays between the access tubes from measurement to measurement reflects the change in total bulk density between measurements. The gamma ray attenuation is calibrated to both the total bulk density and soil moisture content (bulk density and soil moisture both determined by soil sampling, using a hydraulic coring device at the time of the installation of the access tubes). A computer program was then used to transform the raw data (gamma ray attenuation) to volumetric moisture content for the profile. The maximum depth of monitoring alternated between 60 cm and 100 cm. The 60 cm depth (in 2 cm depth intervals to 40 cm, 4 cm intervals below 60 cm), monitored daily, was chosen to ensure that a both the 30 cm control volume and a depth below the 30 cm boundary were monitored for a change in soil moisture. The 100 cm depth (depth intervals as above) monitored every second day, was chosen to additionally check instrumentation drift.

Microlysimeters were used to monitor evaporation by measuring the 24-hour change in soil mass within the enclosed volume. The microlysimeters were constructed of aluminum, cylindrical in shape (17.8 cm ID, 18.2 cm OD, 32.0 cm length). The sleeve length ensured that a full 30 cm profile could be contained and allowed a 2 cm lip at the soil surface to prevent runoff to and from the surrounding soil and guard against

the loss of mass (water or soil) due to raindrop splash. To fully ensure that mass loss did not occur due to raindrop splash would have required a wall higher than 2 cm, however this would have significantly altered the aerodynamic regime, and thus evaporation from the soil surface within the microlysimeter. The microlysimeters were hydraulically pushed into the soil. During the observation period the microlysimeters were removed, weighed, and replaced within a pit defined by a PVC sleeve (20.8 cm ID) that acted as a retaining wall against the surrounding soil. The PVC cylinder was hydraulically driven into the soil to a depth of 40 cm to ensure that preferential flow did not enter the microlysimeter from the area outside the pit via the lower perimeter. To eliminate evaporative losses or the collection of soil and debris between the microlysimeter and the PVC sleeve, a gum rubber band was stretched from the outer PVC wall to the wall of the microlysimeter. This also minimized convective heating between the two walls which might alter the thermal and hence the moisture regime of the microlysimeter. A mechanical balance with a 5 g resolution was employed for the daily weighing. The resolution of the scale gave an equivalent depth of resolution of 0.2 mm of water

A traditional microlysimeter has a capped lower boundary (Boast and Robertson 1982, Lascano and van Bavel 1986) to isolate the control volume from upward or downward flux of moisture. In capped microlysimeters an assumption is made that the bottom of the microlysimeter represents a zero flux plane. To fully explore the concept that the base of the microlysimeter could be represented as a no flow boundary, three different types of microlysimeters were installed:

1. a traditional, barrier-capped microlysimeter,

2. a microlysimeter with a lower boundary of fabric allowing hydraulic as well as thermal contact, and

3. an unbroken microlysimeter, an aluminum cylinder pushed into the soil with no capping or barrier to allow unrestricted flow.

The first type of microlysimeter used a conventional barrier of heavy grade plastic applied to the lower end of one group of the microlysimeters. This type of microlysimeter requires that the capping be repeated on additional microlysimeters at approximately two-week intervals (Walker 1983). For the study period from August 5th to September 9th a second capping occurred on a group of microlysimeters on August 20th. This set of microlysimeters, aluminum sleeves of soil within the retaining walls PVC, were previously unbroken and had been allowed unrestricted hydraulic contact at the 30 cm depth. On August 20th, the aluminum contained soil was broken at 30 cm, capped with plastic, weighed and returned to the pit contained by the PVC cylinder. The weighing on August 21st represented the first recorded change in soil moisture within the second set of capped microlysimeters.

The second type of microlysimeter was constructed to allow hydraulic contact at the base of the microlysimeter. After the aluminum cylinder containing the control volume of soil was initially excavated and removed from the microlysimeter pit, cotton fabric was stretched across the bottom of the microlysimeter and affixed to the lower perimeter of the aluminum sleeve. A supply of ground and sieved soil from the 30 cm depth was applied to both the lower boundary of the soil core in the microlysimeter and the soil at the bottom of the pit, ensuring better hydraulic contact across the cotton sheet. This potentially allowed for 'natural' movement of soil water through the lower

boundary, and thus an improved representation of evaporation and drainage. It also necessitated that the moisture flow at the bottom of the lower boundary of the contacting microlysimeter must be quantified in order to determine evaporation. This could be accomplished with the evaluation of the gravimetric sampling, twin probe data, and a comparison between the contacting and traditional microlysimeters.

The final type of microlysimeter was installed and left undisturbed and uncapped for the entire season. They were used as a control set and were cored and excavated at the end of the monitoring regime. The moisture content and bulk density of these microlysimeters were compared to both the plastic capped and cotton-capped microlysimeters. There were five nested sites, or repetitions, (Figure 3.1), each of four types of microlysimeters; hydraulically contacting, barrier-capped (first capping and second capping) and undisturbed. There was a slight slope (approximately 1% north to south) from Site 1 down to Site 3 and a greater slope (approximately 2% east to west) from Site 5 down to Site 4.

For all the microlysimeters, a post season laboratory drying of the soil within the aluminum sleeve allowed for a calculation of the daily absolute moisture content, not just the daily gain or loss of soil moisture.

It was suspected that the field installation of the microlysimeters might introduce some compaction of the soil contained in the microlysimeter. The bulk density of the soil within microlysimeters was evaluated by sectioning (in 5 cm increments) the microlysimeters at the end of the monitoring season, and compared to the bulk densities of the undisturbed cores taken on June 10th. The soil texture was also determined for the depths within the sectioned microlysimeters.

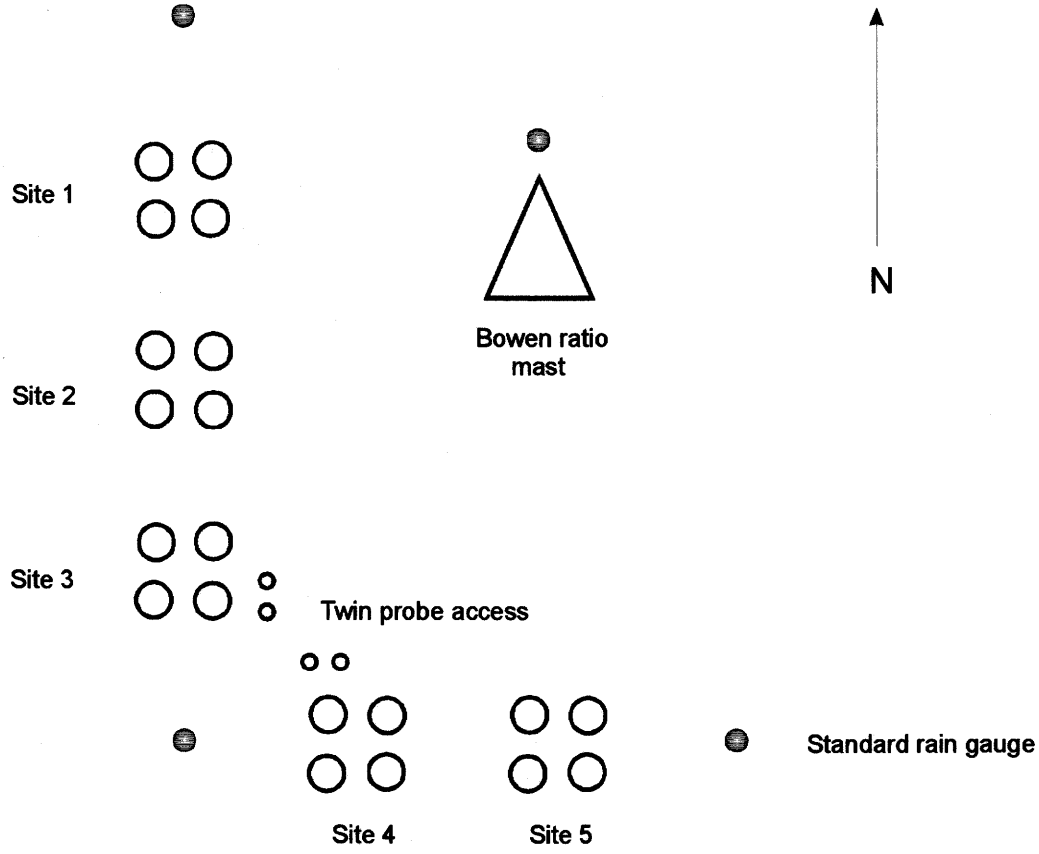

Figure 3.1 Field installation of the four types of microlysimeters within five sites (or repetitions), rain gauges, twin gamma probes and meteorological mast (Bowen ratio mast).

3.2.4 The Measurement of the Energy Budget and Aerodynamic Parameters

Several types of instruments were used to monitor the components of the energy budget and aerodynamic factors. The instruments, their resolution and accuracy, and the parameters measured are summarized in Table 3.5. All instruments were connected to a Campbell Scientific, Inc. (CSI) CR10 datalogger and all output data were recorded every 5 seconds, stored, and computed to yield 10 minute averages.

Table 3.5 Field instrumentation for the determination of the components of the energy balance and aerodynamic equations.

Parameter	Sensor	Manufacturer	Height or Depth (m)	Comments
Net radiation	Net pyrradiometer	Middleton	1.2	Calibration according to manufacturer
Soil heat flux	Heat flow transducer	Radiation and Energy Balance Systems	two at 0.05 depth	Calibration according to manufacturer
Sensible heat flux	Fenwal Electronics thermistor (model HMP35C)	Campbell Scientific	2.0 0.52 0.12	0.4 °C accuracy from -33 °C to +48 °C
Latent heat flux	Vaisala capacitive relative humidity sensor (model HMP35C)	Campbell Scientific	2.0 0.52 0.12	1% RH accuracy
Windspeed	Micro-response cup anemometer (model 2031)	Weather measure Weathertronics	2.0 0.32	0.23 m s^{-1} stall speed

Net radiation was measured using a Middleton net pyrradiometer mounted at 1.2 m above and parallel to the ground surface with the head of the instrument facing south. This direction of installation is recommended in the northern hemisphere. The receiving surface of a net pyrradiometer is a blackened, dual faced, thermal detector using multiple thermocouples in series (a thermopile). One set of junctions from the thermopile is in contact with the upper face while a second set of junctions is attached to a lower face. When the plate is parallel to the soil surface, the thermopile voltage output is proportional to the difference between incoming and outgoing radiative fluxes at all

wavelengths. The voltage output of the pyrradiometer is converted into an energy flux using the manufacturer's calibration (Table A.1, Appendix A). The manufacturer states two calibrations, one for use in converting voltage to longwave radiation and the other for calibrating voltage to shortwave radiation. The average of the short wave and long wave calibrations was used for positive voltage situations (daytime) and the long wave calibration was used for negative voltages (nighttime conditions). To simplify the programming for data collection, the datalogger was instructed to give output in voltages and the calibrations were applied to a spreadsheet of the output data to obtain net radiative flux in W m^{-2}.

Soil heat flux was measured using Radiation Energy Balance Systems heat flow transducers. A heat flow transducer consists of a thermopile encapsulated in a flat black disk of high thermal conductivity epoxy. The epoxy prevents ground potential pickup and the voltage output from the instrument is proportional to the heat flux into the soil using a linear calibration. Two heat flux plates were positioned horizontally at a 5 cm depth, parallel to the soil surface. Installation was performed to ensure good thermal contact between the soil and the upper and lower faces of the transducer. Programming instructions for the CR10 used the manufacturer's calibration coefficients (Table A.1, Appendix A) and gave output data directly as heat flux in W m^{-2}.

A Campbell Scientific model HMP35C temperature and humidity probe was used to obtain measures of sensible and latent heat flux. The probe consists of a Vaisala capacitive relative humidity sensor and Fenwal Electronics thermistor, both contained in a radiation shield. These dual sensor units were employed at heights of 0.12 m, 0.52 m and 2 m to obtain temperature and humidity profiles. The 2 m height was monitored by

a stationary HMP35C probe. The 0.12 m and 0.52 m heights were monitored with another probe installed at the end of a 0.2 m arm that oscillated between these two elevations from a pole parallel to the soil surface at a nominal height of 0.32 m (Figure 3.2).

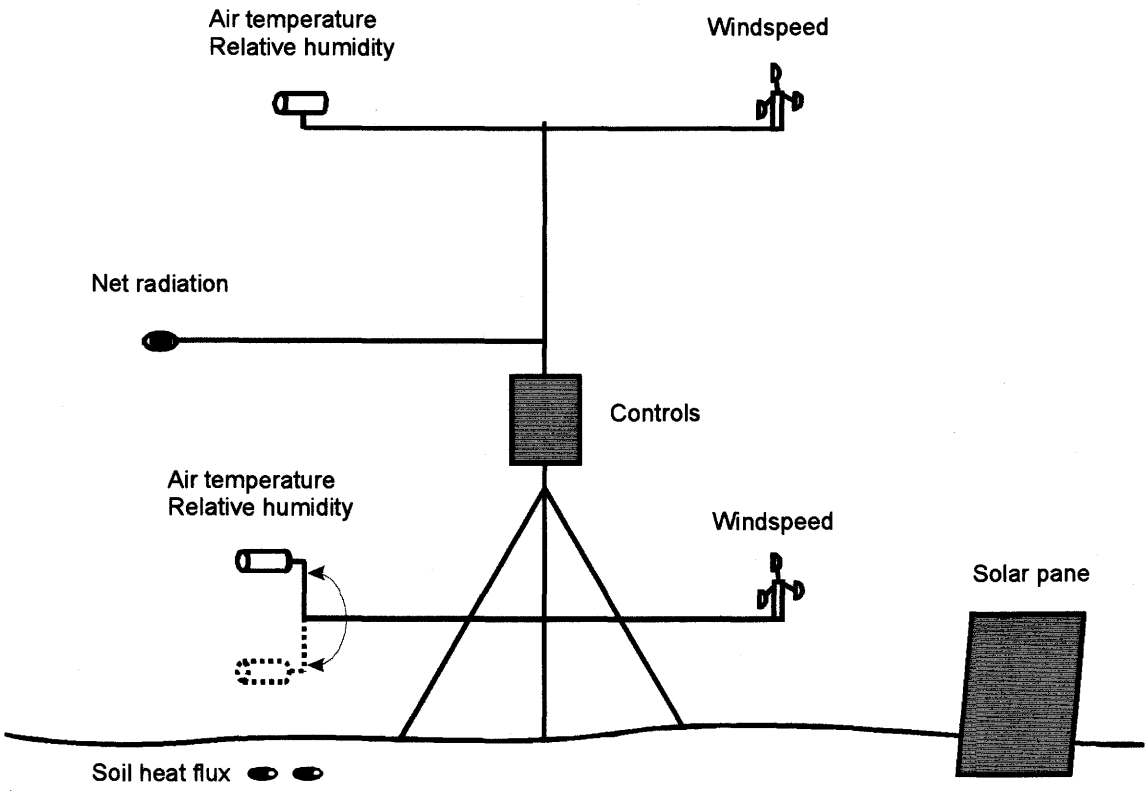

Figure 3.2 The Bowen ratio mast and instrumentation for the determination of the components of the energy balance and aerodynamic equations.

With this oscillating probe the temperature and relative humidity were monitored every 5 s for 5 min at one elevation after which a drive motor was activated by the datalogger causing the probe to swing to the alternate elevation for the next five minutes. The five-second readings were averaged over each of the five-minute intervals. Thus for

any ten minute interval there was an average temperature and relative humidity calculated for both the upper (0.52 m) and lower elevation (0.12 m) using data collected from one sensor. This technique assists in lowering the significance of sensor inaccuracies or systematic offsets in instrument calibration (Cellier and Olioso 1993) when measuring small gradients of temperature and relative humidity. Programming instructions at the datalogger converted the measured voltages, using the manufacturer's calibrations, to an output of temperature in °C and % RH.

Wind profiles were measured using Weathertronics micro-response cup anemometers at heights of 2 m and at 0.32 m. These anemometers had a stall speed of 0.23 m s^{-1}. The CR10 was programmed to convert the output frequency of these rotating cups to windspeed in m s^{-1}, using the manufacturer's calibration conversion.

Monitoring equipment measuring atmospheric parameters were supported by a Campbell Scientific Bowen ratio mast system. All instruments were provided by the Division of Hydrology.

3.3 Analytical Methods

3.3.1 The Water Balance and Evaporation

The soil water budget equation defines that for any volume of soil the change in soil moisture storage is equal to the precipitation input less the evaporation combined with losses and gains due to surface runoff and run on and flow between the root zone and groundwater (Equation 3.1). In semi-arid environments, the practical evaluation of the water balance usually assumes that surface inflow (run on) and outflow (runoff) and

fluxes between root zone and groundwater stores are negligible. The evaporation term can then be calculated from precipitation and the change in soil moisture storage.

The water budget was evaluated with the use of the daily differential weighing of the microlysimeters and Equation 3.1 was restated as:

$$E = P - dS \qquad [3.3]$$

where:

E = daily evaporative loss (mm d^{-1}),
P = daily precipitation received (mm d^{-1}), and
dS = daily mass change of the microlysimeters (converted to mm of water).

The major drawback of this method is that evaporation is determined as a residual term and errors associated with the measurement of the other terms or assumptions about their values accumulate in the estimate of evaporation. It is therefore desirable to employ an independent means of estimating evaporation.

3.2.2 The Energy Budget and Aerodynamic Considerations in Evaporation

Various energy budget equations and aerodynamic expressions were used to evaluate evaporation, namely the Bowen ratio method, the Penman-Monteith equation, and the G-D approach.

The Bowen Ratio Method

Energy received at the earth's surface may be used to heat the air (sensible heat), heat the soil (ground heat) or evaporate water (latent heat). Solving the surface energy balance requires the determination of the sensible, latent and ground heat fluxes. Ground heat flux is an easily measured; however, the determination of turbulent (latent and sensible heat) fluxes is more difficult. This can be accomplished by employing the

Bowen Ratio Energy Balance (BREB). The Bowen ratio is the ratio of the sensible heat to latent flux and can be written (for full development see Appendix E.1):

$$B = \gamma \frac{\partial T}{\partial e} \qquad [3.4]$$

where:

B = Bowen ratio (dimensionless),
γ = psychrometric constant (kPa °C^{-1}),
∂T = difference in air temperature (°C) between two levels, and
∂e = difference in vapor pressure (kPa) between the same two levels.

Substituting the Bowen ratio into the surface energy equation (Equation 3.4) yields the following expression for the latent heat flux:

$$Q_e = \frac{Q_n - Q_g}{1 + B} \qquad [3.5]$$

where:

Qe = latent flux (W m^{-2}),
Q_n = net radiation (W m^{-2}), and
Q_g = ground heat flux (W m^{-2}).

The advantage of the reformulation of the energy equation in terms of the Bowen ratio is that evaporation can be estimated independent of windspeed. The Bowen ratio can be calculated from the gradients of temperature and vapour (Equation 3.4). Equations 3.4 and 3.5 indicate that the required inputs for the estimation of evaporation are a measurement of net radiative flux, soil heat flux in addition to the temperature and relative humidity measurements (to calculate vapour pressure) at two elevations.

There are problems that arise with the Bowen ratio estimation in practice. The first is the possibility of obtaining the wrong signs for the turbulent fluxes. Calculations involving the Bowen ratio may yield a flux direction the same as that of the gradient,

inconsistent with the definition of the flux/gradient relationship. The second problem with the Bowen ratio method is the estimation of latent flux when the ratio approaches a value close to -1. At these times any small measurement error may cause an unrealistic estimate of the sensible and latent heat fluxes. Instrument resolution therefore can be considered significant when employing the BREB method and equations [3.4] and [3.5] cannot be employed successfully as the Bowen ratio nears -1. Ohmura (1982) defined criteria for rejecting Bowen ratio values that take into account the resolution limits of the temperature and humidity sensors (Table 3.5) and for those cases when the flux and gradient are in the same direction. These criteria reduce to the following expression for the BREB system employed:

Accept data (gradient and flux in opposing directions) only if:

when $Q_n - Q_g > 0$

$$T_1 - T_2 > -(15.975 \times (e_1 - e_2)) \quad [3.6]$$

or when $Q_n - Q_g < 0$

$$T_1 - T_2 < -(15.975 \times (e_1 - e_2)) \quad [3.7]$$

and reject data (due to possible instrument error when the Bowen ratio equals or approaches -1) when:

$$(-15.37) \times (e_2 - e_1) - 0.809 < T_2 - T_1 < (-15.37) \times (e_2 - e_1) + 0.809 \quad [3.8]$$

where:

T_1, T_2 = air temperatures at levels 1 and 2 (°C),
e_1, e_2 = vapour pressures at levels 1 and 2 (kPa),
Q_n = net radiation (W m^{-2}), and

Q_g = soil heat flux (W m^{-2}).

At those times when the Bowen ratio data were considered unsuitable the evaporation was estimated by interpolating values on either side of the period of rejection.

The accurate estimation of evaporation using the Bowen ratio and the energy balance methods often employs a correction of the measured soil heat flux term. In practice, soil heat flux is not measured at the earth's surface, but within the soil matrix. The damping of the soil heat flux is due primarily to the increased storage of heat and reduced gradients that occur with depth. Accurate assessment of soil heat flux is often accomplished by using heat flux plates and a calorimetric method, necessitating a soil temperature measurement, to determine the true ground heat flux at the surface (Tanner 1963, Tanner et al. 1985, Campbell Scientific 1988). However there may be errors associated with this combination method (Tanner et al. 1985, Massman 1992) due to inaccuracies in soil temperature measurement. Recent work by Passerat de Silans et al. (1997) suggested an analytical method that does not rely on soil temperature measurement; however the application of the corrected soil heat flux did not significantly alter their estimation of latent heat flux. For this reason the soil heat flux measurements at 5 cm depth were deemed to represent the surface ground heat flux and used in the determination of evaporation.

The Penman-Monteith Method

Combined energy budget and aerodynamic equations, such as Penman's expression for saturated surfaces, describe the evaporation process as one that can only occur if there is: 1) sufficient energy available for evaporation, and 2) a vapour pressure

gradient away from the surface that ensures the removal of the saturated vapour layer over an evaporating surface, by diffusion or air movement. Work by Penman and others such as Monteith (1965) and Thom (1972), modified the Penman equation in an attempt to quantify evaporation when a supply of water was not freely available. This work utilizes resistance terms to evaluate evaporation for vegetative and non-saturated surfaces. Evaporative flux may be calculated using the Penman-Monteith equation (Appendix E.2):

$$Q_e = \frac{\Delta (Q_n - Q_g) + \rho_a C_p \dfrac{(e^*_a - e_a)}{r_a}}{\Delta + \gamma (1 + \dfrac{r_s}{r_a})} \qquad [3.9]$$

where:

Q_e = latent heat flux (W m^{-2}),
Q_n = net radiative flux (W m^{-2}),
Q_g = ground heat flux (W m^{-2}),
ρ_a = density of moist air (kg m^{-3}),
C_p = the specific heat of air at constant pressure (equal to 1013 J kg^{-1} $°C^{-1}$),
e^*_a = saturated vapour pressure evaluated the air temperature (kPa),
e_a = air vapor pressure (kPa),
γ = psychrometric constant (kPa $°C^{-1}$),
Δ = slope of saturated vapour pressure vs air temperature curve (kPa $°C^{-1}$),
r_a = aerodynamic resistance to vapour transfer by turbulence (s m^{-1}), and
r_s = the surface or soil resistance to vapour flow (s m^{-1}).

The saturated vapour pressure (e^*) is temperature dependent and, when utilizing the Penman-Monteith estimation, is evaluated at the ambient air temperature (T_a).

For temperatures equal or greater than 0 °C:

$$e^*_a = 0.611 \, exp\left(\frac{17.27 \, T_a}{T_a + 237.3} \right) \qquad [3.10]$$

and for temperatures below 0 °C:

$$e^{*}_{a} = 0.611 \exp\left(\frac{21.88\, T_a}{T_a + 265.5}\right) \qquad [3.11]$$

where T_a is in °C and e^{*}_{a} is in kPa.

The vapour pressure (e_a) is a function of the relative humidity.

The slope of the saturated vapour pressure vs. temperature curve (Δ, kPa °C $^{-1}$) may be evaluated at the ambient air temperature (T_a, °C).

For temperatures equal or greater than 0° C:

$$\Delta = \frac{4098.17\, e^{*}_{a}}{(T_a + 237.3)^2} \qquad [3.12]$$

while for temperatures less than 0° C:

$$\Delta = \frac{5809.14\, e^{*}_{a}}{(T_a + 265.5)^2} \qquad [3.13]$$

The density of moist air (ρ_a, kg m^{-3}) can be evaluated from:

$$\rho_a = 10000 \frac{P_a}{R\,(273.15 + T_a)}\left[1 - 0.379\left(\frac{e_a}{P_a}\right)\right] \qquad [3.14]$$

where:

P_a = atmospheric air pressure (equal to 95.395 kPa at 511.8 m ASL),
e_a = air vapor pressure (kPa),
R = universal gas constant (2.87 x 10^3), and
T_a = ambient air temperature (°C).

The psychrometric constant (γ, kPa °C^{-1}) has a dependancy on atmospheric air pressure (P_a) and the latent heat of vaporization (h_v):

$$\gamma = 1.63\frac{P_a}{h_v} \qquad [3.15]$$

where:

h_v = latent heat of vaporization (kJ kg^{-1}).

The latent heat of vaporization has a slight temperature dependency and:

$$h_v = 2501 - 2.361\,T_a \qquad [3.16]$$

with h_v in kJ kg^{-1} and T_a measured in °C

The aerodynamic resistance (r_a, s m^{-1}) describes the role of windspeed and the logarithmic wind profile on vapour transfer and can be defined as:

$$r_a = \frac{\left(ln\,\frac{(z - d_o)}{z_o}\right)^2}{k^2\,u_z} \qquad [3.17]$$

where:

z = height (m) of measurement of wind speed, u_z,
u_z = windspeed (m sec^{-1}),
d_o = zero plane displacement height (m) for surface roughness ($d_o = 0.67\,h$),
z_o = aerodynamic roughness height (m) ($z_o = 0.13\,h$),
h = crop or roughness height (m), and
k = 0.41, the von Karman constant.

The surface (stomatal or soil) resistance to vapour transfer defines the availability of the supply of water to the demand of an evaporative flux. For unvegetated wet surfaces r_s = 0; for non-saturated surfaces the term is difficult to evaluate because its magnitude is affected by complex interactions between climatological, soil and vegetative factors. In this study (involving a bare fallow field) an expression was found to estimate the surface resistance (r_s) that was a function of soil parameters alone (van de Griend and Owe 1994):

$$r_s = 10\, e^{0.3563\,(\,19\,-\,\theta\,)} \qquad [3.18]$$

where:

r_s = surface resistance (s m^{-1}),

θ = measured volumetric moisture (%) of the 0 to 1.0 cm layer of soil.

This model predicts a small resistance at saturation, increasing to a value 1467 s m^{-1} when the soil is very dry. For use within this project, the soil moisture of the top 2 cm of soil was substituted for the θ variable.

The input parameters for evaporative estimation using the Penman equation are measurements of net radiative flux, air temperature, relative humidity, windspeed at a known height, and a measurement of ground heat flux. The evaluation of aerodynamic resistance further requires a knowledge of roughness height (the roughness or ridge height was taken to be 2.5 cm), while the surface resistance of the soil is inferred from the soil moisture content and Equation 3.18.

The G-D Method

Granger and Gray (1989) studied 158 evaporation periods in the semi-arid environment of western Canada. They defined evaporation during these periods as:

$$E = \frac{\Delta G Q}{(\Delta G + \gamma)} + \frac{\gamma G E_a}{(\Delta G + \gamma)} \quad [3.19]$$

where:

- E = evaporation flux (mm d^{-1}),
- Δ = slope of the saturation vapor pressure curve at given air temperature (kPa $°C^{-1}$),
- G = relative evaporation (the ratio of actual to potential evaporation),
- Q = daily total net energy available for evaporation (Q_n - Q_n) expressed as an equivalent depth of water (mm d^{-1}),
- E_a = drying power of the air (mm d^{-1}), and
- γ = psychrometric constant (kPa $°C^{-1}$).

The relative evaporation, G, is determined by the expression (Granger 1991):

$$G = \frac{1}{0.793 + exp^{4.902\,D}} + 0.006\,D \quad [3.20]$$

where D is the relative drying power (mm d^{-1}), determined by:

$$D = \frac{E_a}{E_a + Q} \quad [3.21]$$

while the drying power of the air, E_a (mm d^{-1}), is given by:

$$E_a = f(u)\,(e^*_a - e_a) \quad [3.22]$$

where:

- $f(u)$ = wind function (mm d^{-1} kPa^{-1}),
- e^*_a = saturation vapor pressure at the daily average air temperature (kPa), and
- e_a = atmospheric vapor pressure (kPa).

The wind function for a fallow land surface is:

$$f(u) = 7.50 + 1.3\, u_2 \qquad [3.23]$$

where:

u_2 = average daily horizontal winds speed (m s^{-1}) measured at 2 m.

The G-D method requires the calculation of the wind function (*f(u)*) the drying power of the air (E_a) the relative drying power (D) the relative evaporation (G) to determine the daily values of evapotranspiration. The inputs required are net radiation, air temperature, humidity and windspeed measured at a 2 m height and a measurement of ground heat flux.

Recent work with the G-D method has proven its validity for the estimations of evapotranspiration within forested environments (Elliott et al. 1998). This work also developed the use of the G-D method within a hydrological model that calculated the water balance on an hourly basis (Pomeroy et al. 1997). The application of the G-D estimation of evaporation for periods of time shorter than one day required that the wind function be examined and that special consideration be given to periods of time when net radiation is negative.

The wind function, *f(u)*, was reformulated to represent a dynamic wind profile. An appropriate expression of the wind function for short time periods (in the order of one hour) is:

$$f(u) = \frac{0.622\, k^2\, \rho_a\, u_z}{P_a \left[ln\left(\frac{z - d_o}{z_o} \right) \right]^2} \qquad [3.24]$$

where:

$f(u)$ = wind function (mm h^{-1} kPa^{-1}),
k = 0.41, the von Karman constant,
ρ_a = density of moist air (kg m^{-3}),
u_z = windspeed (m s^{-1}),
z = height at which windspeed is measured (m),
P_a = atmospheric air pressure (equal to 95.395 kPa at 511.8 m ASL kPa),
d_o = zero plane displacement height (m) for surface roughness ($d_o = 0.67\ h$),
z_o = aerodynamic roughness height (m) ($z_o = 0.13\ h$), and
h = crop or roughness height (m).

with the remainder of the energy flux terms (E, Q, D and E_a) expressed in the proper measurements of vapour flux (mm h^{-1}).

Consideration was given to periods when the net radiation available for evaporation (i.e., Q_n - Q_g) is negative. In the development of Granger's method, it is assumed that the available energy remains positive (a reasonable assumption for daylight hours in summer). For those periods when the net available energy is negative, the relationship between G and D no longer holds. In such cases, the G-D estimate was set to zero.

4.0 RESULTS AND DISCUSSION

4.1 Precipitation

Precipitation data was collected with a TBRG system 150 meters from the site, with standard rain gauges on site and Appendix B outlines the occurrence of rainfall for the observation period. Consistent with the measurement regime of the project, daily rainfall was measured from noon to noon each day. A rainfall event was deemed to have been completed once a subsequent noon to noon period passed without the occurrence of precipitation.

A total of 59.9 mm of precipitation was received between August 5 and September 9, 1994. This depth was higher than the normal for August (39.6 mm). An examination of the frequency distribution of the daily rainfall amounts (Table 4.1) shows that, for the lower daily rainfall amounts (i.e., up to 10 mm), the observation period experienced precipitation amounts proportional to seasonal norms. For those depth intervals above 10 mm, daily rainfall depths from 10 mm to 20 mm contributed 46% of the total rainfall depth received during the observation period. There were no daily rainfall amounts exceeding 20 mm during August of 1994.

Table 4.1 The distribution of the daily rainfall amounts by depth interval for the observation period and the normals averaged from 1922 to 1990.*

	Depth Interval (mm)					Total
	< 5	5 - 10	10 - 20	20 - 35	35 - 60	(mm)
August 1994 rainfall depths	17.5 (29%)	15.0 (25%)	27.4 (46%)	0 (0%)	0 (0%)	59.9
August normal rainfall depths	10.1 (26%)	10 (26%)	11.2 (29%)	5.3 (14%)	2.3 (6%)	38.9
August 1994 number of days in interval	10	2	2	0	0	

*the percentage contribution of the depth interval to the total monthly precipitation is in parenthesis.

The precipitation for the observation period (August 5 to September 9, 1994) fell during 14 days and in eight events. Five of these events were followed by two to six day drying periods (Figure 4.1) providing an opportunity to monitor a drying regime. The other three of these events were followed by a period of at least a day with no rainfall, allowing measurement of the soil moisture losses 24 hours following the cessation of a rainfall event.

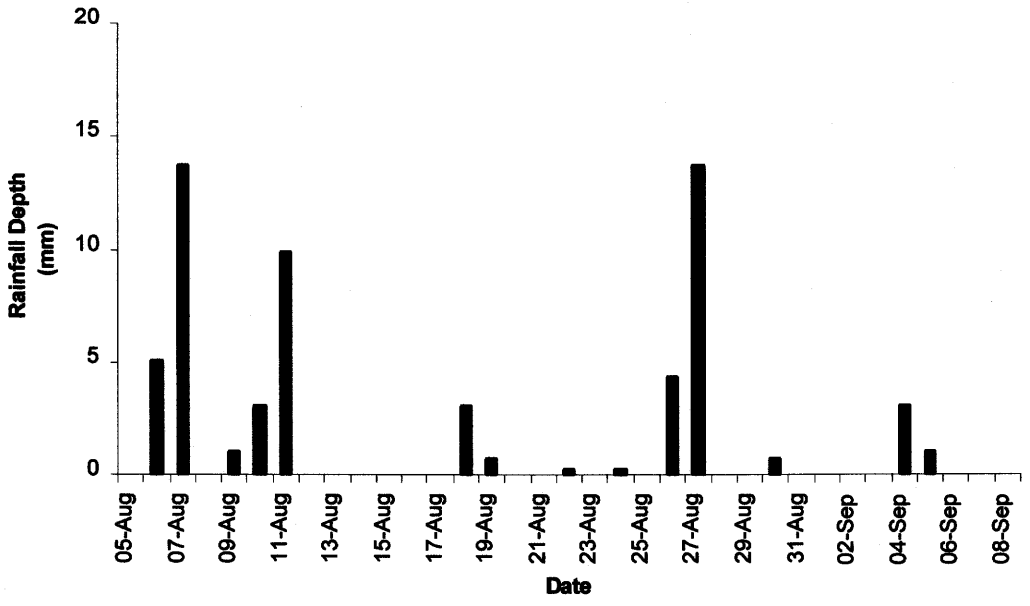

Figure 4.1 Daily precipitation 150 m from the site for August 5 to September 9, 1994.

4.2 Soil Properties

Soil moisture retention curve, the soil texture, and the bulk density of the soil within the microlysimeters and for the surrounding field were investigated.

The soil moisture retention curve (SMRC) was evaluated using undisturbed soil cores (three replicates) obtained from the surrounding field at depth intervals to 30 cm. The SMRC is shown in Appendix C. For the top 10 cm of soil, the mass moisture contents for field capacity and permanent wilting points were 32% and 19%, respectively, with standard deviations ranging from less than 1% to 2%.

The soil textural analysis was completed at depth intervals to 30 cm for both the field (replicated undisturbed cores above) and the installed microlysimeters. The textural classification for the top 10 cm of the soil profile is an average 44% clay, 11% sand and 45% silt. The standard deviations for the textures of the samples at all depth intervals ranged from less than 1% to 3.4%. The variation in texture with increasing depth showed an increase in clay content to 51% at the 30 cm depth, primarily at the expense of the sand fraction. In general the textural class of the soil was a silty clay. The soil texture within the microlysimeters was representative of field conditions at all depths. An illustration of the variation of soil texture with depth and the similarity between the soil textures found in the microlysimeters and the adjoining field is presented in Appendix C.

After the installation of the microlysimeter, the soil surface within the aluminum sleeve was lower than the soil surface of the surrounding field. It was suspected that the

installation of the microlysimeters had introduced some compaction of the soil within the microlysimeter. For each type of microlysimeter, barrier-capped, cotton-capped, and the unbroken or control, there were five field-operational microlysimeters (replicates). In the post monitoring period, all microlysimeters were excavated and sliced into layers to discover the distribution of bulk density with depth (Figure 4.2). The microlysimeters showed similar bulk densities, 1060 and 1029 kg m^{-3} ($\pm$ 20 and 70 kg m^{-3}) for the cotton and barrier-capped respectively in the top 5 cm; while at the 25 to 30 cm depth, bulk densities were 1275 and 1330 kg m^{-3} ($\pm$ 119 and 68 kg m^{-3}) for the cotton and barrier-capped respectively (Table C.3). The bulk density distribution of the unbroken or control microlysimeters varied from the capped microlysimeters, primarily in the top 5 cm, where the average bulk density of the five control or unbroken microlysimeters was 940 kg m^{-3} ($\pm$ 111 kg m^{-3}). However it should be noted that the unbroken microlysimeter bulk density values in the top 5 cm showed significant variability and are within one standard deviation of the values determined for the capped microlysimeters.

The difference in surface bulk density between the two types of microlysimeters could be attributed to the way in which they were used in the field. The capped microlysimeters were removed from the soil profile, weighed, and replaced each day while the unbroken or control microlysimeters remained stationary throughout the season. The extra handling of the capped microlysimeters may have caused some settling of the soil within the microlysimeter which would be most noticeable in the looser surface layers.

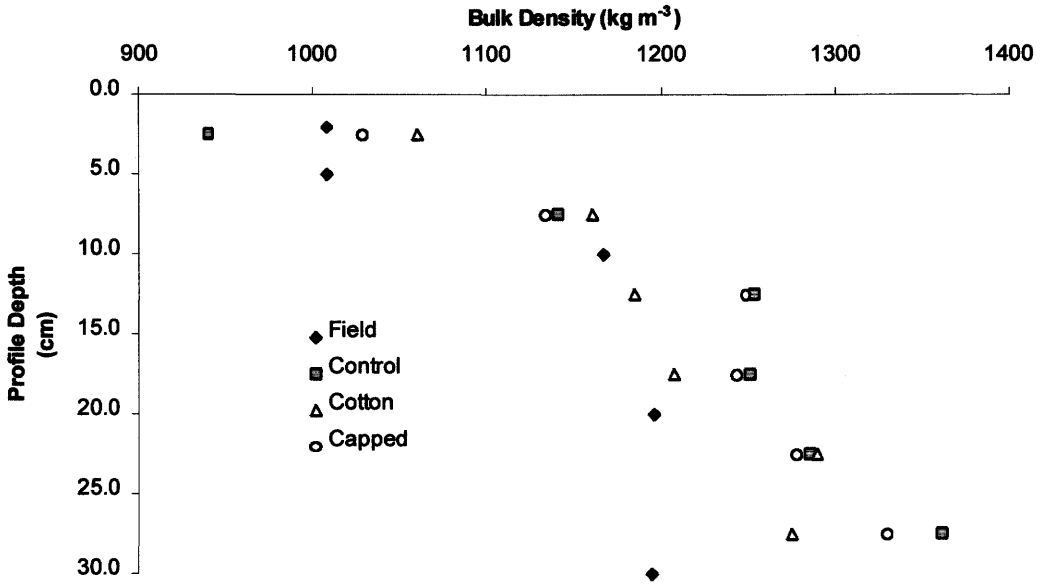

Figure 4.2 Variation of soil bulk density with depth, comparing the microlysimeters (three treatments – control, cotton and capped) with undisturbed cores representing field conditions. The field condition data represent an average of three sampling replicates, while the microlysimeter data is an average of the five sites.

The field bulk density was assessed using the same undisturbed cores taken for the determination of the SMRC. Bulk density increased with depth, varying from 1008 kg m^{-3} (± 45 kg m^{-3}) in the top 3.5 cm to 1196 kg m^{-3} (± 25 kg m^{-3}) in the 27.5 to 32.5 cm layer.

Figure 4.2 indicates that, when compared to field conditions, slight compaction within the microlysimeters did occur, primarily in the depth intervals below 10 cm. A comparison of the bulk densities of both the microlysimeters and the undisturbed soil cores taken from the field can be found in Appendix C. For all depths the range of values within one standard deviation of the average microlysimeter bulk densities overlap

the range of values encompassing one standard deviation of the undisturbed core bulk densities.

4.3 Evaporation Estimates from the Water Balance Method

Measurements taken to evaluate evaporation from the water balance included precipitation monitoring, microlysimetric weighing, twin gamma probe readings and gravimetric sampling (see Table 3.4). The gravimetric soil moisture data obtained from daily coring with the Oakfield corer yielded variable results attributed to spatial variability in soil properties and were not utilized. The twin gamma probe measurements were not used in the water balance, but were useful in the assessment of evaporation in the Penman-Monteith method (Section 4.4.3). The evaporation estimates using the water balance were derived from precipitation measurements and the daily weighing of the microlysimeters.

4.3.1 Evaluation of the Site Locations and Types of Microlysimeters

There were five sites established around the two sets of twin probe access tubes, each site consisting of four differently completed microlysimeters. Each site contained an unbroken or control microlysimeter, a cotton-capped microlysimeter and two barrier-capped microlysimeters, arranged randomly within the site. From August 5th to August 20th the daily weighing of two microlysimeters, a cotton-capped and one of the barrier-capped microlysimeters, within each site was performed. On August 20th the second barrier-capped microlysimeters, previously unbroken at the lower boundary, were removed from the soil pit, completed with a plastic barrier at the lower end. Mass measurements were then taken on three of the microlysimeters at each site until

September 9th. Appendix D (Tables D.1 - D.3) contains the raw data from the weighing of the microlysimeters.

Site Locations

For each type of microlysimeter, the five sites yielded significantly different (two factor analysis of variance without replication, $\alpha = 0.05$) moisture contents (Appendix D, Tables D.4 - D.6). Figure 4.3 portrays the variability in moisture content (average of cotton, first barrier and second barrier capping) between sites. The difference in moisture content between sites reflects the variability of the moisture regime of the field due primarily to the slope position. Sites 3 and 4 at the lower positions on the slope exhibit a higher soil moisture content than sites 1 and 5 at higher elevations.

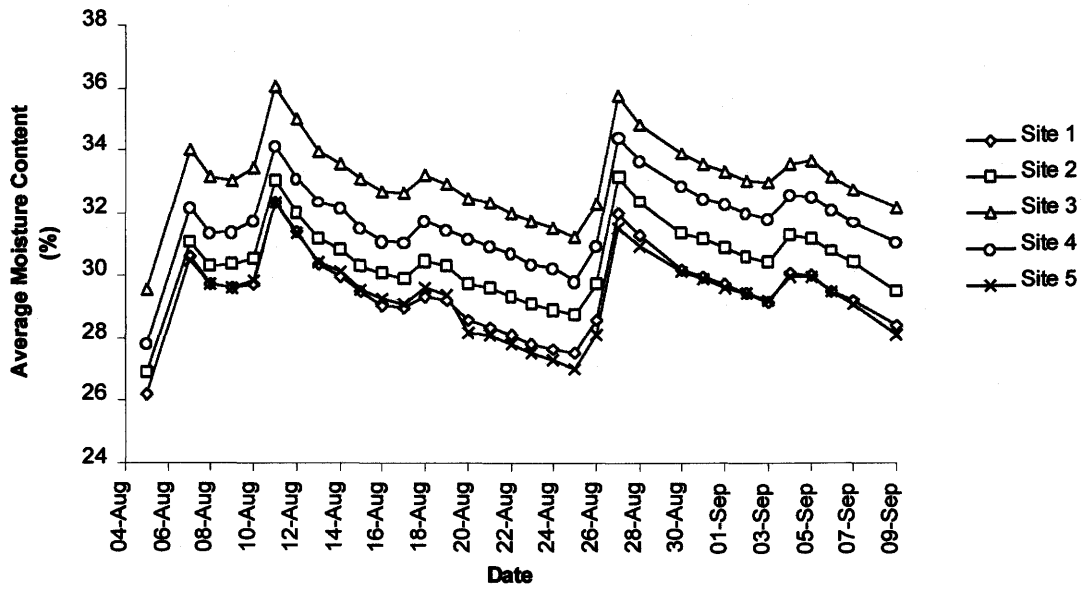

Figure 4.3 The average moisture content for each site of microlysimeters over the observation period. Note that August 20th represents the first weighing of the second set of barrier-capped microlysimeters.

Figure 4.3 illustrates that the response of the sets of microlysimeters within each site to precipitation input or evaporative demand was very similar, despite moisture content variation. Appendix D, Tables D.7 – D.9, presents the daily mass change (converted to mm of soil water) of the microlysimeters for each of the sites, performs a two factor analysis of variance without replication ($\alpha = 0.05$), and demonstrates that there were no significant difference in microlysimeter response. So while there was significant between-site variability in moisture content, the response by each site to evaporation or precipitation, as judged by the soil moisture change, was not significantly different.

Microlysimeter Types

The purpose of installing five sites of microlysimeters was to monitor the areal response of the soil profile to precipitation and evaporation while replicating the different types of capping mechanisms. To determine the statistical significance of the responses of the different types of microlysimeters, the five sites were considered as five replicates of each of the three operational types of microlysimeters: cotton-capped, the first set of barrier-capped and the second set of barrier-capped. The responses of the microlysimeters to precipitation and evaporation were judged to be represented by the change in soil water of the microlysimeters. The average soil water changes of the five replicates was compared for the three types of microlysimeters. At the 5% level, the daily response (mm of water) of the cotton-capped microlysimeters was similar to the barrier-capped microlysimeters (Appendix D, Table D.10).

However, the mass moisture contents of the different types of microlysimeters experienced drift according to capping mechanism over the entire observation period as shown in Figure 4.4. Initially, the first barrier-capped microlysimeters showed good agreement with the cotton-capped microlysimeter but subsequently allowed less flux, either evaporative or drainage, and retained more moisture. Upon completion of the second set of barrier-capped microlysimeters, this same phenomena was repeated. Initially the second capped microlysimeters were at the same moisture content as the cotton-capped microlysimeters. However the second capped microlysimeters retained more soil moisture over time (e.g., after the rainfall event on August 26th to 27th).

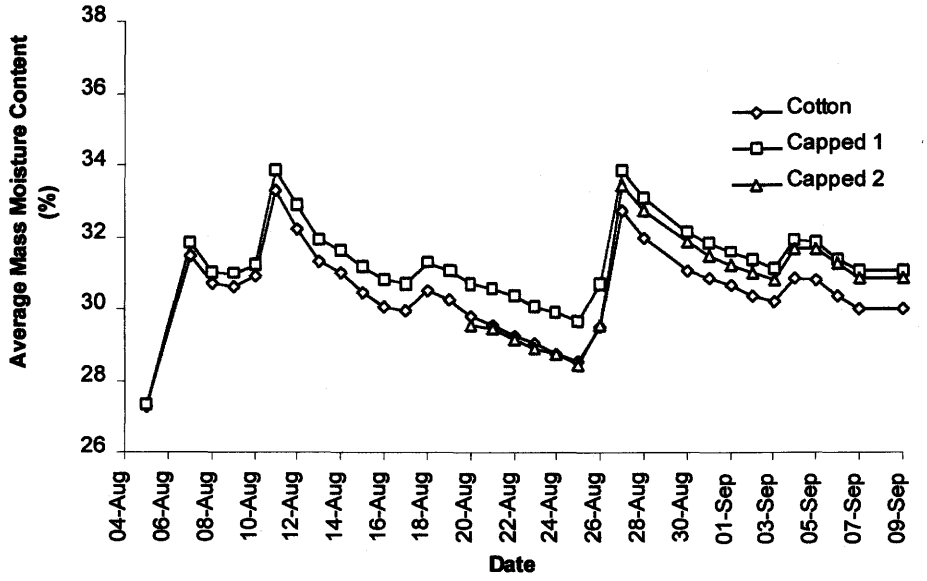

Figure 4.4 Average mass moisture content for each type of microlysimeter over the observation period with the second set of barrier-capped microlysimeters completed on August 20th.

The cumulative change in soil moisture (mm of water) for each type of microlysimeter was significantly different (Appendix D, Tables D.10 a, b, c). For both the entire period and the period from August 5th to 20th, the cumulative soil moisture change for the first set of barrier-capped microlysimeters differed from the cotton-capped microlysimeters. Similarly the cumulative soil moisture change in the second barrier-capped microlysimeters differed significantly from the cotton-capped microlysimeters for the period August 21st to September 9th.

This deviation in microlysimeter response could be attributed to either heightened moisture loss from the cotton-capped microlysimeters in drainage or evaporative flux or a reduction of drainage flux from the barrier-capped microlysimeters. The moisture content of the soil within the cotton-capped microlysimeters matched the moisture content of the second set of microlysimeters at the time of the second capping and was lower than the first set of capped microlysimeters that had not been allowed free drainage. The good agreement between the cotton-capped microlysimeters and the set of barrier-capped microlysimeters that were broken off and capped well into the observation period indicates that the cotton-capped microlysimeters were more representative of field conditions.

4.3.2 Soil Moisture Changes in the Microlyimeters

Soil water changes in the microlysimeters were due to precipitation, evaporation and drainage. During periods of precipitation all microlysimeters should increase in soil water (for precipitation depths exceeding evaporative demand) while the cotton-capped microlysimeters would allow free drainage. During periods of evaporation, all

microlysimeters should give up soil water to evaporation, however any artificial drainage retention by the barrier-capped microlysimeters might then increase subsequent evaporation by increasing the soil moisture content.

The average cumulative change in mm of water (August 5th to August 20th) from the cotton-capped microlysimeters was a gain of 9.6 mm compared to the cumulative gain of 12.6 mm from the first set of barrier-capped microlysimeters (Table 4.2). Thus, from August 5th to 20th, the cotton-capped microlysimeters allowed 3.0 mm more soil water loss, either as drainage or evaporation than the first set of barrier-capped microlysimeters. From August 20th to September 9th the cotton microlysimeters lost 1.8 mm of soil water, the second set of barrier-capped microlysimeters gained 3.0 mm of water, while the first set of barrier-capped microlysimeters lost 0.4 mm of soil. Hence, from August 21st to September 9th the cotton-capped microlysimeters lost an additional 4.8 mm of soil water over the second set of capped microlysimeters. It should also be noted that from August 21st to September 9th the second capped microlysimeters lost 3.4 mm less than the first barrier-capped microlysimeters that were at a higher soil water content on August 20th (Figure 4.4).

Table 4.2 The cumulative changes in soil water for each type of microlysimeter (replicated over five sites) for the periods August 5th to 20th, and August 21st to September 9th.

Cumulative change of soil water (mm), average of five sites						
Date	Cotton	Cap 1	Date	Cotton	Cap 1	Cap 2
5-Aug	0.0	0.0 *	20-Aug	0.0	0.0	0.0 *
7-Aug	16.0	16.6	21-Aug	-1.0	-0.5	-0.4
8-Aug	13.1	13.6	22-Aug	-2.2	-1.4	-1.5
9-Aug	12.7	13.6	23-Aug	-3.0	-2.5	-2.4
10-Aug	13.8	14.4	24-Aug	-4.1	-3.1	-3.1
11-Aug	22.8	24.3	25-Aug	-4.8	-4.0	-4.0
12-Aug	18.7	20.6	26-Aug	-1.2	0.0	0.0
13-Aug	15.4	17.1	27-Aug	11.0	11.6	14.3
14-Aug	14.2	16.0	28-Aug	8.2	8.8	11.5
15-Aug	12.0	14.2	30-Aug	4.7	5.2	8.4
16-Aug	10.6	12.9	31-Aug	4.0	4.2	7.0
17-Aug	10.2	12.5	1-Sep	3.1	3.2	6.1
18-Aug	12.3	14.6	2-Sep	2.0	2.3	5.3
19-Aug	11.2	13.9	3-Sep	1.5	1.5	4.6
20-Aug	9.6	12.6	4-Sep	4.0	4.4	7.7
			5-Sep	3.8	4.4	7.7
			6-Sep	2.1	2.5	6.2
			7-Sep	0.8	1.3	4.7
			9-Sep	-1.8	-0.4	3.0

* denotes the initialization of a set of barrier-capped microlysimeters

To examine the drainage past the 30 cm boundary, an assessment of the soil water retained during a precipitation event within the different types of microlysimeters was completed. During 11 of the 14 days with rainfall the barrier-capped microlysimeters retained more precipitation than the cotton-capped microlysimeters (see Table 4.3). The first set of barrier-capped microlysimeters retained a total of 2.3 mm of additional soil water over that retained by the cotton-capped microlysimeters (August 5th to 20th). Additionally, the second capped microlysimeters retained an excess 2.6 mm of soil water (August 20th to September 9th) above that held by the cotton-capped microlysimeters during the 24-hour periods with precipitation. The excess retention was deemed to be drainage that was not allowed in the barrier-capped microlysimeters; thus the drainage

that occurred in conjunction with precipitation for the cotton-capped microlysimeters was 4.9 mm total over the entire observation period.

Table 4.3 Comparison of soil moisture change (average of five sites, mm of water), with particular emphasis on drainage by the cotton-capped microlysimeters, during rainfall.

Date	**Cotton** Average of five sites (mm)	**Cap 1 or Cap 2**	**Precipitation** rec'd in past 24 hours (mm)	**Capped less cotton** excess retention rainfall (mm)	other
06-Aug			5.1		
07-Aug	16.0	16.6	13.7	0.6	
08-Aug	-2.9	-3.0			-0.2
09-Aug	-0.4	0.0	1.0	0.4	
10-Aug	1.0	0.8	3.0	-0.2	
11-Aug	9.0	9.9	9.9	0.9	
12-Aug	-4.0	-3.7			0.4
13-Aug	-3.3	-3.5			-0.1
14-Aug	-1.2	-1.1			0.1
15-Aug	-2.1	-1.8			0.3
16-Aug	-1.5	-1.3			0.2
17-Aug	-0.4	-0.4			-0.1
18-Aug	2.1	2.1	3.0	0.0	
19-Aug	-1.1	-0.7	0.8	0.4	
20-Aug	-1.6	-1.3			0.2
21-Aug	-1.0	-0.4			0.6
22-Aug	-1.2	-1.1	0.3	0.1	
23-Aug	-0.8	-0.9			-0.1
24-Aug	-1.0	-0.6	0.3	0.4	
25-Aug	-0.8	-1.0			-0.2
26-Aug	3.6	4.0	4.3	0.4	
27-Aug	12.2	14.3	13.7	0.6	
28-Aug	-2.8	-2.7			0.0
29-Aug					
30-Aug	-3.6	-3.2	0.8	0.4	
31-Aug	-0.7	-1.4			-0.6
01-Sep	-0.8	-0.9			0.0
02-Sep	-1.1	-0.8			0.3
03-Sep	-0.5	-0.7			-0.2
04-Sep	2.5	3.2	3.0	0.6	
05-Sep	-0.2	0.0	1.0	0.2	
06-Sep	-1.8	-1.5			0.2
07-Sep	-1.3	-1.5			-0.2
08-Sep					
09-Sep	-2.5	-1.7			0.8
Totals	7.9	15.5	59.9 *	4.9 **	1.5

* blank value is a measured 0.0 mm of precipitation

** includes only positive values

The net change in microlysimeter mass is equal to the precipitation input less drainage and evaporation (Figure 4.5) or evaporation within the microlysimeter is precipitation less the change in mass and drainage component combined. Thus, the total evaporative loss from the soil surface is equal to the measured precipitation less the change in mass of the cotton-capped microlysimeters, corrected for the drainage, and was equal to 47.1 mm (Figure 4.6). The barrier-capped microlysimeters, where mass change represents only evaporation (drainage is prevented), showed a 44.4 mm loss for the entire observation period.

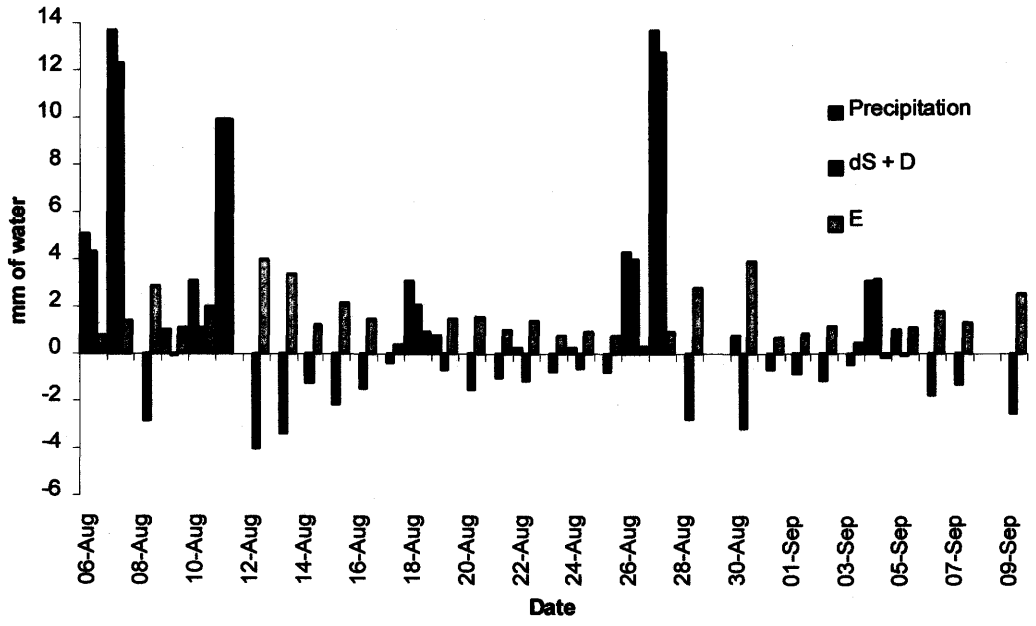

Figure 4.5 Precipitation is equal to the change in storage (dS) in the cotton-capped microlysimeters plus evaporation (E) and drainage (D) from the microlysimeters, thus $E = P - (dS + D)$.

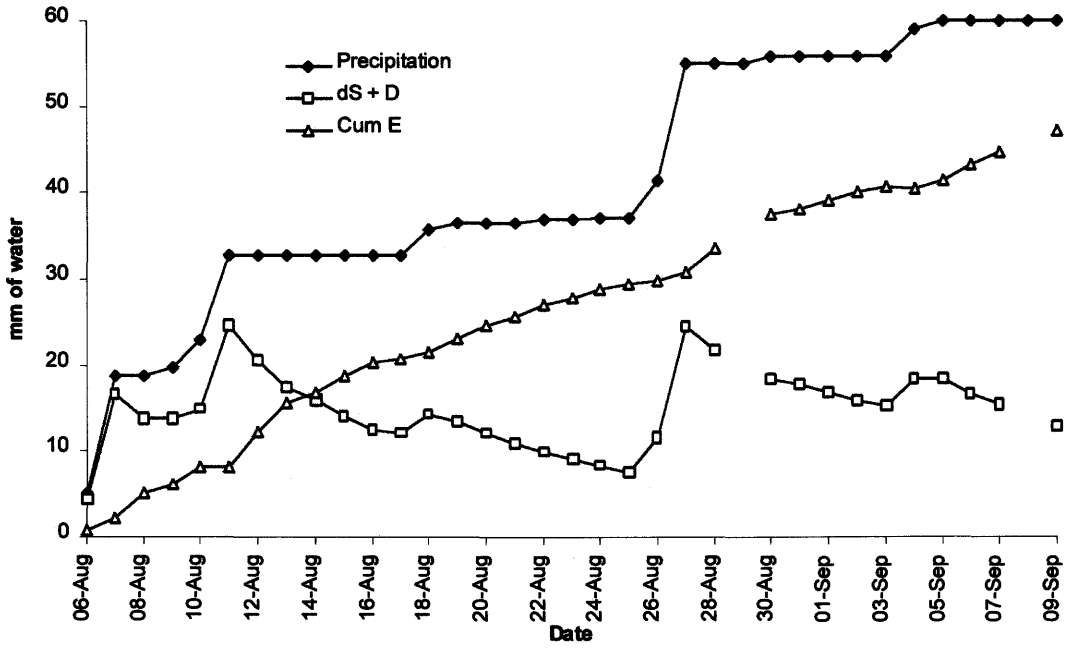

Figure 4.6 Cumulative precipitation (P), water storage (dS), and evaporation (E) for the cotton-capped microlysimeters where E = P - (dS + D).

The impeded drainage characteristics of the barrier-capped microlysimeters resulted in higher moisture after rainfall events exhibited in Figure 4.4. It would have been reasonable to assume that the higher moisture contents might have translated into higher evaporation losses; that once the drainage had been quantified and accounted for, the barrier-capped microlysimeters would be seen to lose more soil moisture than the cotton-capped microlysimeters. This is not supported by the data and the cotton-capped showed slightly higher losses over the entire observation period and for the 24-hour periods following rainfall. (Table 4.4).

Table 4.4 Comparison of change in soil moisture, with particular emphasis on the losses from the microlysimeters for the 24 hours immediately following daily rainfall where E = P - (dS + D).

Date	Cotton, corrected mass change, average of five sites (mm)	Barrier-capped	Precipitation past 24 hours (mm)	Cotton, corrected post rain 24 hour evaporative loss (mm)	Capped
06-Aug			5.1		
07-Aug	16.6	16.6	13.7	1.4	1.6
08-Aug	-2.9	-3.0	0.0	2.9	3.0
09-Aug	0.0	0.0	1.0		
10-Aug	1.0	0.8	3.0	2.0	2.2
11-Aug	9.9	9.9	9.9	0.0	0.0
12-Aug	-4.0	-3.7	0.0	4.0	3.7
13-Aug	-3.3	-3.5	0.0		
14-Aug	-1.2	-1.1	0.0		
15-Aug	-2.1	-1.8	0.0		
16-Aug	-1.5	-1.3	0.0		
17-Aug	-0.4	-0.4	0.0		
18-Aug	2.1	2.1	3.0		
19-Aug	-0.7	-0.7	0.8	1.4	1.4
20-Aug	-1.6	-1.3	0.0	1.6	1.3
21-Aug	-1.0	-0.4	0.0		
22-Aug	-1.1	-1.1	0.3		
23-Aug	-0.8	-0.9	0.0	0.8	0.9
24-Aug	-0.6	-0.6	0.3		
25-Aug	-0.8	-1.0	0.0	0.8	1.0
26-Aug	4.0	4.0	4.3		
27-Aug	12.8	14.3	13.7	0.9	-0.6
28-Aug	-2.8	-2.7	0.0	2.8	2.7
29-Aug			0.0		
30-Aug	-3.2	-3.2	0.8		
31-Aug	-0.7	-1.4	0.0	0.7	1.4
01-Sep	-0.8	-0.9	0.0		
02-Sep	-1.1	-0.8	0.0		
03-Sep	-0.5	-0.7	0.0		
04-Sep	3.2	3.2	3.0		
05-Sep	0.0	0.0	1.0	1.1	1.1
06-Sep	-1.8	-1.5	0.0	1.8	1.5
07-Sep	-1.3	-1.5	0.0		
08-Sep			0.0		
09-Sep	-2.5	-1.7	0.0		
Totals	12.8	15.5	59.9	22.2	21.4

4.4 Evaporation Estimates from Energy Balance Methods

The measurements taken to evaluate evaporative flux using various energy balance and aerodynamic methods are summarized in Appendix F (Tables F.1 – F.3).

4.4.1 The Energy Balance Components

Representative energy fluxes, values and diurnal variation, are presented to provide the reader with a framework from which to view the evaporation estimates from the energy balance and energy balance/aerodynamic approaches. The energy balance components: measured net radiation, measured ground heat, sensible and latent heats partitioned by the Bowen ratio method, are presented for a typical day (August 14th) without precipitation in Figure 4.7. For this 24-hour period, three days following a 14 mm rainfall event, the magnitude of energy fluxes (during daylight hours) in descending order are: net radiation, latent energy with ground heat flux equal in magnitude but lagging in time, and sensible heat. Latent flux was the prevailing energy flux from the soil surface on 35 of the 36 days during the observation period and ground heat during daylight hours was predominant over sensible flux on 20 of the 36 days. The diurnal variation of these fluxes presented in Figure 4.7 is typical. Net radiation peaks at approximately 1200 hours while the ground heat flux at 5 cm lags the net radiation peak by roughly an hour. Latent and sensible heat appear to peak before noon local time, however this could be due to the heat stored within the top 5 cm of soil and not properly attributed to the turbulent exchange fluxes, or an advection of local energy from the surrounding field.

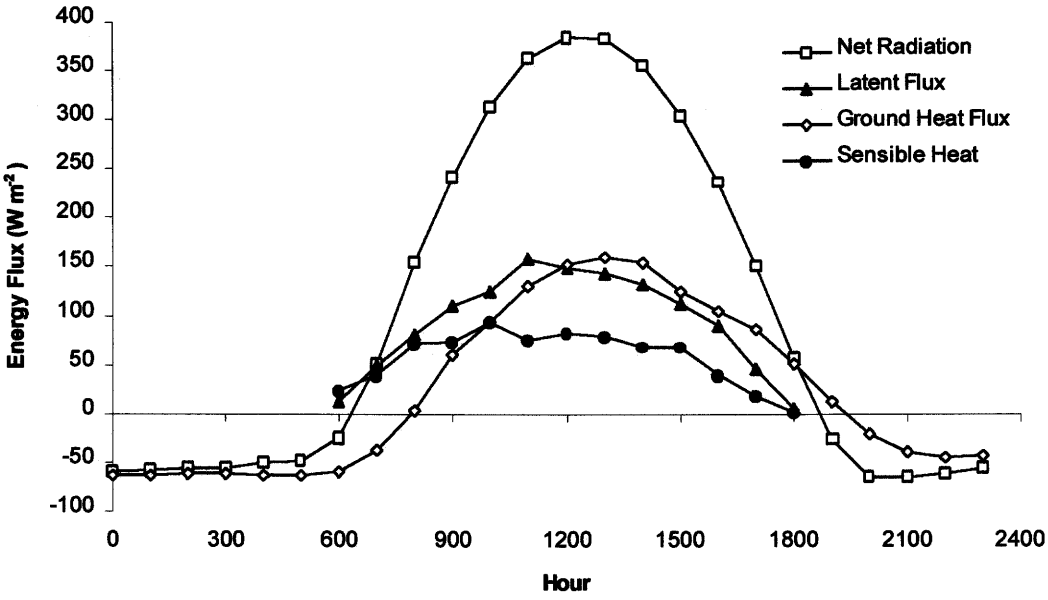

Figure 4.7 Components of the energy balance during a precipitation-free day showing the typical magnitude and diurnal cycling of energy fluxes.

4.4.2 The Bowen Ratio Method

The Bowen ratio (BR) estimation technique required that the net radiation, ground heat flux, as well as temperature and vapour pressure profiles be monitored. The temperature and vapour pressure gradients were established utilizing the data from the temperature relative humidity sensor that oscillated between 0.12 m and 0.52 m. The BR method allowed a determination of evaporative flux on an hourly basis. The Ohmura criteria were used to reject measurements if they indicated that the definition of the flux/gradient relationship was violated, or at times when the Bowen ratio neared –1 and instrument error became significant.

If the data was rejected during periods of condensation and precipitation, the evaporation estimate was set to zero. If data were rejected at other times when evaporation might reasonably have occurred, the estimation was made as an interpolation

of those evaporation estimates on either side of the period of rejected data. At times the period of rejected data was so extensive (over several daylight hours) that interpolation yielded unreasonable evaporation estimates. In these cases, and the occasional hour of data where evaporative flux far exceeded the net radiation, evaporation was deemed to have depleted half of the energy available for sensible and latent transfer (measured net radiation less measured soil heat flux).

The daily evaporative flux (evaluated from noon to noon each day) is presented in Figure 4.8. Also presented are the daily precipitation depths for the observation period. The elevation of the latent flux on the day following precipitation events is evident. For those days with precipitation, the evaporation is not as high as experienced on previous or subsequent rain-free days. This indicates lower evaporative demand due to lower air temperatures and higher relative humidity with rainfall.

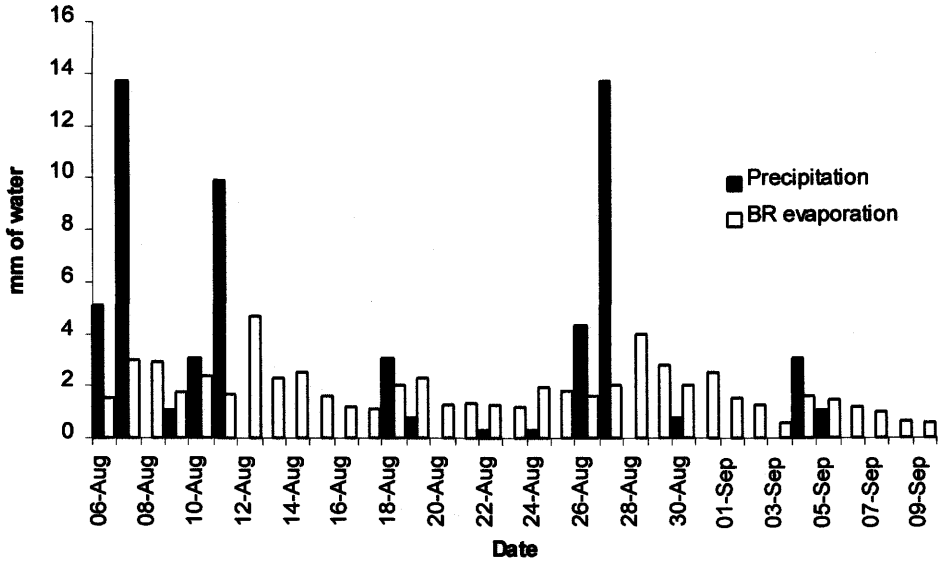

Figure 4.8 Evaporation estimated by the Bowen ratio method and precipitation for the observation period.

The Bowen ratio method of estimating evaporation yielded a total evaporative flux of 64.4 mm from August 5th to September 9th, 1994. This estimate is higher than that provided by the differential weighing of the cotton or barrier-capped microlysimeters (47.1 and 44.4 mm respectively) and exceeds the precipitation for the observation period (59.9 mm) by 7.5%.

The estimation of evaporative flux by the Bowen ratio method may also be influenced by the rejection of data during condensation periods (almost every night) and the evaporative flux subsequently set to zero instead of negative values (condensation). This rejection of data occurred on every day of the study period, for periods from 1 to 11 hours, with an average time span of 6.6 hours. The most common period of rejection were the hours just prior to sunrise and as the day cooled toward sunset. The partial representation of calculated latent and sensible heat flux in Figure 4.7 is typical of the data rejection period.

4.4.3 The Penman-Monteith Method

The data collected at the 2 m height was employed with the Penman-Monteith method to estimate latent flux on an hourly basis. A knowledge of the aerodynamic and surface or soil resistance to vapour flux is also necessary to utilize the Penman-Monteith method. The evaluation of the aerodynamic resistance demands the windspeed be measured and the zero plane displacement as well as the aerodynamic roughness heights be known. The surface resistance (for a non-vegetated surface) can be estimated from the measurement of soil surface moisture content.

The surface resistance to evaporative flux is a function of the soil water availability. While measurements of the soil moisture at the 2 cm depth were made daily using two sets of twin gamma probes, these readings were as low as 1% volumetric moisture content. This was well below the range of the values (permanent wilting point to field capacity) indicated by the SMRC analysis (19% to 32% by volume). Although field moisture conditions at the soil surface may extend beyond the PWP to FC range, air-dried soil was found to be at a minimum of 5% moisture content. Therefore the 1% moisture content measured by the twin gamma probe is unrealistically low, illustrating the inherent problem in measuring soil moisture very near the soil surface. Additionally the twin probe soil moisture readings taken on days immediately following rainfall were less than the field capacity moisture content expected. Despite these factors, the soil moisture measured by the twin gamma probe showed a good response to the occurrence of precipitation.

The range of soil moisture values, determined by the twin gamma probes, was scaled to match the range of possible soil moisture from air dry to saturation values (determined by the SMRC). These scaled values established a daily estimate of the soil surface moisture content (see Figure 4.9). The scaled volumetric moisture contents were used to establish a daily estimate of the surface resistance. Hourly surface resistance values, required the Penman-Monteith equation, were obtained by interpolation (Figure 4.10). The interpolated surface resistance values obtained ranged in value from 0 to 1467 s m^{-1}, compared to aerodynamic resistance values of 30 to 850 s m^{-1} for the same period.

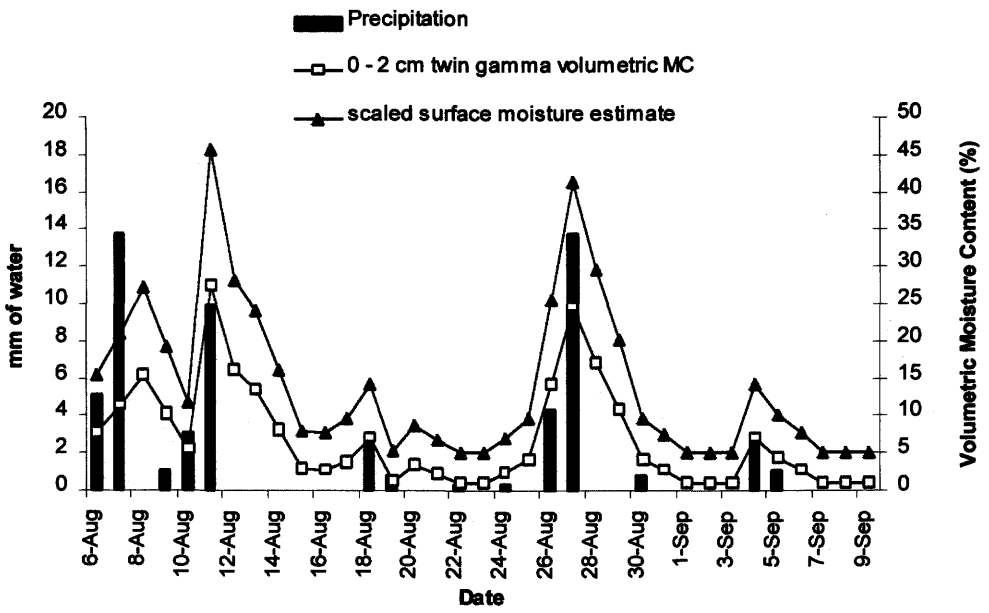

Figure 4.9 The occurrence of precipitation and soil surface moisture as measured by twin probe gamma, soil sampling and an estimate of the moisture content.

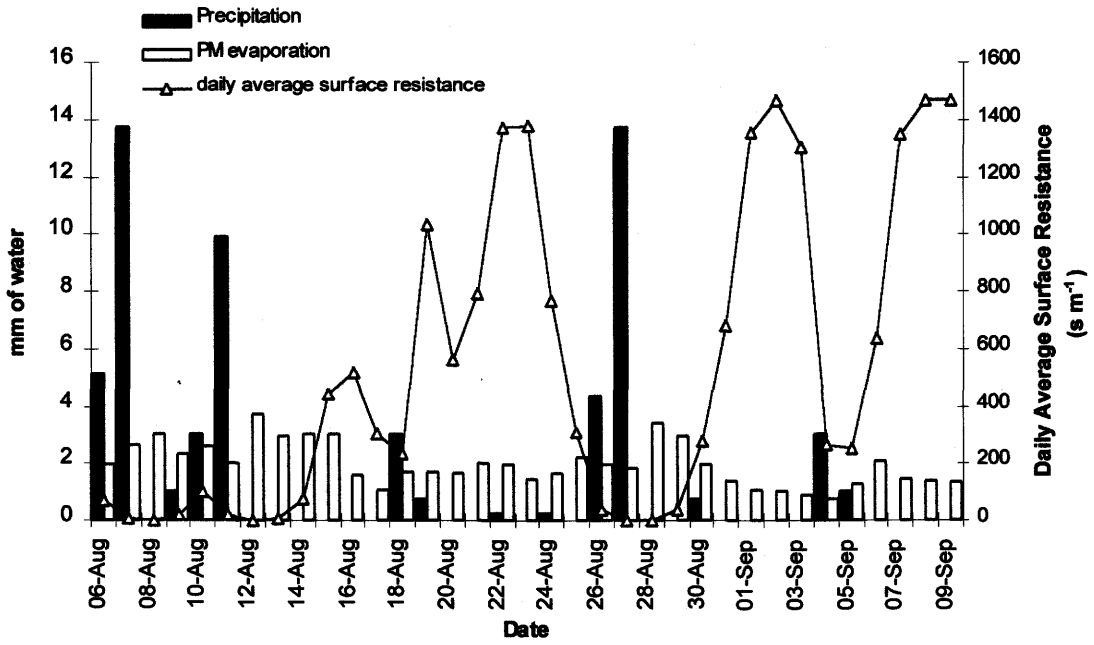

Figure 4.10 Evaporative flux estimated by the Penman-Monteith equation (influenced by the surface resistance and its dependence on soil water availability).

The total daily evaporative flux estimated using the Penman-Monteith method is shown in Figure 4.10, along with daily rainfall and calculated surface resistance. The surface resistance dropped and evaporative estimate rose on days immediately following precipitation. The total evaporative flux from August 5th to September 9th, 1994 was estimated to be 64.0 mm.

Surface resistance linearly interpolated from noon to noon inaccurately estimates the diurnal cycling of soil moistures. Measurement or estimation of the formation of dew or capillary rise of soil moisture during the night hours, or desiccation during the afternoon period is lacking. Surface resistance has been inaccurately estimated for these hours resulting in a calculated evaporative flux that may also be inaccurate. Additionally, as can be seen from Figure 4.10, the linear interpolation from noon to noon has resulted in a drop in the estimate of surface resistance for a few hours preceding the actual wetting of the surface on days with rain, yielding an elevated evaporation estimate.

4.4.4 The G-D Method

Daily averages of the energy components, temperature and windspeed at the 2 m height were used to assess the evaporative flux on a daily basis. The evaporative flux was also calculated on an hourly basis by replacing Granger's empirical wind function with a Dalton type of dynamic wind function setting the estimate to zero at times of the day when the net energy available for turbulent transfer was negative.

The daily flux and daily totals of hourly flux are presented in Figure 4.11. The cumulative evaporative fluxes were 43.1 and 53.2 mm for the daily and daily totals of

hourly evaporative estimates respectively. The daily totals of hourly flux exceeded the daily estimate on 30 of the 36 days within the observation period. Figure 4.12 shows that the hourly G-D method provided systematically higher evaporation estimates.

For both time intervals of estimation, the evaporative flux quantifed by the G-D method shows an increased evaporation immediately following days of rainfall.

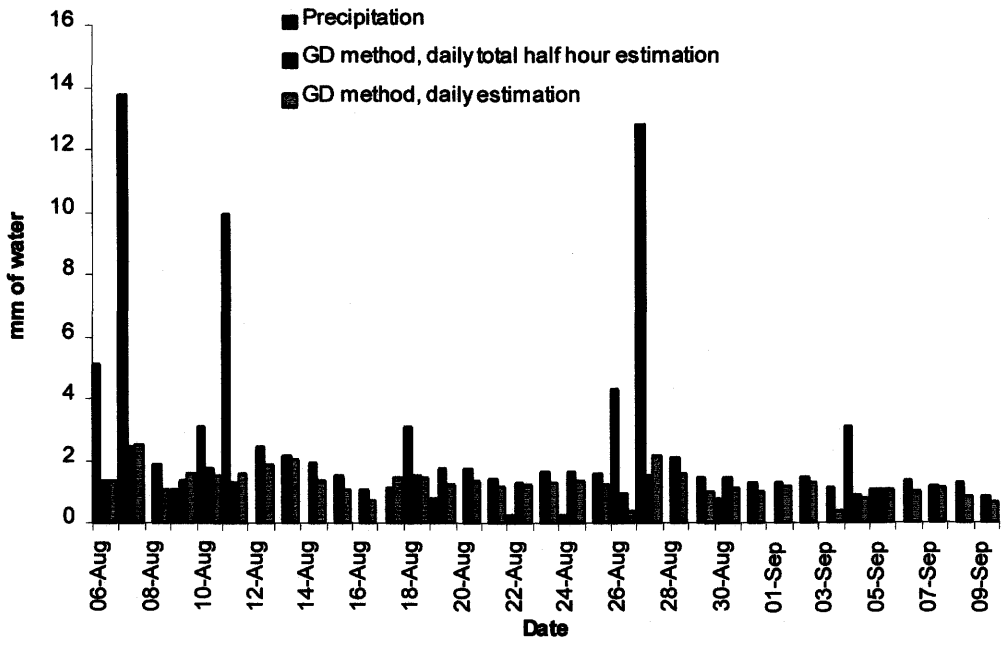

Figure 4.11 Daily precipitation and evaporation estimated using the G-D method, applied to hourly and daily data.

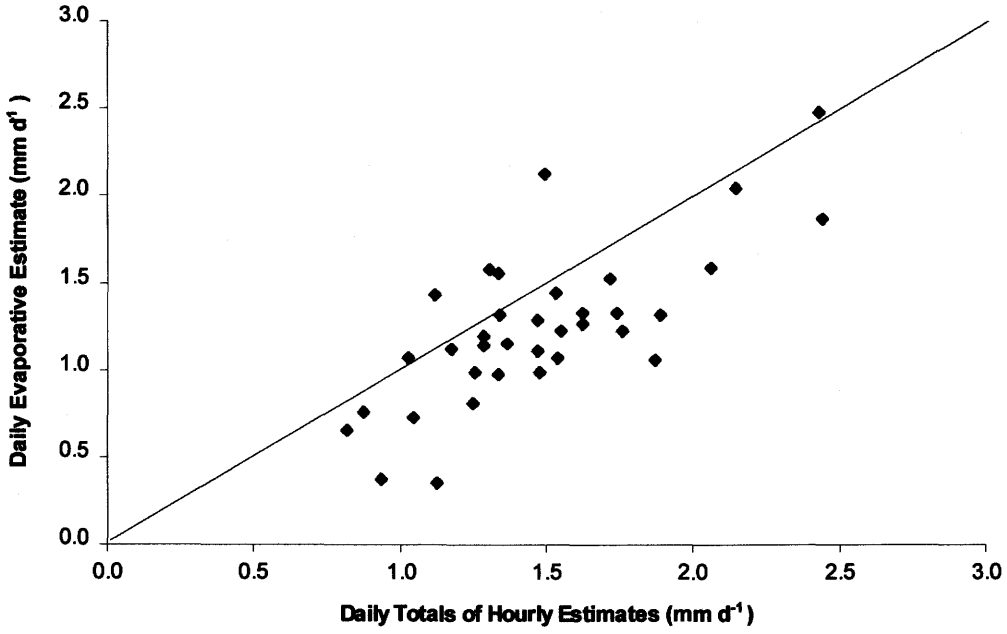

Figure 4.12 Comparison of daily G-D evaporation estimated from hourly and daily data. A 1:1 line is plotted for convenience.

4.5 The Comparison of Evaporative Estimates

4.5.1 Cumulative Evaporation Losses

The cumulative estimates of evaporation determined by all methods are presented in Figure 4.13. The Bowen ratio approach and the Penman-Monteith equation gave the highest evaporative estimates, 64.4 mm and 64.0 mm, respectively. The hourly G-D method resulted in a 53.2 mm estimate. The microlysimetric measurements (both cotton-capped corrected for drainage and barrier-capped), as well as the daily G-D model provided estimates that agreed closely (47.1 mm, 44.4 mm and 43.1 mm respectively).

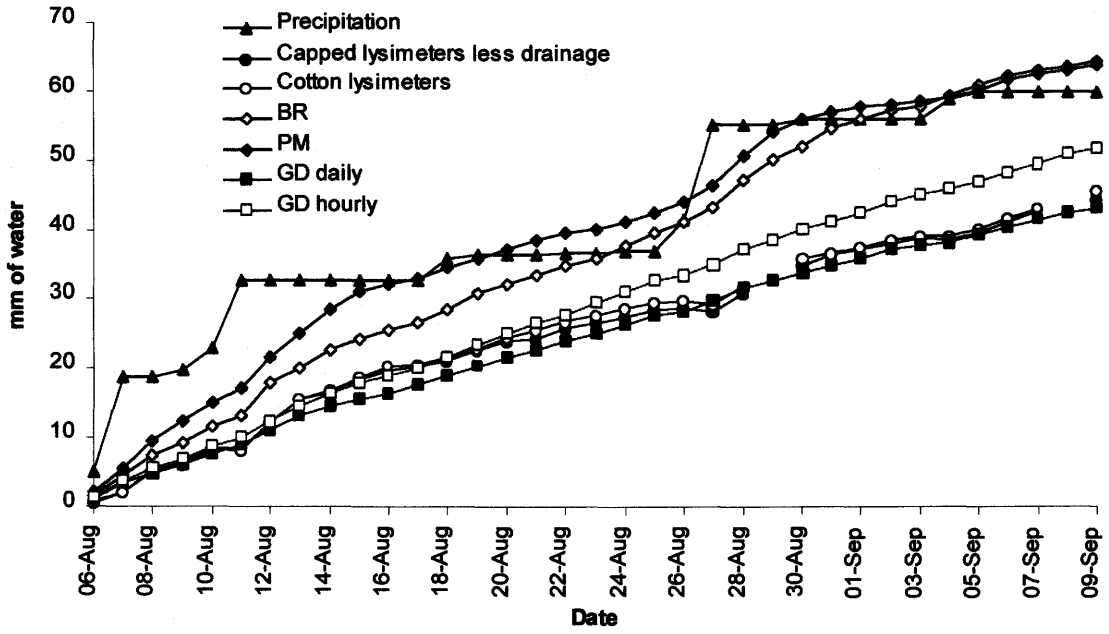

Figure 4.13 Cumulative precipitation and evaporation estimates from August 5th to September 9th.

4.5.2 Twenty-four Hour Losses Following Rainfall Days

To allow an evaluation of effective precipitation, evaporative losses subsequent to days with rainfall were determined. Table 4.5 outlines the days of precipitation and the concomitant 24-hour evaporative losses using all evaporation estimation techniques.

Table 4.5 Days with rainfall, and the subsequent 24-hour evaporative loss assessed by all evaporative estimation techniques.

Date	Precipitation	BR	PM	GD		Lysimeter	
				hourly	daily	cotton, corrected	capped
				(mm)			
06-Aug	5.1						
07-Aug	13.7	3.0	3.4	2.6	2.4	1.4	1.6
08-Aug		2.9	3.7	2.0	1.3	2.9	3.0
09-Aug	1.0						
10-Aug	3.0	2.4	2.9	1.8	1.5	2.0	2.2
11-Aug	9.9	1.7	2.0	1.4	1.3	0.0	0.0
12-Aug		4.6	4.4	2.6	2.0	4.0	3.7
13-Aug							
14-Aug							
15-Aug							
16-Aug							
17-Aug							
18-Aug	3.0						
19-Aug	0.8	2.3	1.3	1.8	1.3	1.4	1.4
20-Aug		1.3	1.2	1.8	1.3	1.6	1.3
21-Aug							
22-Aug	0.3						
23-Aug		1.2	0.7	1.6	1.3	0.8	0.9
24-Aug	0.3						
25-Aug		1.8	1.5	1.5	1.2	0.8	1.0
26-Aug	4.3						
27-Aug	13.7	2.0	2.3	1.6	1.7	0.9	-0.6
28-Aug		4.0	4.2	2.1	1.7	2.8	2.7
29-Aug							
30-Aug	0.8						
31-Aug		2.5	1.0	1.3	1.0	0.7	1.4
01-Sep							
02-Sep							
03-Sep							
04-Sep	3.0						
05-Sep	1.0	1.5	1.1	1.1	1.0	1.1	1.1
06-Sep		1.2	1.4	1.3	1.0	1.8	1.5
07-Sep							
08-Sep							
09-Sep							
Totals	59.9 *	32.3	31.1	24.6	20.1	22.2	21.4

* blank value indicates no precipitation

4.6 The Determination of the Rainfall-Evaporation Relationship

Table 4.6 depicts days with precipitation divided into depth intervals. The table also shows the subsequent 24-hour evaporative losses evaluated using microlysimetry (cotton-capped, corrected for drainage during rainfall) and the G-D estimation techniques as well as the potential evaporation. Potential evaporation (PE) was evaluated using the Penman-Monteith equation with the surface resistance set to zero (Maidment 1993).

For days with rainfall in the 10 - 20 mm interval, an estimated average of 2.1 mm, 1.5 mm and 2.8 mm (G-D hourly, daily and microlysimeter estimates) were lost to subsequent 24-hour evaporation of the average 13.7 mm received. In the 5 - 10 mm interval, similar average 24-hour evaporative losses were apparent (2.6 mm, hourly G-D, 2.2 mm daily G-D, and 2.7 mm, microlysimeter estimates).

Daily rainfall of less than 5 mm produced a range of losses from 0.0 to 1.8 mm. The 0.0 mm loss was derived from mass measurements taken on August 11th. The gain of mass of the microlysimeters exactly matched the 9.9 mm of precipitation that fell, indicating no evaporative loss. However, all other estimation techniques specify evaporative losses in excess of 1.3 mm. Of the rainfall depths between 1 - 5 mm an average of 1.2 mm was lost to evaporation, with a similar (1.4 mm) average 24-hour loss for those daily rainfall amounts of less than 1 mm. The examination of these two associations of depth intervals, 5 - 20 mm (with average losses of 1.5 to 2.8 mm) and 0.3 - 5 mm daily rainfall depths (with average losses at 1.3 mm) show a grouping of evaporative losses.

Table 4.6 Days with precipitation and subsequent 24-hour evaporation partitioned into depth intervals as well as the potential evaporation on the days following rain.

Precipitation Depth Interval	Date	Precipitation	PE	Evaporation		
				G-D Hourly	G-D Daily	Corrected Cotton
		(mm)	(mm)	(mm)	(mm)	(mm)
10 mm - 20 mm	**07-Aug**	**13.7**				
	08-Aug	0.0	3.8	2.0	1.3	2.9
	27-Aug	**13.7**				
	28-Aug	0.0	4.2	2.1	1.7	2.8
average		**13.7**	**4.0**	**2.1**	**1.5**	**2.8**
5 mm - 10 mm	**11-Aug**	**9.9**				
	12-Aug	0.0	4.4	2.6	2.0	4.0
	06-Aug	**5.1**				
	07-Aug	13.7	3.8	2.6	2.4	1.4
average		**7.5**	**4.1**	**2.6**	**2.2**	**2.7**
	26-Aug	**4.3**				
1 mm - 5 mm	27-Aug	13.7	2.3	1.6	1.7	0.9
	10-Aug	**3.0**				
	11-Aug	9.9	2.5	1.4	1.3	1.3
	18-Aug	**3.0**				
	19-Aug	0.8	3.2	1.8	1.3	1.4
	04-Sep	**3.0**				
	05-Sep	1.0	2.2	1.1	1.0	1.1
average		**3.4**	**2.5**	**1.5**	**1.3**	**1.2**
	09-Aug	**1.0**				
less than or equal to 1 mm	10-Aug	3.0	3.6	1.8	1.5	2.0
	05-Sep	**1.0**				
	06-Sep	0.0	4.0	1.3	1.0	1.8
	19-Aug	**0.8**				
	20-Aug	0.0	2.8	1.8	1.3	1.6
	30-Aug	**0.8**				
	31-Aug	0.0	2.1	1.3	1.0	0.7
	22-Aug	**0.3**				
	23-Aug	0.0	4.3	1.6	1.3	0.8
	24-Aug	**0.3**				
	25-Aug	0.0	4.5	1.5	1.2	0.8
average		**0.7**	**3.5**	**1.6**	**1.2**	**1.3**

The estimated daily potential evaporation following rainfall ranged from 2.1 to 4.5 mm. In each rainfall depth interval, the associated average evaporative 24-hour loss was less than the average daily potential evaporation. The dataset is limited and does not lend itself to rigorous statistical tests or regressions; however certain trends are evident. Potential and actual evaporation are higher for the larger rainfall depths. The precipitation data and evaporation estimates (cotton-capped microlysimeters) were normalized using potential evaporation for each depth interval. The ratios of P/PE (precipitation as a fraction of potential evaporation) and E/PE (evaporation as a portion of potential evaporation) are presented in Table 4.7.

Table 4.7 Normalized precipitation data and evaporation estimates for each depth interval.

Precipitation Depth Interval	**P/PE**	**E/PE**
10 mm - 20 mm	3.45	0.71
5 mm - 10 mm	1.83	0.66
1 mm - 5 mm	1.33	0.34
less than or equal to 1 mm	0.19	0.36

While it is difficult to assess concomitant 24-hour losses due to the differing meteorological conditions following the small number of rainfall events monitored it would appear that evaporation, as a fraction of potential evaporation, increases to some limiting value of P/PE. Evaporation rises to approximately 70% of the potential for evaporation as precipitation increases to about twice the depth necessary to satisfy

potential evaporation. Therefore, for a constant potential evaporation following rainfall, evaporation increases with increasing precipitation.

While the researcher would have liked to test the ability of rainfall to suppress subsequent evaporative losses, an examination of the effect of rainfall occurring during the following 24-hour period when evaporative loss was evaluated was not possible, due to the limited dataset. However potential evaporation did not appear to be reduced for those days where subsequent 24-hour evaporative losses were assessed while experiencing rainfall except for August 11th and August 27th (Figure 4.14). This coincided with the actual evaporative estimates given by the Bowen ratio, Penman-Monteith, and G-D methods, which all displayed an elevation of evaporation for those days immediately following days with precipitation (Figures 4.8, 4.10, 4.11).

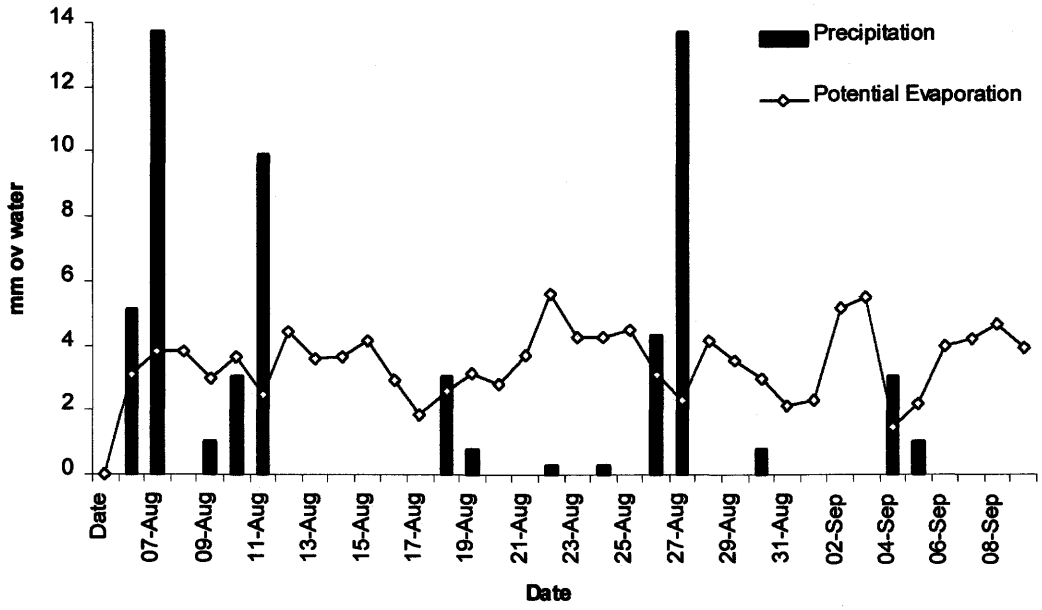

Figure 4.14 Precipitation and its influence on subsequent 24-hour potential evaporative losses.

5.0 SUMMARY AND CONCLUSIONS

The semi-arid environment of the Prairies experiences a potential for evaporation that exceeds the supply of precipitation and data shows a significant portion of its precipitation falls in lighter daily intensities. The hypothesis was that lighter daily rainfall amounts cannot be held within the soil against evaporative demand and do not increase storage of soil water in the root zone. The objective of this project was to establish the relationship between daily rainfall amounts and that portion of the rainfall lost to evaporation in the following 24-hour period. The scope of the project was limited to the examination of the top 30 cm of a fallow plot, bare of residue, during the growing season.

Evaporation is the link between the hydrological cycle and the surface energy budget, therefore evaporative losses were assessed using both the water budget and combined energy balance-aerodynamic methods. The energy balance methods included the Bowen ratio, the Penman-Monteith and the G-D equations. The soil water balance was evaluated with precipitation measurements as well as replicates of two different types of microlysimeters that allowed evaluation of the drainage component. The dataset consisted of daily soil moisture changes from microlysimeters, soil moisture measurements, and daily rainfall; additional measurements included net radiation, ground

heat flux, air temperatures, relative humidities, and windspeed. This dataset spanned 36 days in August and early September 1994. Data analysis was completed using the four techniques to estimate 24-hour evaporative losses following days of rainfall and allow the determination of effective precipitation.

The water budget, using both a barrier-capped and a cotton-capped microlysimeters, yielded estimates with a 2.7 mm range (44.4 mm, barrier-capped and 47.1 mm, cotton-capped) for the entire season and a 0.8 mm range (21.4 and 22.2 mm, respectively) for only those 24-hour periods following rainfall. The cotton-capped microlysimeters allowed flux through the bottom, drainage during rainfall, and were more representative of field conditions. While the barrier-capped microlysimeters behaved similarly to the cotton-capped microlysimeters until rain occurred (see August 5th to 9th and August 21st to 26th in Figure 4.4), post rainfall moisture content within the barrier-capped microlyimeter was higher than the cotton-capped microlysimeters. It is reasonable to assume that the barrier-capped microlysimeters, at a higher moisture content, might experience greater evaporative losses than the cotton-capped microlysimeters. However this is not supported by the data (Table 4.4) which shows that the barrier-capped microlysimeters retain more soil moisture over the study period. It is possible that the cotton-capped microlysimeters, while allowing drainage during rainfall to be isolated, could also have allowed drainage at other times.

The barrier-capped microlysimeters should be considered to be evaporating at a higher rate due to higher soil moisture content, and provide an upper bound on evaporative losses. Thus, the barrier-capped microlysimetric estimate of 44.1 mm is the higher limit of the seasonal evaporation estimate. However, for the purposes of this

project where 24-hour losses following rainfall were assessed the cotton-capped microlysimeters, which allowed drainage, were more representative of normal hydrologic cycling. Drainage during these 24-hour periods was also quantifiable. Therefore the 24-hour evaporative estimate was derived from the cotton-capped microlyimeters and equals 22.2 mm.

The Bowen ratio and Penman-Monteith approaches both indicate evaporative losses in excess of the values determined by microlysimetry. Significant portions of the Bowen ratio data were rejected (Figure 4.7), particularly in the early morning and evening hours when condensation might reasonably have occurred, resulting in an elevated evaporation estimate (64.6 mm and 32.3 mm total and subsequent 24-hour). The Penman-Monteith estimate used surface resistance factors difficult to quantify for any period of the day other than the time when the soil surface moisture was measured and has resulted in an estimate that is inaccurate (64.0 mm and 31.1 mm total and subsequent 24-hour evaporation).

The G-D method, developed in a semi-arid environment, with minimal reliance on empirical parameters, appears to yield reasonable estimates of cumulative and 24-hour evaporation subsequent to rainfall days (43.1 mm and 20.1 mm respectively).

The dataset was limited, and no rigorous regression techniques could be used to establish a quantifiable relationship between daily rainfall amounts and subsequent 24-hour evaporative loss. However, trends of evaporative loss (evaluated using the G-D equation and the cotton-capped microlysimeters) as a function of daily rainfall amounts were evident. For daily rainfall depths totaled for the 10 - 20 mm depth interval, 11% and 21% were estimated (by the G-D equation and capped microlysimetry respectively)

to have been lost to subsequent 24-hour evaporation. These percentages climbed for rainfall depths of 5 - 10 mm daily; 30% and 36% were lost from total of the precipitation that was received. An assumed 1.3 mm microlysimetric loss on August 11th resulted in an average evaporation loss of 35% of the rainfall in the 1 – 5 mm depth interval, while the G-D method indicates that 39% is lost to subsequent evaporation. Daily rainfall depths of 1 mm or less did not contribute to effective precipitation or precipitation that was be stored within the root zone.

Data normalization of precipitation and evaporation by potential evaporation shows that E/PE increases to approximately 70% as P/PE rises to a value of approximately 2. Additional increases in P/PE do not seem to induce an increase in the ratio of E/PE beyond the limit of 70%. For a constant potential on the day following rainfall, evaporation increases for increasing precipitation. The potential for evaporation following rainfall does not appear to decrease, but has a tendency to increase.

6.0 REFERENCE LIST

Allen, S.J. 1990. Measurement and estimation of evaporation from soil under sparse barley crops in norther Syria. *Agricultural and Forest Meteorology* 49:291-309.

Angus, D.E. and P.J. Watts. 1984. Evapotranspiration - how good is the Bowen ratio method? *Agricultural Water Management* 8:133-150.

Black, T.A., W.R. Gardner and G.W. Thurtell. 1969. The prediction of evaporation, drainage, and soil water storage for a bare soil. *Soil Science Society of America Proceedings* 33:655-660.

Blaney, H. F. and W. D. Criddle. 1950. Determining water requirements in irrigated areas from climatological and irrigation data. *U.S. Department of Agriculture, Soil Conservation Service TP-96*. Washington, D.C.

Blanken, P.D. and W.R. Rouse. 1995. Modelling evaporation from a high subarctic willow-birch forest. *International Journal of Climatology* 15:97-106.

Boast, C.W. 1986. Evaporation from Bare Soil Measured with High Spatial Resolution. In: *Methods of soil analysis, Part I.* Agronomy Monograph 9:889-900. American Society of Agronomy. Madison, Wisconsin. Edited by A. Klute.

Boast, C.W. and T.M. Robertson. 1982. A microlysimeter method for determining evaporation from bare soil: Description and laboratory evaluation. *Soil Science of America Journal* 46:689-696.

Bos, M.G., J. Vos and R.A. Feddes. 1996. CRIWAR 2.0: *A Simulation Model on Crop Irrigation Water Requirements*. International Institute for Land Reclamation and Improvement (ILRI), Wageningen, Netherlands. 117 pages.

Bowen, I.S. 1926. The ratio of heat losses by conduction and by evaporation from any water surface. *Physics Review* 27:779-787.

Brutsaert, W. 1982. *Evaporation into the Atmosphere, Theory, History and Applications*. D. Reidel Publishing Company, The Netherlands. 299 pages.

Brutsaert, W. and D. Chen. 1995. Desorption and the two stages of drying of natural tallgrass prairie. *Water Resources Research* 31(5):1305-1313.

Brutsaert, W. and D. Chen. 1996. Diurnal variation of surface fluxes during thorough drying (or severe drought) of natural prairie. *Water Resources Research* 32(7):2013-2019.

Camillo, P.J. and R.J.Gurney 1986. A resistance parameter for bare-soil evaporation models. *Soil Science* 141(2):95-105.

Campbell Scientific Inc. 1988. *CSI Bowen Ratio Instrumentation Manual.*

Cellier, P. and A. Olioso. 1993. A simple system for automated long-term Bowen ratio measurement. *Agricultural and Forest Meteorology* 66:81-92.

Daamen, C.C. and L.P. Simmonds. 1996. Measurement of evaporation from bare soil and its estimation using surface resistance. *Water Resources Research* 32(5):1393-1402.

Daamen, C.C., L.P. Simmonds, J.S. Wallace, K.B. Laryea and M.V.K. Sivakumar. 1993. Use of microlysimeters to measure evaporation from sandy soils. *Agricultural and Forest Meteorology* 65:159-173.

Department of Agricultural Engineering, University of Saskatchewan. 1989. *Handbook on Conservation Agriculture.* Prepared with support from the Conservation Awareness Program, Prairie Farm Rehabilitation Administration. Saskatoon Saskatchewan, Canada.

Doorenbos, J., A.H. Kassam, C.L.M. Bentvelsen, V. Branscheid, J.M.G.A. Plusje, M. Smith, G.O. Uittenbogaard and H.K. van Der Wal. 1986. Yield response to water. *FAO Irrigation and Drainage Paper No. 33.* 193 pages.

Elliott, J.A., B.M. Toth, R.J. Granger and J.W. Pomeroy. 1998. Soil moisture storage in mature and replanted sub-humid boreal forest stands. *Canadian Journal of Soil Science* 78:17-27.

Evett, S.R., A.W. Warrick and A.D. Matthias. 1995. Wall material and capping effects on microlysimeter temperatures and evaporation. *Soil Science Society of America Journal* 59:329-336.

Feddes, R.A., P. Kabat, P.J.T van Bakel, J.J.B. Bronswijk and J. Halbertsma. 1988. Modelling soil water dynamics in the unsaturated zone - state of the art. *Journal of Hydrology* 100:69-111.

Fleagle, R.G. and J.A. Businger. 1980. *An Introduction to Atmospheric Physics.* International Geophysics Series, Volume 25. Academic Press, New York. 432 pages.

Gardner, H.R. and W.R. Gardner. 1969. Relation of water application to evaporation and storage of soil water. *Soil Science Society of America Proceedings* 33(2):192-196.

Granger, R.J. 1991. Evaporation from natural non-saturated surfaces. Ph.D. Thesis. Department of Agricultural Engineering, University of Saskatchewan. 141 pages

Granger, R.J. 1996. Summer energy balance at Wolf Creek research basin, Yukon. In: *Hydro-ecology Workshop on the Arctic Enviromental Strategy - Action on Water.* Canadian Geophysical Union, Hydrology Section Annual Meeting, May 5-10 1996 in Banff, Canada. NHRI Symposium No. 16:325-342. Edited by David Milburn.

Granger, R.J. 1997. Comparison of surface and satellite-derived estimates of evapotranspiration using a feedback algorithm. In: *Application of Remote Sensing in Hydrology.* Proceedings of the Third International Workshop, NHRI Symposium No. 17, October, 1996; NASA, Goddard Space Flight Center, Greenbelt, Marland. Edited by G.W. Kite, A. Pietroniro and T.J. Pultz.

Granger, R.G. and D.M. Gray. 1989. Evaporation from natural nonsaturated surfaces. *Journal of Hydrology* 111:21-29.

Heermann, D.F. and H.H. Shull. 1976. Effective precipitation of various application depths. *Transactions of the ASAE* 19(4):708-712.

Indorante, S. J., L. R. Follmer, R.D. Hammer and P.G. Koenig. 1990. Particle-size analysis by a modified pipette procedure. *Soil Science Society of America Journal* 54:560-563.

Jones, H.G. 1992. *Plants and Microclimates* (2nd Edition). Cambridge University Press. 428 pages.

Hillel, Daniel. 1982. *Introduction to Soil Physics.* Academic Press, New York. 364 pages.

Kondo, J., N. Saigusa and T. Sato. 1990. A parameterization of evaporation from bare soil surfaces. *Journal of Applied Meteorology* 29:385-389.

Klute, A. 1986. Water Retention: Laboratory Methods. In: *Methods of Soil Analysis. Part 1.* Agronomy Monograph 9:635-662. American Society of Agronomy. Madison, Wisconsin. Edited by A. Klute.

Lascano, R.J. and C.H.M. van Bavel. 1986. Simulation and measurement of evaporation from a bare soil. *Soil Science Society of America Journal* 50:1127-1132.

Maidment, D.R. 1993. *Handbook of Hydrology*. McGraw-Hill, New York

Malek, E. and G.E. Bingham. 1993. Comparision of the Bowen ratio-energy balance and the water balance methods for measurement of evapotranspiration. *Journal of Hydrology* 146:209-220.

Marshall, T.J. and J.W. Holmes. 1988. *Soil Physics*. Cambridge University Press, New York. 374 pages.

Martin, D.L., N.L Klocke and D.H. DeHann. 1985. Measuring Evaporation Using Mini-lysimeters. In: *Advances in Evpotranspiration*:231-240. Proceedings of the American Society of Agricultural Engineers, Chicago, Illinois.

Massman, W.J. 1992. Correcting errors associated with soil heat flux measurements and estimating soil thermal properties from soil temperature and heat flux plate data. *Agricultural and Forest Meteorology* 59:249-266.

Matthias, A.D., R. Salehi and A.W. Warrick. 1986. Bare soil evaporation near a surface point-source emitter. *Agricultural Water Management* 11:257-277.

Menenti, M. 1984. Physical aspects and determination of evaporation in deserts applying remote sensing techniques. *Institute of Land Water Management Research*. Report 10, 202 pages.

Monteith, J.L. 1965. Evaporation and Environment. In: *The State and Movement of Water in Living Organisms*, The Proceedings of the 19th Symposium of the Society of Experimental Biology 19:205-234.

Ohmura, A. 1982. Objective criteria for rejecting data for Bowen ratio flux calculations. *Journal of Applied Meteorology* 21:595-598.

Oke, T.R. 1993. *Boundary Layer Climates*. Cambridge University Press, Cambridge. 435 pages.

Passerat de Slians, A., B.A. Monteny and J.P. Lhomme. 1997. The correction of soil heat flux measurments to derive accurate surface energy balance by the Bowen ratio method. *Journal of Hydrology* 188-189:453-465.

Patwardhan, A.S., J.L. Nieber and I.L.L. Bakovic. 1987. Effective Precipitation in Irrigation Design and Management. In: *Irrigation Systems for the 21st Century*. Proceedings of a conference sponsored by the Irrigation and Drainage Division of

the ASCE in cooperation with the Irrigation Association of the ASAE. Portland Oregon, July 1987. Edited by L.G. James and M.J. English. 768 pages.

Payne, W.A., C.W. Wendt and R.J. Lascano. 1990. Bare fallowing on sandy fields of Niger, West Africa. *Soil Science of America Journal* 54:1079-1084.

Penman, H.L. 1948. Natural evaporation from open water, bare soil and grass. *Proceedings of the Royal Society of London, Series A* 193:120-145.

Philip, J.R. 1957. Evaporation and moisture and heat fields in the soil. *Journal of Meteorology* 14:354-366.

Pierce, L. T. 1960. A practical method of determining evapotranspiration from temperature and rainfall. *Transactions of the ASAE* 3(1):77-81.

Pomeroy, J.W., R.J. Granger, A. Pietroniro, J.A. Elliott, B. Toth and N. Hedstrom. 1997. *Hydrological Pathways in the Prince Albert Model Forest.* National Hydrology Research Institute Contribution Series No. CS-97004, Environment Canada. 154 pages.

Priestley, C.H.B and R.J. Taylor. 1972. On the assessment of surface heat flux and evaporation using large-scale parameters. *Monthly Weather Review* 100(2):81-92.

Robins, J.S. 1965. Evapotranspiration. In: *Methods of Soil Analysis, Part 1.* Agronomy 9:286-298. American Society of Agronomy. Madison, Wisconsin. Edited by C.A. Black.

Rouse, W.R. and R.G. Wilson. 1971/1972. A test of the potential accuracy of the water-budget approach to estimating evapotranspiration. *Agricultural Meteorology* 9:421-446.

Russell, G. 1980. Crop evaporation, surface resistance and soil water status. *Agricultural Meteorology* 21:213-226.

Sherratt, D.J. and H.S. Wheater. 1984. The use of surface resistance-soil moisture relationships in soil water budget models. *Agricultural and Forest Meteorology* 31:143-157.

Shu Fen Sun. 1982. Moisture and heat transport in a soil layer forced by atmospheric conditions. M.Sc. thesis, University of Connecticut.

Shuttleworth, W.J. and J.S. Wallace. 1985. Evaporation from sparse crops - an energy combination theory. *Quarterly Journal of the Royal Meteorological Society* 111:839-855.

Sinclair, T.R., L.H. Allen and E.R. Lemon. 1975. An analysis of errors in the calculation of energy flux densities above vegetation by a Bowen-ratio profile method. *Boundary Layer Meteorology* 8:129-139.

Slayter, R.O. 1967. *Plant-Water Relationships*. CSIRO Division of Land Research. Academic Press, London. 366 pages.

Shawcroft, R.W. and H.R. Gardner. 1983. Direct evaporation from soil under a rowcrop canopy. *Agricultural Meteorology* 28:229-238.

Tanner, B.D., M.S. Tanner, W.A. Dugas, E.C. Campbell and B.L. Bland. 1985. Evaluation of an operational eddy correlation system for evapotranspiration. *ASAE Publication 14-85*:87-99. ASAE Michigan.

Tanner, C.B. 1963. Basic instrumentation and measurements for plant environment and micrometeorology. University of Wisconsin Soils Bulletin 6.

Tanner, C.B. 1967. Measurement of Evaporation. In: *Irrigation of Agricultural Lands*. Agronomy 11:534-574. American Society of Agronomy. Madison, Wisconsin. Edited by R.M. Hagen.

Thom, A.S. 1972. Momentum, mass and heat exchange of vegetation. *Quarterly Journal of the Royal Meteorological Society* 98:124-134.

van Bavel, C.H.M. 1961. Lysimetric measurements of evapotranspiration rates in the eastern United States. *Soil Science Society of America Proceedings* 25:138-141.

van Bavel, C.H.M. 1966. Potential evaporation: the combination concept and its experimental verification. *Water Resources Research* 2(3):455-467.

van de Griend, A.A. and M. Owe. 1994. Bare soil surface resistance to evaporation by vapor diffusion under semi arid conditions. *Water Resources Research* 30(2):181-188.

Villagra, M.M., O.O.S Bacchi, R.L. Turon and K. Reichardt. 1995. Difficulties of estimating evapotranspiration from the water balance equation. *Agricultural and Forest Meteorology* 72:317-325.

Villalobos, R.J and E. Fereres. 1990. Evaporation measurements beneath corn, cotton and sunflower canopies. *Agronomy Journal* 82:1153-1159.

Wallace, J.S. 1995. Calculating evaporation: Resistance to factors. *Agricultural and Forest Meteorology* 73:353-366.

Wallace, J.S., C.R. Lloyd and M.V.K. Sivakumar. 1992. Measurements of soil, plant and total evaporation from millet in Niger. *Agricultural and Forest Meteorology* 63:149-169.

Walker, G.K. 1983. Measurement of evaporation from soil beneath crop canopies. *Canadian Journal of Soil Science* 63:137-141.

APPENDIX A

INSTRUMENT CALIBRATIONS

Table A.1 Manufacturer, serial number, and calibration coefficient of the net pyrradiometers and heat flow plates used in this study.

Manufacturer	Serial Number	Heat Flow Plate	Net Pyrradiometer	
		calibration	short wave calibration	long wave calibration
		$Wm^{-2}\ mV^{-1}$	$Wm^{-2}\ mV^{-1}$	$Wm^{-2}\ mV^{-1}$
Radiation and Energy	923132	26.8		
Balance Systems	923133	25.0		
Middleton	885		23.76	22.29

APPENDIX B

PRECIPITATION

Table B.1 Precipitation at Kernen Farm during the observation period, 1994.

Until		Rec'd in past 24 hours		Event
Date	**time**	**(in)**	**(mm)**	**(mm)**
6-Aug	1200	0.20	5.1	
7-Aug	1200	0.54	13.7	18.8
8-Aug	1200	0.00	0.0	
9-Aug	1200	0.04	1.0	
10-Aug	1200	0.12	3.0	
11-Aug	1200	0.39	9.9	14.0
12-Aug	1200	0.00	0.0	
13-Aug	1200	0.00	0.0	
14-Aug	1200	0.00	0.0	
15-Aug	1200	0.00	0.0	
16-Aug	1200	0.00	0.0	
17-Aug	1200	0.00	0.0	
18-Aug	1200	0.12	3.0	
19-Aug	1200	0.03	0.8	3.8
20-Aug	1200	0.00	0.0	
21-Aug	1200	0.00	0.0	
22-Aug	1200	0.01	0.3	0.3
23-Aug	1200	0.00	0.0	
24-Aug	1200	0.01	0.3	0.3
25-Aug	1200	0.00	0.0	
26-Aug	1200	0.17	4.3	
27-Aug	1200	0.54	13.7	18.0
28-Aug	1200	0.00	0.0	
29-Aug	1200	0.00	0.0	
30-Aug	1200	0.03	0.8	0.8
31-Aug	1200	0.00	0.0	
1-Sep	1200	0.00	0.0	
2-Sep	1200	0.00	0.0	
3-Sep	1200	0.00	0.0	
4-Sep	1200	0.12	3.0	
5-Sep	1200	0.04	1.0	4.1
6-Sep	1200	0.00	0.0	
7-Sep	1200	0.00	0.0	
8-Sep	1200	0.00	0.0	
9-Sep	1200	0.00	0.0	
Total		2.36	59.9	59.9

APPENDIX C

SOIL MOISTURE RETENTION CURVE

SOIL TEXTURAL ANALYSIS

SOIL BULK DENSITY

Table C.1 Summary data (average of three samples) for the soil moisture retention curves at specific nominal depths. The standard deviation of the three samples is presented in parenthesis.

	Mass moisture content (%)					
	Suction (kPa)					
Soil Depth (cm)	25	50	100	300	500	1500
2	38 (1.9)	37 (1.8)	35 (1.7)	32 (1.8)	29 (2.0)	19 (0.8)
5	39 (1.3)	37 (1.2)	36 (1.1)	34 (1.5)	32 (1.0)	19 (0.4)
10	34 (0.9)	33 (0.8)	32 (0.7)	30 (0.8)	30 (1.3)	19 (0.1)
20	30 (1.3)	30 (1.4)	29 (1.5)	27 (1.2)	27 (0.5)	20 (0.7)
30	30 (0.6)	29 (0.7)	28 (0.8)	26 (1.0)	25 (0.7)	19 (0.9)

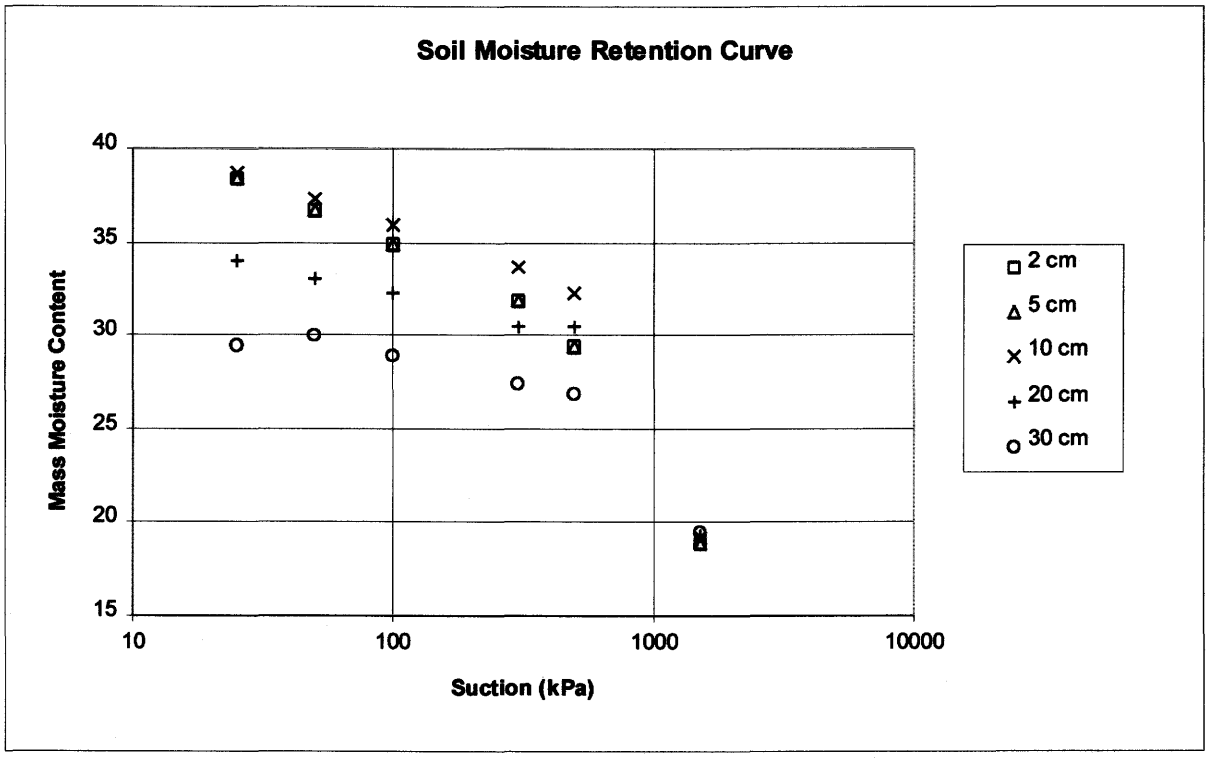

Figure C.1 Soil moisture retention as a function of depth.

Table C.2 Summary of soil textural analysis (average of three replicates) for the microlysimeters and the surrounding field conditions. The standard deviation of the three replicates are presented in parenthesis.

Lysimeter			Field		
Depth (cm)	Clay (%)	Sand (%)	Depth (cm)	Clay (%)	Sand (%)
0 - 5	43 (0.3)	11 (0.6)	0.5 - 3.5	43 (1.6)	12 (1.0)
5 - 10	46 (3.4)	11 (1.8)	2.5 - 7.5	44 (1.5)	11 (0.8)
10 - 15	45 (2.4)	9 (2.0)	7.5 - 12.5	48 (1.2)	10 (0.1)
15 - 20	48 (0.8)	8 (0.9)	17.5 - 22.5	49 (2.1)	8 (1.7)
20 - 25	48 (1.0)	8 (1.6)	27.5 - 32.5	51 (0.5)	7 (1.0)
25 - 30	52 (1.8)	7 (1.1)			

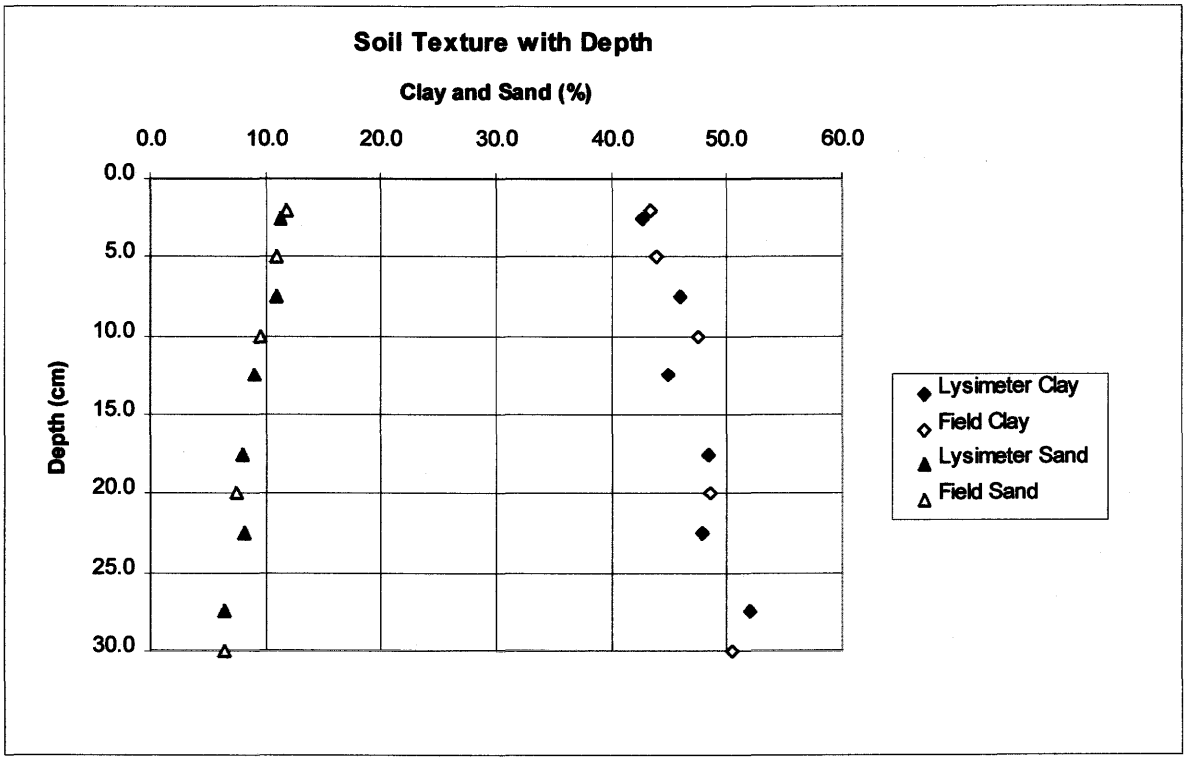

Figure C.2 Comparison of soil texture with depth for the installed microlysimeters and the surrounding field.

Table C.3 Bulk densities of the undisturbed cores (average of three samples) for each type (average of five replicates) of lysimeter. The standard deviation of all samples is presented in parenthesis.

Lysimeter				Field	
Depth (cm)	Bulk Density (kg m^{-3}) capped	cotton	control	Depth (cm)	Bulk Density (kg m^{-3})
0 - 5	1029 (70)	1060 (20)	940 (111)	0.5 - 3.5	1008 (45)
5 - 10	1134 (62)	1160 (56)	1141 (62)	2.5 - 7.5	1008 (101)
10 - 15	1250 (57)	1185 (115)	1254 (108)	7.5 - 12.5	1167 (52)
15 - 20	1244 (25)	1208 (162)	1252 (123)	17.5 - 22.5	1196 (89)
20 - 25	1278 (63)	1290 (130)	1286 (85)	27.5 - 32.5	1196 (25)
25 - 30	1330 (68)	1275 (119)	1361 (41)		

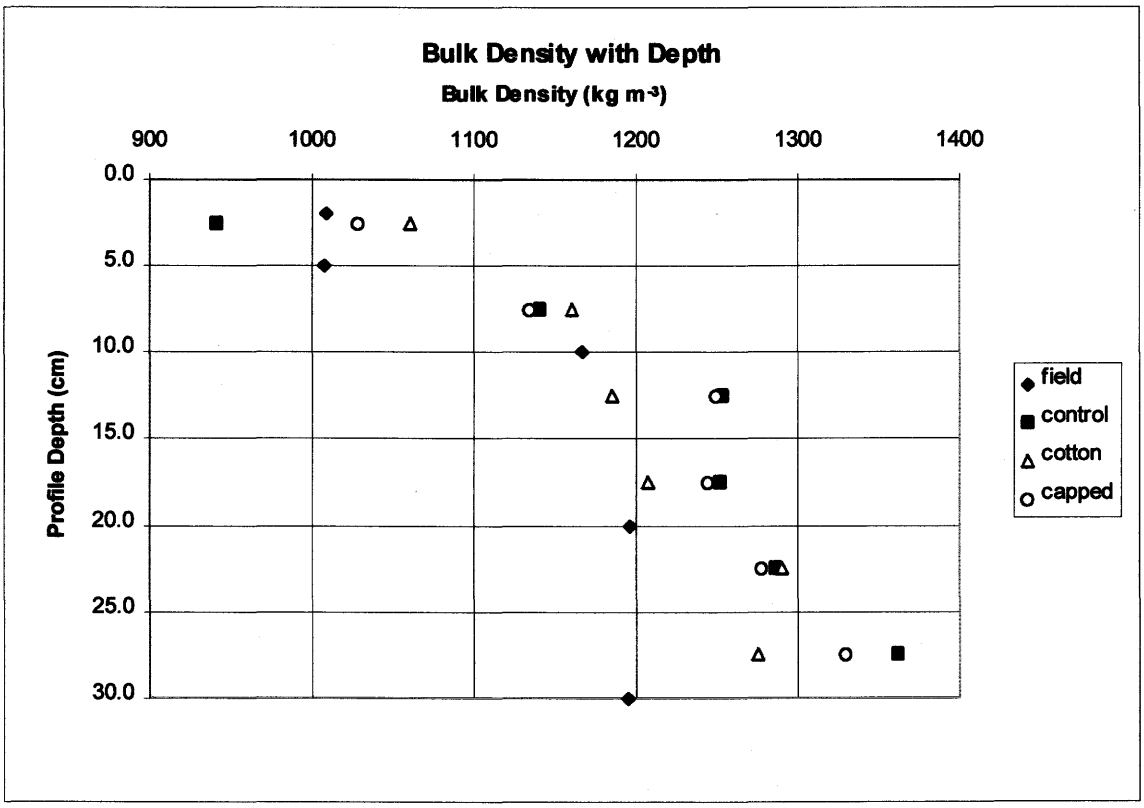

Figure C.3 Bulk density variation with depth, comparing the lysimeters (three treatments and an average) with the undisturbed cores representing field conditions.

APPENDIX D

DAILY MICROLYSIMETER MEASUREMENTS

DAILY MICROLYSIMETER MASS MOISTURE CONTENTS
with
STATISTICAL ANALYSIS

DAILY MICROLYSIMETER SOIL WATER CHANGES
with
STATISTICAL ANALYSIS

CUMULATIVE MICROLYSIMETER SOIL WATER CHANGES
with
STATISTICAL ANALYSIS

Table D.1 Mass measurements for the cotton-capped microlysimeters, Kernen Farm 1994.

Date	Mass of the Cotton-capped Microlysimeters (g)				
	Site				
	1	2	3	4	5
5-Aug	13380	13055	12370	12885	12365
7-Aug	13770	13455	12780	13265	12765
8-Aug	13695	13380	12705	13200	12700
9-Aug	13680	13380	12680	13205	12685
10-Aug	13675	13395	12740	13235	12715
11-Aug	13900	13635	12970	13440	12930
12-Aug	13805	13535	12860	13340	12835
13-Aug	13705	13445	12775	13270	12765
14-Aug	13675	13415	12745	13245	12730
15-Aug	13625	13350	12705	13185	12680
16-Aug	13575	13330	12665	13150	12645
17-Aug	13575	13310	12660	13140	12635
18-Aug	13630	13355	12715	13200	12680
19-Aug	13595	13335	12685	13175	12655
20-Aug	13570	13295	12645	13130	12610
21-Aug	13525	13270	12625	13105	12600
22-Aug	13500	13240	12590	13085	12560
23-Aug	13480	13220	12575	13055	12545
24-Aug	13455	13195	12545	13035	12515
25-Aug	13450	13175	12530	13000	12495
26-Aug	13555	13265	12615	13080	12585
27-Aug	13835	13575	12930	13400	12875
28-Aug	13770	13500	12850	13335	12815
30-Aug	13665	13405	12765	13255	12740
31-Aug	13650	13390	12740	13230	12730
1-Sep	13625	13360	12725	13210	12715
2-Sep	13595	13335	12695	13190	12680
3-Sep	13575	13330	12685	13170	12675
4-Sep	13655	13400	12735	13220	12740
5-Sep	13645	13385	12745	13220	12730
6-Sep	13590	13345	12700	13180	12690
7-Sep	13565	13315	12660	13150	12655
9-Sep	13495	13250	12585	13100	12600

Table D.2 Mass measurements for the first set of barrier-capped microlysimeters, Kernen Farm 1994.

	Mass of the First Barrier-capped Microlysimeters (g)				
	Site				
Date	1	2	3	4	5
5-Aug	12515	12970	12865	12810	12340
7-Aug	12930	13370	13275	13215	12770
8-Aug	12850	13305	13190	13140	12700
9-Aug	12840	13315	13190	13145	12690
10-Aug	12865	13330	13200	13175	12710
11-Aug	13125	13565	13455	13405	12955
12-Aug	13040	13470	13365	13315	12860
13-Aug	12950	13400	13265	13245	12760
14-Aug	12910	13365	13220	13240	12745
15-Aug	12875	13330	13180	13180	12690
16-Aug	12835	13310	13145	13145	12665
17-Aug	12825	13290	13140	13145	12645
18-Aug	12840	13360	13190	13215	12700
19-Aug	12850	13340	13165	13180	12685
20-Aug	12825	13295	13130	13160	12645
21-Aug	12810	13285	13120	13140	12635
22-Aug	12785	13265	13095	13115	12625
23-Aug	12760	13235	13070	13085	12595
24-Aug	12745	13220	13055	13075	12575
25-Aug	12730	13205	13025	13050	12545
26-Aug	12830	13285	13140	13155	12640
27-Aug	13145	13555	13440	13440	12910
28-Aug	13070	13480	13360	13375	12855
30-Aug	12975	13395	13250	13305	12775
31-Aug	12950	13375	13220	13275	12750
1-Sep	12930	13355	13190	13260	12720
2-Sep	12905	13330	13170	13230	12710
3-Sep	12880	13305	13160	13225	12675
4-Sep	12960	13385	13230	13280	12750
5-Sep	12955	13375	13225	13290	12750
6-Sep	12905	13335	13185	13240	12700
7-Sep	12885	13295	13150	13215	12665
9-Sep	12840	13260	13110	13170	12630

Table D.3 Mass measurements for the second set of barrier-capped microlysimeters, Kernen Farm 1994.

	Mass of the Second Barrier-capped Microlysimeters (g)				
Date	Site				
	1	2	3	4	5
20-Aug	13145	12630	13865	12600	11515
21-Aug	13130	12625	13860	12585	11510
22-Aug	13110	12600	13815	12565	11480
23-Aug	13090	12575	13795	12535	11460
24-Aug	13070	12565	13775	12530	11435
25-Aug	13055	12555	13745	12490	11410
26-Aug	13140	12655	13835	12600	11525
27-Aug	13510	13035	14185	12930	11865
28-Aug	13445	12965	14085	12860	11830
30-Aug	13345	12860	14030	12790	11765
31-Aug	13315	12845	13980	12740	11740
1-Sep	13295	12815	13965	12725	11710
2-Sep	13275	12790	13940	12700	11705
3-Sep	13245	12775	13930	12680	11690
4-Sep	13345	12865	13985	12770	11750
5-Sep	13330	12860	14005	12755	11760
6-Sep	13305	12820	13945	12735	11715
7-Sep	13265	12790	13915	12680	11690
9-Sep	13225	12755	13880	12640	11625

Table D.4 Mass moisture contents and a statistical analysis of the cotton-capped microlysimeters in the five sites.

Mass Moisture Content of the Cotton Capped Lysimeters (%)

Date	Site				
	1	2	3	4	5
5-Aug	26.9	26.0	30.6	26.9	25.9
7-Aug	31.1	30.1	35.1	31.1	30.1
8-Aug	30.3	29.3	34.3	30.4	29.4
9-Aug	30.1	29.3	34.0	30.5	29.3
10-Aug	30.0	29.5	34.6	30.8	29.6
11-Aug	32.5	31.9	37.2	33.1	31.8
12-Aug	31.4	30.9	36.0	32.0	30.8
13-Aug	30.4	30.0	35.0	31.2	30.1
14-Aug	30.0	29.7	34.7	30.9	29.7
15-Aug	29.5	29.0	34.3	30.2	29.2
16-Aug	29.0	28.8	33.8	29.9	28.9
17-Aug	29.0	28.6	33.8	29.7	28.7
18-Aug	29.6	29.1	34.4	30.4	29.2
19-Aug	29.2	28.9	34.0	30.1	29.0
20-Aug	28.9	28.5	33.6	29.6	28.5
21-Aug	28.4	28.2	33.4	29.4	28.4
22-Aug	28.2	27.9	33.0	29.1	28.0
23-Aug	27.9	27.7	32.8	28.8	27.8
24-Aug	27.7	27.4	32.5	28.6	27.5
25-Aug	27.6	27.2	32.3	28.2	27.3
26-Aug	28.7	28.2	33.3	29.1	28.2
27-Aug	31.8	31.3	36.7	32.6	31.3
28-Aug	31.1	30.5	35.9	31.9	30.6
30-Aug	29.9	29.6	34.9	31.0	29.8
31-Aug	29.8	29.4	34.6	30.7	29.7
1-Sep	29.5	29.1	34.5	30.5	29.6
2-Sep	29.2	28.9	34.1	30.3	29.2
3-Sep	29.0	28.8	34.0	30.1	29.2
4-Sep	29.8	29.5	34.6	30.6	29.8
5-Sep	29.7	29.4	34.7	30.6	29.7
6-Sep	29.1	29.0	34.2	30.2	29.3
7-Sep	28.9	28.7	33.8	29.9	29.0
9-Sep	28.1	28.0	32.9	29.3	28.4

Statistical Analysis of Cotton Capped

Anova: Two-Factor Without Replication

Date	Count	Sum	Average	Variance
5-Aug	5	136.3	27.3	3.6
7-Aug	5	157.5	31.5	4.3
8-Aug	5	153.7	30.7	4.1
9-Aug	5	153.1	30.6	3.8
10-Aug	5	154.5	30.9	4.6
11-Aug	5	166.4	33.3	5.0
12-Aug	5	161.1	32.2	4.6
13-Aug	5	156.7	31.3	4.5
14-Aug	5	155.1	31.0	4.5
15-Aug	5	152.2	30.4	4.7
16-Aug	5	150.3	30.1	4.6
17-Aug	5	149.8	30.0	4.7
18-Aug	5	152.6	30.5	4.9
19-Aug	5	151.2	30.2	4.8
20-Aug	5	149.1	29.8	4.7
21-Aug	5	147.7	29.5	4.8
22-Aug	5	146.1	29.2	4.7
23-Aug	5	145.1	29.0	4.7
24-Aug	5	143.7	28.7	4.6
25-Aug	5	142.7	28.5	4.6
26-Aug	5	147.5	29.5	4.6
27-Aug	5	163.7	32.7	5.3
28-Aug	5	160.0	32.0	4.9
30-Aug	5	155.3	31.1	5.0
31-Aug	5	154.3	30.9	4.7
1-Sep	5	153.2	30.6	4.9
2-Sep	5	151.7	30.3	4.8
3-Sep	5	151.0	30.2	4.8
4-Sep	5	154.4	30.9	4.4
5-Sep	5	154.1	30.8	4.9
6-Sep	5	151.8	30.4	4.8
7-Sep	5	150.1	30.0	4.6
9-Sep	5	146.7	29.3	4.3
Sites				
1	33	972.0	29.5	1.5
2	33	958.4	29.0	1.4
3	33	1127.3	34.2	1.6
4	33	997.6	30.2	1.5
5	33	963.1	29.2	1.4

ANOVA

Source of Variation	SS	df	MS	F	P-value	F crit
Rows (Date)	232.7916	32	7.274739	285.6425	4.1E-104	1.534094
Columns (Sites)	606.85	4	151.7125	5956.988	2.5E-144	2.442455
Error	3.259902	128	0.025468			
Total	842.9015	164				

Table D.5 Mass moisture contents and a statistical analysis of the first set of barrier-capped microlysimeters in the five sites.

ass Moisture Content of the First Barrier Capped Lysimeters (%)

Date	Site				
	1	2	3	4	5
5-Aug	25.6	27.8	28.6	28.7	26.0
7-Aug	30.1	32.0	33.0	33.1	30.8
8-Aug	29.2	31.3	32.1	32.3	30.0
9-Aug	29.1	31.4	32.1	32.4	29.9
10-Aug	29.4	31.6	32.2	32.7	30.1
11-Aug	32.2	34.1	34.9	35.2	32.9
12-Aug	31.3	33.1	34.0	34.2	31.8
13-Aug	30.3	32.3	32.9	33.5	30.7
14-Aug	29.9	32.0	32.4	33.4	30.5
15-Aug	29.5	31.6	32.0	32.8	29.9
16-Aug	29.1	31.4	31.6	32.4	29.6
17-Aug	29.0	31.2	31.5	32.4	29.4
18-Aug	29.1	31.9	32.1	33.1	30.0
19-Aug	29.2	31.7	31.8	32.8	29.9
20-Aug	29.0	31.2	31.4	32.5	29.4
21-Aug	28.8	31.1	31.3	32.3	29.3
22-Aug	28.5	30.9	31.0	32.1	29.2
23-Aug	28.3	30.6	30.8	31.7	28.9
24-Aug	28.1	30.4	30.6	31.6	28.6
25-Aug	27.9	30.3	30.3	31.4	28.3
26-Aug	29.0	31.1	31.5	32.5	29.4
27-Aug	32.5	34.0	34.8	35.6	32.4
28-Aug	31.6	33.2	33.9	34.9	31.7
30-Aug	30.6	32.3	32.7	34.1	30.9
31-Aug	30.3	32.1	32.4	33.8	30.6
1-Sep	30.1	31.9	32.1	33.6	30.2
2-Sep	29.8	31.6	31.9	33.3	30.1
3-Sep	29.6	31.3	31.7	33.3	29.7
4-Sep	30.4	32.2	32.5	33.9	30.6
5-Sep	30.4	32.1	32.4	34.0	30.6
6-Sep	29.8	31.6	32.0	33.4	30.0
7-Sep	29.6	31.2	31.6	33.1	29.6
9-Sep	29.1	30.8	31.2	32.7	29.2

Statistical Analysis of the First Set of Barrier Capped

Anova: Two-Factor Without Replication

Date	Count	Sum	Average	Variance
5-Aug	5	136.7	27.3	2.1
7-Aug	5	159.1	31.8	1.8
8-Aug	5	155.0	31.0	1.8
9-Aug	5	154.9	31.0	2.0
10-Aug	5	156.0	31.2	1.9
11-Aug	5	169.4	33.9	1.7
12-Aug	5	164.4	32.9	1.7
13-Aug	5	159.7	31.9	1.9
14-Aug	5	158.2	31.6	2.0
15-Aug	5	155.7	31.1	1.9
16-Aug	5	154.1	30.8	1.9
17-Aug	5	153.5	30.7	2.1
18-Aug	5	156.3	31.3	2.7
19-Aug	5	155.4	31.1	2.2
20-Aug	5	153.6	30.7	2.2
21-Aug	5	152.9	30.6	2.2
22-Aug	5	151.7	30.3	2.1
23-Aug	5	150.2	30.0	2.1
24-Aug	5	149.4	29.9	2.1
25-Aug	5	148.1	29.6	2.1
26-Aug	5	153.5	30.7	2.2
27-Aug	5	169.2	33.8	2.0
28-Aug	5	165.4	33.1	2.0
30-Aug	5	160.6	32.1	2.1
31-Aug	5	159.2	31.8	2.0
1-Sep	5	157.9	31.6	2.1
2-Sep	5	156.7	31.3	2.0
3-Sep	5	155.6	31.1	2.3
4-Sep	5	159.6	31.9	2.0
5-Sep	5	159.5	31.9	2.2
6-Sep	5	156.9	31.4	2.2
7-Sep	5	155.3	31.1	2.2
9-Sep	5	153.1	30.6	2.2
Sites				
1	32	976.9	29.6	1.7
2	32	1043.2	31.6	1.3
3	32	1057.2	32.0	1.5
4	32	1088.9	33.0	1.5
5	32	990.4	30.0	1.5

ANOVA

Source of Variation	SS	df	MS	F	P-value	F crit
Rows (Date)	234.8187	32	7.338084	174.0741	1.2E-90	1.534094
Columns (Sites)	265.6551	4	66.41378	1575.468	8.7E-108	2.442455
Error	5.395832	128	0.042155			
Total	505.8696	164				

Table D.6 Mass moisture contents and a statistical analysis of the second set of barrier-capped microlysimeters in the five sites.

ass Moisture Content of the Second Barrier Capped Lysimeters (%)

Date	Site				
	1	2	3	4	5
20-Aug	27.9	29.6	32.4	31.3	26.7
21-Aug	27.8	29.5	32.3	31.1	26.6
22-Aug	27.5	29.2	31.9	30.9	26.2
23-Aug	27.3	28.9	31.7	30.5	26.0
24-Aug	27.1	28.8	31.4	30.5	25.7
25-Aug	27.0	28.7	31.1	30.0	25.4
26-Aug	27.9	29.8	32.1	31.3	26.8
27-Aug	31.8	34.1	35.7	35.0	30.9
28-Aug	31.1	33.3	34.6	34.2	30.4
30-Aug	30.0	32.1	34.1	33.4	29.7
31-Aug	29.7	31.9	33.6	32.8	29.4
1-Sep	29.5	31.6	33.4	32.7	29.0
2-Sep	29.3	31.3	33.1	32.4	28.9
3-Sep	29.0	31.2	33.0	32.2	28.8
4-Sep	30.0	32.2	33.6	33.2	29.5
5-Sep	29.9	32.1	33.8	33.0	29.6
6-Sep	29.6	31.7	33.2	32.8	29.1
7-Sep	29.2	31.3	32.9	32.2	28.8
9-Sep	27.9	29.6	32.4	31.3	26.7

Statistical Analysis of the Second Barrier Capped Lysi

Anova: Two-Factor Without Replication

Date	Count	Sum	Average	Variance
20-Aug	5	147.8	29.6	5.5
21-Aug	5	147.3	29.5	5.5
22-Aug	5	145.7	29.1	5.3
23-Aug	5	144.5	28.9	5.3
24-Aug	5	143.6	28.7	5.5
25-Aug	5	142.2	28.4	5.3
26-Aug	5	147.8	29.6	5.0
27-Aug	5	167.3	33.5	4.3
28-Aug	5	163.6	32.7	3.5
30-Aug	5	159.3	31.9	3.9
31-Aug	5	157.4	31.5	3.5
1-Sep	5	156.2	31.2	3.7
2-Sep	5	155.1	31.0	3.4
3-Sep	5	154.1	30.8	3.6
4-Sep	5	158.5	31.7	3.4
5-Sep	5	158.4	31.7	3.5
6-Sep	5	156.3	31.3	3.4
7-Sep	5	154.3	30.9	3.3
9-Sep	5	147.8	29.6	5.5
Sites				
1	18	549.5	28.9	1.9
2	18	586.9	30.9	2.5
3	18	626.3	33.0	1.3
4	18	610.5	32.1	1.8
5	18	534.0	28.1	3.0

ANOVA

Source of Variation	SS	df	MS	F	P-value	F crit
Rows (Date)	182.0683	18	10.11491	118.9991	3.75E-46	1.748926
Columns (Sites)	323.8795	4	80.96989	952.5884	1.65E-61	2.498922
Error	6.11999	72	0.085			
Total	512.0678	94				

Table D.7 Daily change of soil moisture (mm of water) and a statistical analysis of the cotton-capped microlysimeters within the five sites.

Moisture change in mm soil water, Cotton Capped

Date	Site				
	1	2	3	4	5
7-Aug	15.74	16.14	16.55	15.33	16.14
8-Aug	-3.03	-3.03	-3.03	-2.62	-2.62
9-Aug	-0.61	0.00	-1.01	0.20	-0.61
10-Aug	-0.20	0.61	2.42	1.21	1.21
11-Aug	9.08	9.69	9.28	8.27	8.68
12-Aug	-3.83	-4.04	-4.44	-4.04	-3.83
13-Aug	-4.04	-3.63	-3.43	-2.82	-2.82
14-Aug	-1.21	-1.21	-1.21	-1.01	-1.41
15-Aug	-2.02	-2.62	-1.61	-2.42	-2.02
16-Aug	-2.02	-0.81	-1.61	-1.41	-1.41
17-Aug	0.00	-0.81	-0.20	-0.40	-0.40
18-Aug	2.22	1.82	2.22	2.42	1.82
19-Aug	-1.41	-0.81	-1.21	-1.01	-1.01
20-Aug	-1.01	-1.61	-1.61	-1.82	-1.82
21-Aug	-1.82	-1.01	-0.81	-1.01	-0.40
22-Aug	-1.01	-1.21	-1.41	-0.81	-1.61
23-Aug	-0.81	-0.81	-0.61	-1.21	-0.61
24-Aug	-1.01	-1.01	-1.21	-0.81	-1.21
25-Aug	-0.20	-0.81	-0.61	-1.41	-0.81
26-Aug	4.24	3.63	3.43	3.23	3.63
27-Aug	11.30	12.51	12.71	12.91	11.70
28-Aug	-2.62	-3.03	-3.23	-2.62	-2.42
30-Aug	-4.24	-3.83	-3.43	-3.23	-3.03
31-Aug	-0.61	-0.61	-1.01	-1.01	-0.40
1-Sep	-1.01	-1.21	-0.61	-0.81	-0.61
2-Sep	-1.21	-1.01	-1.21	-0.81	-1.41
3-Sep	-0.81	-0.20	-0.40	-0.81	-0.20
4-Sep	3.23	2.82	2.02	2.02	2.62
5-Sep	-0.40	-0.61	0.40	0.00	-0.40
6-Sep	-2.22	-1.61	-1.82	-1.61	-1.61
7-Sep	-1.01	-1.21	-1.61	-1.21	-1.41
9-Sep	-2.82	-2.62	-3.03	-2.02	-2.22

Statistical Analysis of Cotton Capped

Anova: Two-Factor Without Replication

Date	Count	Sum	Average	Variance
7-Aug	5	79.90	15.98	0.21
8-Aug	5	-14.33	-2.87	0.05
9-Aug	5	-2.02	-0.40	0.24
10-Aug	5	5.25	1.05	0.92
11-Aug	5	45.00	9.00	0.30
12-Aug	5	-20.18	-4.04	0.06
13-Aug	5	-16.75	-3.35	0.28
14-Aug	5	-6.05	-1.21	0.02
15-Aug	5	-10.69	-2.14	0.15
16-Aug	5	-7.26	-1.45	0.19
17-Aug	5	-1.82	-0.36	0.09
18-Aug	5	10.49	2.10	0.07
19-Aug	5	-5.45	-1.09	0.05
20-Aug	5	-7.87	-1.57	0.11
21-Aug	5	-5.04	-1.01	0.26
22-Aug	5	-6.05	-1.21	0.10
23-Aug	5	-4.04	-0.81	0.06
24-Aug	5	-5.25	-1.05	0.03
25-Aug	5	-3.83	-0.77	0.19
26-Aug	5	18.16	3.63	0.14
27-Aug	5	61.14	12.23	0.48
28-Aug	5	-13.92	-2.78	0.11
30-Aug	5	-17.76	-3.55	0.24
31-Aug	5	-3.63	-0.73	0.07
1-Sep	5	-4.24	-0.85	0.07
2-Sep	5	-5.65	-1.13	0.05
3-Sep	5	-2.42	-0.48	0.09
4-Sep	5	12.71	2.54	0.28
5-Sep	5	-1.01	-0.20	0.16
6-Sep	5	-8.88	-1.78	0.07
7-Sep	5	-6.46	-1.29	0.05
9-Sep	5	-12.71	-2.54	0.18
Sites				
1	32	4.64	0.15	19.10
2	32	7.87	0.25	20.26
3	32	8.68	0.27	20.76
4	32	8.68	0.27	18.34
5	32	9.48	0.30	18.38

ANOVA

Source of Variation	SS	df	MS	F	P-value	F crit
Rows (Date)	2980.992	31	96.16104	563.8733	5.2E-119	1.543949
Columns (Sites)	0.447847	4	0.111962	**0.656527**	0.623369	**2.444764**
Error	21.14654	124	0.170537			
Total	3002.587	159				

Table D.8 Daily change of soil moisture (mm of water) and a statistical analysis of the first barrier-capped microlysimeters within the five sites.

Moisture change in mm soil water, First Barrier Capped

Date	Site				
	1	2	3	4	5
7-Aug	16.75	16.14	16.55	16.34	17.35
8-Aug	-3.23	-2.62	-3.43	-3.03	-2.82
9-Aug	-0.40	0.40	0.00	0.20	-0.40
10-Aug	1.01	0.61	0.40	1.21	0.81
11-Aug	10.49	9.48	10.29	9.28	9.89
12-Aug	-3.43	-3.83	-3.63	-3.63	-3.83
13-Aug	-3.63	-2.82	-4.04	-2.82	-4.04
14-Aug	-1.61	-1.41	-1.82	-0.20	-0.61
15-Aug	-1.41	-1.41	-1.61	-2.42	-2.22
16-Aug	-1.61	-0.81	-1.41	-1.41	-1.01
17-Aug	-0.40	-0.81	-0.20	0.00	-0.81
18-Aug	0.61	2.82	2.02	2.82	2.22
19-Aug	0.40	-0.81	-1.01	-1.41	-0.61
20-Aug	-1.01	-1.82	-1.41	-0.81	-1.61
21-Aug	-0.61	-0.40	-0.40	-0.81	-0.40
22-Aug	-1.01	-0.81	-1.01	-1.01	-0.40
23-Aug	-1.01	-1.21	-1.01	-1.21	-1.21
24-Aug	-0.61	-0.61	-0.61	-0.40	-0.81
25-Aug	-0.61	-0.61	-1.21	-1.01	-1.21
26-Aug	4.04	3.23	4.64	4.24	3.83
27-Aug	12.71	10.90	12.11	11.50	10.90
28-Aug	-3.03	-3.03	-3.23	-2.62	-2.22
30-Aug	-3.83	-3.43	-4.44	-2.82	-3.23
31-Aug	-1.01	-0.81	-1.21	-1.21	-1.01
1-Sep	-0.81	-0.81	-1.21	-0.61	-1.21
2-Sep	-1.01	-1.01	-0.81	-1.21	-0.40
3-Sep	-1.01	-1.01	-0.40	-0.20	-1.41
4-Sep	3.23	3.23	2.82	2.22	3.03
5-Sep	-0.20	-0.40	-0.20	0.40	0.00
6-Sep	-2.02	-1.61	-1.61	-2.02	-2.02
7-Sep	-0.81	-1.61	-1.41	-1.01	-1.41
9-Sep	-1.82	-1.41	-1.61	-1.82	-1.41

Statistical Analysis of First Barrier Capped

Anova: Two-Factor Without Replication

Date	Count	Sum	Average	Variance
7-Aug	5	83.13	16.63	0.22
8-Aug	5	-15.13	-3.03	0.10
9-Aug	5	-0.20	-0.04	0.13
10-Aug	5	4.04	0.81	0.10
11-Aug	5	49.44	9.89	0.26
12-Aug	5	-18.36	-3.67	0.03
13-Aug	5	-17.35	-3.47	0.37
14-Aug	5	-5.65	-1.13	0.48
15-Aug	5	-9.08	-1.82	0.22
16-Aug	5	-6.26	-1.25	0.11
17-Aug	5	-2.22	-0.44	0.13
18-Aug	5	10.49	2.10	0.83
19-Aug	5	-3.43	-0.69	0.46
20-Aug	5	-6.66	-1.33	0.18
21-Aug	5	-2.62	-0.52	0.03
22-Aug	5	-4.24	-0.85	0.07
23-Aug	5	-5.65	-1.13	0.01
24-Aug	5	-3.03	-0.61	0.02
25-Aug	5	-4.64	-0.93	0.09
26-Aug	5	19.98	4.00	0.27
27-Aug	5	58.11	11.62	0.62
28-Aug	5	-14.12	-2.82	0.16
30-Aug	5	-17.76	-3.55	0.38
31-Aug	5	-5.25	-1.05	0.03
1-Sep	5	-4.64	-0.93	0.07
2-Sep	5	-4.44	-0.89	0.09
3-Sep	5	-4.04	-0.81	0.24
4-Sep	5	14.53	2.91	0.18
5-Sep	5	-0.40	-0.08	0.09
6-Sep	5	-9.28	-1.86	0.05
7-Sep	5	-6.26	-1.25	0.11
9-Sep	5	-8.07	-1.61	0.04
Sites				
1	32	13.12	0.41	21.22
2	32	11.70	0.37	18.31
3	32	9.89	0.31	21.11
4	32	14.53	0.45	18.81
5	32	11.70	0.37	20.12

ANOVA

Source of Variation	SS	df	MS	F	P-value	F crit
Rows (Date)	3062.347	31	98.78539	501.8556	6.7E-116	1.543949
Columns (Sites)	0.378126	4	0.094531	**0.480244**	0.750187	**2.444764**
Error	24.40819	124	0.19684			
Total	3087.133	159				

Table D.9 Daily change of soil moisture (mm of water) and a statistical analysis of the second barrier-capped microlysimeters within the five sites.

Moisture change in mm soil water, Second Barrier Capped

Date	Site				
	1	2	3	4	5
21-Aug	-0.61	-0.20	-0.20	-0.61	-0.20
22-Aug	-0.81	-1.01	-1.82	-0.81	-1.21
23-Aug	-0.81	-1.01	-0.81	-1.21	-0.81
24-Aug	-0.81	-0.40	-0.81	-0.20	-1.01
25-Aug	-0.61	-0.40	-1.21	-1.61	-1.01
26-Aug	3.43	4.04	3.63	4.44	4.64
27-Aug	14.93	15.33	14.12	13.32	13.72
28-Aug	-2.62	-2.82	-4.04	-2.82	-1.41
30-Aug	-4.04	-4.24	-2.22	-2.82	-2.62
31-Aug	-1.21	-0.61	-2.02	-2.02	-1.01
1-Sep	-0.81	-1.21	-0.61	-0.61	-1.21
2-Sep	-0.81	-1.01	-1.01	-1.01	-0.20
3-Sep	-1.21	-0.61	-0.40	-0.81	-0.61
4-Sep	4.04	3.63	2.22	3.63	2.42
5-Sep	-0.61	-0.20	0.81	-0.61	0.40
6-Sep	-1.01	-1.61	-2.42	-0.81	-1.82
7-Sep	-1.61	-1.21	-1.21	-2.22	-1.01
9-Sep	-1.82	-1.41	-1.61	-1.82	-1.41

Statistical Analysis of Second Barrier Capped

Anova: Two-Factor Without Replication

Date	Count	Sum	Average	Variance
21-Aug	5	-1.82	-0.36	0.05
22-Aug	5	-5.65	-1.13	0.18
23-Aug	5	-4.64	-0.93	0.03
24-Aug	5	-3.23	-0.65	0.11
25-Aug	5	-4.84	-0.97	0.23
26-Aug	5	20.18	4.04	0.26
27-Aug	5	71.43	14.29	0.70
28-Aug	5	-13.72	-2.74	0.87
30-Aug	5	-15.94	-3.19	0.80
31-Aug	5	-6.86	-1.37	0.39
1-Sep	5	-4.44	-0.89	0.09
2-Sep	5	-4.04	-0.81	0.12
3-Sep	5	-3.63	-0.73	0.09
4-Sep	5	15.94	3.19	0.66
5-Sep	5	-0.20	-0.04	0.39
6-Sep	5	-7.67	-1.53	0.42
7-Sep	5	-7.26	-1.45	0.23
9-Sep	5	-8.68	-1.74	0.26
Sites				
1	32	3.23	0.18	16.89
2	32	5.04	0.28	17.70
3	32	0.61	0.03	15.32
4	32	1.61	0.09	14.46
5	32	4.44	0.25	14.23

ANOVA

Source of Variation	SS	df	MS	F	P-value	F crit
Rows (Date)	1313.396	17	77.25861	230.197	3.69E-53	1.775177
Columns (Sites)	0.775364	4	0.193841	**0.577562**	0.679869	**2.506624**
Error	22.82212	68	0.335619			
Total	1336.994	89				

Table D.10 Average (over 5 sites) and statistical analysis of the daily moisture change (mm of soil water) for each type of microlysimeter over the full observation period.

Moisture change in mm soil water, average of five sites

Date	Cotton	Cap 1	Cap 2
7-Aug	15.98	16.63	
8-Aug	-2.87	-3.03	
9-Aug	-0.40	-0.04	
10-Aug	1.05	0.81	
11-Aug	9.00	9.89	
12-Aug	-4.04	-3.67	
13-Aug	-3.35	-3.47	
14-Aug	-1.21	-1.13	
15-Aug	-2.14	-1.82	
16-Aug	-1.45	-1.25	
17-Aug	-0.36	-0.44	
18-Aug	2.10	2.10	
19-Aug	-1.09	-0.69	
20-Aug	-1.57	-1.33	
21-Aug	-1.01	-0.52	-0.36
22-Aug	-1.21	-0.85	-1.13
23-Aug	-0.81	-1.13	-0.93
24-Aug	-1.05	-0.61	-0.65
25-Aug	-0.77	-0.93	-0.97
26-Aug	3.63	4.00	4.04
27-Aug	12.23	11.62	14.29
28-Aug	-2.78	-2.82	-2.74
30-Aug	-3.55	-3.55	-3.19
31-Aug	-0.73	-1.05	-1.37
1-Sep	-0.85	-0.93	-0.89
2-Sep	-1.13	-0.89	-0.81
3-Sep	-0.48	-0.81	-0.73
4-Sep	2.54	2.91	3.19
5-Sep	-0.20	-0.08	-0.04
6-Sep	-1.78	-1.86	-1.53
7-Sep	-1.29	-1.25	-1.45
9-Sep	-2.54	-1.61	-1.74

Statistical Analysis of Capping Mechanisms

Anova: Two-Factor Without Replication

Date	Count	Sum	Average	Variance
7-Aug	2	32.61	16.30	0.21
8-Aug	2	-5.89	-2.95	0.01
9-Aug	2	-0.44	-0.22	0.07
10-Aug	2	1.86	0.93	0.03
11-Aug	2	18.89	9.44	0.39
12-Aug	2	-7.71	-3.85	0.07
13-Aug	2	-6.82	-3.41	0.01
14-Aug	2	-2.34	-1.17	0.00
15-Aug	2	-3.95	-1.98	0.05
16-Aug	2	-2.70	-1.35	0.02
17-Aug	2	-0.81	-0.40	0.00
18-Aug	2	4.20	2.10	0.00
19-Aug	2	-1.78	-0.89	0.08
20-Aug	2	-2.91	-1.45	0.03
21-Aug	3	-1.90	-0.63	0.11
22-Aug	3	-3.19	-1.06	0.04
23-Aug	3	-2.87	-0.96	0.03
24-Aug	3	-2.30	-0.77	0.06
25-Aug	3	-2.66	-0.89	0.01
26-Aug	3	11.66	3.89	0.05
27-Aug	3	38.14	12.71	1.95
28-Aug	3	-8.35	-2.78	0.00
30-Aug	3	-10.29	-3.43	0.04
31-Aug	3	-3.15	-1.05	0.10
1-Sep	3	-2.66	-0.89	0.00
2-Sep	3	-2.82	-0.94	0.03
3-Sep	3	-2.02	-0.67	0.03
4-Sep	3	8.64	2.88	0.10
5-Sep	3	-0.32	-0.11	0.01
6-Sep	3	-5.17	-1.72	0.03
7-Sep	3	-4.00	-1.33	0.01
9-Sep	3	-5.89	-1.96	0.25
Cotton	32	7.87	0.25	19.23
Cap 1	32	12.19	0.38	19.76
Cap 2	18	2.99	0.17	15.45

ANOVA

Source of Variation	SS	df	MS	F	P-value	*F crit*
Rows (Dates)	1195.782	31	38.57362	8.671942	4.62E-13	1.636151
Columns (Capping)	1.324441	2	0.66222	**0.148877**	0.861982	**3.14526**
Error	275.7818	62	4.448094			
Total	1472.888	95				

Table D.10a Average (over 5 sites) and statistical analysis of the cumulative moisture change (mm of soil water) for the first set of barrier-capped microlysimeters over the full observation period.

Cumulative change of soil water (mm), average

Date	Cotton, cum	Cap 1, cum
7-Aug	15.98	16.63
8-Aug	13.12	13.60
9-Aug	12.71	13.56
10-Aug	13.76	14.37
11-Aug	22.76	24.25
12-Aug	18.72	20.58
13-Aug	15.38	17.11
14-Aug	14.16	15.98
15-Aug	12.03	14.16
16-Aug	10.57	12.91
17-Aug	10.21	12.47
18-Aug	12.31	14.57
19-Aug	11.22	13.88
20-Aug	9.64	12.55
21-Aug	8.64	12.03
22-Aug	7.43	11.18
23-Aug	6.62	10.05
24-Aug	5.57	9.44
25-Aug	4.80	8.51
26-Aug	8.43	12.51
27-Aug	20.66	24.13
28-Aug	17.88	21.31
30-Aug	14.33	17.76
31-Aug	13.60	16.71
1-Sep	12.75	15.78
2-Sep	11.62	14.89
3-Sep	11.14	14.08
4-Sep	13.68	16.99
5-Sep	13.48	16.91
6-Sep	11.70	15.05
7-Sep	10.41	13.80
9-Sep	7.87	12.19

Statistical Analysis of Capping Mechanisms

Anova: Two-Factor Without Replication

Date	Count	Sum	Average	Variance
7-Aug	2	32.61	16.30	0.21
8-Aug	2	26.72	13.36	0.12
9-Aug	2	26.27	13.14	0.36
10-Aug	2	28.13	14.06	0.18
11-Aug	2	47.01	23.51	1.11
12-Aug	2	39.31	19.65	1.72
13-Aug	2	32.49	16.24	1.51
14-Aug	2	30.15	15.07	1.65
15-Aug	2	26.19	13.10	2.29
16-Aug	2	23.49	11.74	2.74
17-Aug	2	22.68	11.34	2.55
18-Aug	2	26.88	13.44	2.55
19-Aug	2	25.10	12.55	3.55
20-Aug	2	22.20	11.10	4.22
21-Aug	2	20.66	10.33	5.75
22-Aug	2	18.60	9.30	7.04
23-Aug	2	16.67	8.33	5.88
24-Aug	2	15.01	7.51	7.50
25-Aug	2	13.32	6.66	6.89
26-Aug	2	20.94	10.47	8.31
27-Aug	2	44.79	22.40	6.02
28-Aug	2	39.18	19.59	5.88
30-Aug	2	32.08	16.04	5.88
31-Aug	2	30.31	15.15	4.83
1-Sep	2	28.53	14.27	4.58
2-Sep	2	26.51	13.26	5.34
3-Sep	2	25.22	12.61	4.34
4-Sep	2	30.67	15.33	5.48
5-Sep	2	30.39	15.19	5.88
6-Sep	2	26.76	13.38	5.61
7-Sep	2	24.21	12.11	5.75
9-Sep	2	20.06	10.03	9.32
Cotton	32	393.18	12.29	16.69
Cap 1	32	479.94	15.00	13.79

ANOVA

Source of Variation	SS	df	MS	F	P-value	F crit
Rows (Dates)	927.3516	31	29.91457	53.2164	1.57E-19	1.822134
Columns (Capping)	117.6236	1	117.6236	209.246	2.49E-15	4.159617
Error	17.42605	31	0.562131			
Total	1062.401	63				

Table D.10b Average (over 5 sites) and statistical analysis of the cumulative moisture change (mm of soil water) for the for the first set of barrier-capped microlysimeters from August 5th to August 20th.

Cumulative change of soil water (mm), average

Date	Cotton, cum	Cap 1, cum
7-Aug	15.98	16.63
8-Aug	13.12	13.60
9-Aug	12.71	13.56
10-Aug	13.76	14.37
11-Aug	22.76	24.25
12-Aug	18.72	20.58
13-Aug	15.38	17.11
14-Aug	14.16	15.98
15-Aug	12.03	14.16
16-Aug	10.57	12.91
17-Aug	10.21	12.47
18-Aug	12.31	14.57
19-Aug	11.22	13.88
20-Aug	9.64	12.55

Statistical Analysis of Capping Mechanisms

Anova: Two-Factor Without Replication

Date	Count	Sum	Average	Variance
7-Aug	2	32.61	16.30	0.21
8-Aug	2	26.72	13.36	0.12
9-Aug	2	26.27	13.14	0.36
10-Aug	2	28.13	14.06	0.18
11-Aug	2	47.01	23.51	1.11
12-Aug	2	39.31	19.65	1.72
13-Aug	2	32.49	16.24	1.51
14-Aug	2	30.15	15.07	1.65
15-Aug	2	26.19	13.10	2.29
16-Aug	2	23.49	11.74	2.74
17-Aug	2	22.68	11.34	2.55
18-Aug	2	26.88	13.44	2.55
19-Aug	2	25.10	12.55	3.55
20-Aug	2	22.20	11.10	4.22
Cotton	14	192.57	13.76	12.78
Cap 1	14	216.63	15.47	11.16

ANOVA

Source of Variation	SS	df	MS	F	P-value	F crit
Rows (Dates)	307.0644408	13	23.6203416	74.86059	5.03E-10	2.576925
Columns (Capping)	20.66007454	1	20.66007454	65.47853	1.97E-06	4.667186
Error	4.101817195	13	0.3155244			
Total	331.8263325	27				

Table D.10c Average (over 5 sites) and statistical analysis of the cumulative moisture change (mm of soil water) between the cotton-capped and second barrier-capped microlysimeters for the period August 21st to September 9th.

Cumulative change of soil water (mm), average

Date	otton, cum	Cap 2, cum
21-Aug	-1.01	-0.36
22-Aug	-2.22	-1.49
23-Aug	-3.03	-2.42
24-Aug	-4.08	-3.07
25-Aug	-4.84	-4.04
26-Aug	-1.21	0.00
27-Aug	11.02	14.29
28-Aug	8.23	11.54
30-Aug	4.68	8.35
31-Aug	3.95	6.98
1-Sep	3.11	6.09
2-Sep	1.98	5.29
3-Sep	1.49	4.56
4-Sep	4.04	7.75
5-Sep	3.83	7.71
6-Sep	2.06	6.17
7-Sep	0.77	4.72
9-Sep	-1.78	2.99

Statistical Analysis of Capping Mechanisms

Anova: Two-Factor Without Replication

Date	Count	Sum	Average	Variance
21-Aug	2	-1.37	-0.69	0.21
22-Aug	2	-3.71	-1.86	0.26
23-Aug	2	-5.45	-2.72	0.18
24-Aug	2	-7.14	-3.57	0.51
25-Aug	2	-8.88	-4.44	0.33
26-Aug	2	-1.21	-0.61	0.73
27-Aug	2	25.30	12.65	5.34
28-Aug	2	19.77	9.89	5.48
30-Aug	2	13.03	6.52	6.74
31-Aug	2	10.94	5.47	4.58
1-Sep	2	9.20	4.60	4.46
2-Sep	2	7.26	3.63	5.48
3-Sep	2	6.05	3.03	4.70
4-Sep	2	11.78	5.89	6.89
5-Sep	2	11.54	5.77	7.50
6-Sep	2	8.23	4.12	8.47
7-Sep	2	5.49	2.74	7.82
9-Sep	2	1.21	0.61	11.34
Cotton	18	27.00	1.50	17.51
Cap 2	18	75.06	4.17	26.55

ANOVA

Source of Variation	SS	df	MS	F	P-value	F crit
Rows (Dates)	732.1121	17	43.065416	43.42556	1.06E-10	2.271893
Columns (Capping)	64.16799	1	64.167987	64.70461	3.39E-07	4.451323
Error	16.85901	17	0.9917067			
Total	813.1391	35				

APPENDIX E

EQUATION DEVELOPMENT for EVAPORATIVE ESTIMATION TECHNIQUES

BOWEN RATIO EQUATION

PENMAN-MONTEITH EQUATION

G-D EQUATION

E.1 The Bowen Ratio Equation

Net radiation is disposed of in the form of latent, sensible and ground heat fluxes. The transfer mechanism for sensible heat is similar to that of latent transfer as both take place within the turbulent zone. As well, the energy consumed in latent transfer is often supplied by the sensible energy component within a control volume of air. This has led to the development of the Bowen ratio energy balance approach for the evaluation of evaporation (Bowen 1926). The Bowen ratio is the ratio of sensible heat to latent flux:

$$B = \frac{Q_h}{Q_e} = \frac{- \rho_a C_p K_h \frac{dT}{dz}}{- \frac{\rho_a C_p}{\gamma} K_e \frac{de}{dz}} = \gamma \frac{K_h \frac{dT}{dz}}{K_e \frac{de}{dz}} \qquad [E.1]$$

where:

Q_h = sensible heat flux (W m^{-2}),
Q_e = latent heat flux (W m^{-2}),
ρ_a = air density (kg m^{-3}),
C_p = specific heat of air (J kg^{-1} $°C^{-1}$),
K_h = coefficient of heat transfer (m^2 s^{-1}),
K_e = coefficient of vapor transfer (m^2 s^{-1}),
γ = psychrometric constant (kPa $°C^{-1}$),
T = air temperature (°C), and
e = air vapor pressure (kPa).

Note, the psychrometric constant is:

$$\gamma = \frac{P_a C_p}{0.622 h_v} \qquad [E.2]$$

where:

γ = a function of temperature and atmospheric air pressure (equals 0.067 kPa $°C^{-1}$ at 20°C and P_a = 101.3 kPa),
P_a = atmospheric pressure (kPa),
C_p = the specific heat of air at constant pressure (equal to 1013 J kg^{-1} $°C^{-1}$),
h_v = latent heat of vaporization (J kg^{-1}), and
0.622 is the ratio of the molecular weight of water to that of dry air.

To evaluate the Bowen ratio, the transfer coefficients for heat and mass transfer are assumed to be equal ($K_h = K_e$), and the Bowen ratio becomes:

$$B = \gamma \frac{\partial T}{\partial e} \qquad [E.3]$$

where:

∂T = difference in air temperature (°C) between two levels and
∂e = difference in vapor pressures (kPa) between the same two levels.

With the Bowen ratio defined, and combined with the energy balance equation, evaporation may be determined by:

$$Q_e = \frac{Q_n - Q_g}{1 + B} \qquad [E.4]$$

where:

Q_n = net radiation (W m^{-2}) and
Q_g = ground heat flux (W m^{-2}).

E.2 The Penman Equation

Penman's potential evaporation equation quantifies the evaporation occurring if there is an unrestricted supply of water, sufficient energy available for evaporation, and a vapour pressure gradient ensures the removal of the saturated vapour layer over an evaporating surface.

If the evaporating surface is saturated, the Bowen ratio expression (Equation E.3) becomes:

$$B = \gamma \frac{(T_s - T_a)}{(e^*_s - e_a)} \qquad [E.5]$$

where:

T_s, T_a= evaporating surface and air temperature(°C),
e_a = vapour pressure (kPa) evaluated at the air temperature, and
e^*_s = saturated vapor pressure (kPa) evaluated at the surface temperature.

The slope of the saturated vapour pressure curve as a function of temperature, $\Delta = de^*/dT$ can be approximated by a straight line:

$$\Delta = \frac{(e^*_s - e^*_a)}{(T_s - T_a)} \qquad [E.6]$$

where:

e^*_a = saturated vapour pressure (kPa) evaluated at the air temperature.

Since $e_s = e^*_s$ for a saturated surface the Bowen ratio (Equation E.5) becomes:

$$B = \frac{\gamma}{\Delta}\left[1 - \frac{e^*_a - e_a}{e_s - e_a}\right] \qquad [E.7]$$

and substituting into Equation E.4:

$$Q_n - Q_g = \left(1 + \frac{\gamma}{\Delta}\right) Q_e - \frac{\gamma}{\Delta}\left(\frac{e^*_a - e_a}{e_s - e_a}\right) Q_e \qquad [E.8]$$

The second term on the right of E.8 may be expressed by a Dalton-type bulk mass transfer equation as a function of windspeed:

$$Q_e = f(u)\,(e_s - e_a) \qquad [E.9]$$

where:

$f(u)$ = is considered the wind function and can be represented by an empirical relationship to windspeed measurement, or may express the physical process described by the logarithmic wind profile (see Equation E.17).

The drying power of the air can be defined in a Dalton type equation as:

$$E_A = f(u)\,(e^*_a - e_a) \qquad [E.10]$$

Equation E.8 then becomes the Penman (1948) equation:

$$Q_e = \frac{\Delta}{\Delta + \gamma}(Q_n - Q_g) + \frac{\gamma}{\Delta + \gamma} E_A \qquad [E.11]$$

The Penman equation shows the combination of two processes. The first term is the radiant term, concerning itself with the net flux of energy available for evaporation. The second term quantifies the corresponding aerodynamic process of vapour flux from the evaporating surface to the surrounding air and is called the aerodynamic term.

E.2.1 The Penman-Monteith Equation

Equation E.11 is only valid when the vapour pressure at the surface is the saturation vapour pressure at the surface temperature. While this is true for open water or a saturated surface, the vapour pressure at a drying soil surface or a leaf is less than the saturation vapour pressure at the soil surface or leaf temperature. For either of these surfaces the water changes to vapour within the soil surface or leaf and the further path to the atmosphere is by molecular diffusion. The adiabatic cooling and loss of moisture from the air in the diffusion process is described by Monteith (1965). Monteith modified Penman's equation to account for both the surface resistance and the aerodynamic resistance.

The aerodynamic resistance to vapour transport away from the evaporating surface is inversely proportional to windspeed and changes with the height of vegetation:

$$r_a = \frac{\left(ln \frac{(z - d_o)}{z_o} \right)^2}{k^2 u_z} \qquad [E.12]$$

where:

r_a = aerodynamic resistance to turbulent vapour flux (s m^{-1}),
z = height (m) of measurement of wind speed, u_z,
u_z = windspeed (m s^{-1}),
d_o = zero plane displacement height (m) for vegetation or surface roughness
z_o = aerodynamic roughness height (m)
k = 0.41, the von Karman constant.

The two resistances to vapour flux (r_s and r_a) are considered if a evaporating surface is not saturated, and the driving force against resistance (the vapour pressure gradient) can be formulated as (Brutsaert 1982):

$$e_s - e_a = \left(\frac{r_a}{r_a + r_s} \right) \left(e^*_s - e_a \right) \qquad [E.13]$$

As the surface vapor pressure, e_s is not equal to e^*_s, and considering resistance to vapour flux, Equation E.7 becomes:

$$B = \frac{\gamma}{\Delta} \left(\frac{r_s + r_a}{r_a} \right) \left[1 - \frac{e^*_a - e_a}{e^*_s - e_a} \right] \qquad [E.14]$$

and Equation E.8:

$$Q_n - Q_g = \left[1 + \frac{\gamma}{\Delta}\left(\frac{r_s + r_a}{r_a}\right)\right] Q_e - \frac{\gamma}{\Delta}\left(\frac{r_s + r_a}{r_a}\right)\left(\frac{e^*_a - e_a}{e^*_s - e_a}\right) Q_e \qquad [E.15]$$

which simplifies to the Penman-Monteith equation:

$$Q_e = \frac{\Delta (Q_n - Q_g) + \rho_a C_P \dfrac{(e^*_a - e_a)}{r_a}}{\Delta + \gamma\left(1 + \dfrac{r_s}{r_a}\right)} \qquad [E.16]$$

It should be noted that when a vegetated or soil surface is saturated, r_s is zero and the Penman-Monteith equation simplifies to the Penman equation with a wind function associated with the Dalton equation and the drying power of the air, where:

$$f(u) = \frac{0.622\, k^2\, \rho_a\, u_1}{P\, ln\left[\dfrac{z_1 - d_0}{z_0}\right] ln\left[\dfrac{z_2 - d_0}{z_0}\right]} \qquad [E.17]$$

Bare soil resistance has been empirically described as a function of volumetric soil moisture. The near-surface soil layer is considered to be location of the evaporating surface. van de Griend and Owe (1994) developed a soil resistance expression as a function of the soil moisture content of the top 1 cm which describes a soil resistance that grows exponentially as the soil dries (Equation 3.18).

E.3 The G-D Equation

An extension of the Penman approach, the G-D method (Granger and Gray 1989), uses the concept of relative evaporation, G, the ratio of actual (non-saturated) to potential (saturated) evaporation. It also employs a dimensionless relative drying power term, D, which is the ratio of the drying power of the air (E_A) to the sum of the net energy available for turbulent transfer (Q_n - Q_g) and the drying power of the air (E_A).

To develop the G-D method, Granger and Gray (1989) considered the Bowen ratio and the slope of the saturation vapour pressure curve (Equations E.3 and E.4). As the evaporating surface is not saturated, combining the energy balance equation (Equation 3.4) with the Bowen ratio and the slope of the vapour pressure curve relationship yields:

$$Q_n - Q_g = Q_e \left[1 + \frac{\gamma \left(e^*_s - e^*_a \right)}{\Delta \left(e_s - e_a \right)} \right] \qquad \text{[E.18]}$$

Rearranging the Dalton-type bulk transfer (Equation E.9) gives:

$$e_s - e_a = \frac{Q_e}{f(u)} \qquad \text{[E.19]}$$

The substitution of Equation E.19 into E.18 results in:

$$Q_e = \left(Q_n - Q_g \right) + \frac{\gamma}{\Delta} f(u) \left(e^*_a - e^*_s \right) \qquad \text{[E.20]}$$

By adding and subtracting the vapour pressure of the air (e_a) to the term containing the wind function, Equation E.20 becomes:

$$Q_e = \left(Q_n - Q_g \right) + \frac{\gamma}{\Delta} \left[f(u) \left(e^*_a - e_a \right) - f(u) \left(e^*_s - e_a \right) \right] \qquad \text{[E.21]}$$

The first set of terms in the square brackets in Equation E.21 is the drying power of the air, E_A (Equation E.10). The second set of terms is the evaporation rate that would occur with a saturated surface, thus representing potential evaporation, E_p (van Bavel 1966). Equation E.21 is thus a general equation relating evaporation to the net energy available by radiation and conduction, the drying power of the air, and the potential evaporation. The calculation of potential evaporation, in the form $f(u)(e^*_s - e_a)$ can be problematic as surface temperature is rarely measured.
To evaluate evaporation without requiring the estimation of potential evaporation, Granger and Gray (1989) defined relative evaporation:

$$G = \frac{Q_e}{E_p} = \frac{f(u) \left(e_s - e_a \right)}{f(u) \left(e^*_s - e_a \right)} \qquad \text{[E.22]}$$

For a saturated surface, G will be unity; while for a very dry surface e_s will approach e_a and G will approach zero. Substituting the relative evaporation expression into Equation E.21 gives a general expression for evaporation from a non-saturated surface:

$$Q_e = \frac{\Delta G (Q_n - Q_g)}{\Delta + \gamma} + \frac{\gamma G E_A}{\Delta + \gamma} \qquad \text{[E.23]}$$

This equation is similar to the Penman (1948) formulation for evaporation estimation, but includes the relative evaporation (G) to extend the approach to non-saturated surfaces.

Granger and Gray (1989) studied 158 evaporation periods in the semi-arid environment of western Canada and defined relative evaporation in terms of commonly measured parameters. The expression for relative evaporation, G, is empirically expressed (Equation 3.20) as a function of the relative drying power, D, where:

$$D = \frac{E_A}{E_A + (Q_n - Q_g)} \qquad \text{[E.24]}$$

APPENDIX F

ENERGY MEASUREMENTS

METEOROLOGICAL MEASUREMENTS

Table F.1 Daily total radiation measured at Kernen Farm, for the observation period in 1994.

	Daily Total Net Radiation	Daily Total Ground Heat Flux			Daily Total Available Energy
		sensor 1	sensor 2	average	
Date	(MJ m^{-2})		(MJ m^{-2})		(MJ m^{-2})
06-Aug	5.15	-0.98	-1.24	-1.11	6.26
07-Aug	9.50	-1.64	-2.09	-1.87	11.37
08-Aug	4.10	-1.25	-1.54	-1.39	5.49
09-Aug	8.34	0.29	0.80	0.54	7.79
10-Aug	9.20	1.37	2.19	1.78	7.43
11-Aug	7.43	0.17	0.37	0.27	7.16
12-Aug	8.18	-0.71	-0.38	-0.55	8.73
13-Aug	10.43	0.31	1.26	0.78	9.65
14-Aug	8.53	1.21	2.50	1.86	6.68
15-Aug	6.26	0.93	2.20	1.56	4.69
16-Aug	3.01	-0.77	-0.62	-0.70	3.71
17-Aug	7.06	0.38	0.75	0.57	6.49
18-Aug	7.25	0.04	0.56	0.30	6.95
19-Aug	7.47	0.93	1.99	1.46	6.02
20-Aug	8.08	0.96	1.98	1.47	6.61
21-Aug	5.17	0.55	1.09	0.82	4.35
22-Aug	5.39	0.43	0.76	0.60	4.79
23-Aug	7.23	0.54	1.03	0.79	6.44
24-Aug	6.90	0.06	0.13	0.09	6.81
25-Aug	6.82	0.46	0.40	0.43	6.38
26-Aug	0.24	-1.50	-2.08	-1.79	2.02
27-Aug	9.55	-0.38	-0.06	-0.22	9.77
28-Aug	9.18	0.70	1.65	1.17	8.01
29-Aug	3.66	-1.47	-1.56	-1.52	5.18
30-Aug	4.72	-1.05	-0.91	-0.98	5.70
31-Aug	5.25	-0.34	0.18	-0.08	5.32
01-Sep	6.04	-0.35	0.02	-0.16	6.20
02-Sep	6.48	-0.29	-0.02	-0.15	6.63
03-Sep	0.52	-1.10	-1.52	-1.31	1.83
04-Sep	3.67	-0.08	0.23	0.07	3.60
05-Sep	6.23	0.21	1.10	0.66	5.57
06-Sep	6.27	0.86	1.74	1.30	4.97
07-Sep	5.11	0.75	1.20	0.98	4.14
08-Sep	3.75	0.86	1.36	1.11	2.64
09-Sep	2.16	0.39	0.60	0.49	1.66

Table F.2 Daily average air temperature, relative humidity and windspeed measured at 2 m for Kernen Farm, for the observation period 1994.

Date	Air Temperature (degree C)	Daily Average 2 m Relative Humidity (%)	Windspeed ($m\ s^{-1}$)
06-Aug	17.2	81	3.75
07-Aug	12.5	71	2.70
08-Aug	12.7	74	3.09
09-Aug	15.1	71	3.49
10-Aug	18.3	72	2.38
11-Aug	17.7	80	1.94
12-Aug	15.1	75	2.99
13-Aug	12.5	68	1.57
14-Aug	17.9	58	2.10
15-Aug	21.1	53	2.32
16-Aug	16.7	78	3.20
17-Aug	13.7	81	1.90
18-Aug	16.2	77	2.64
19-Aug	17.9	74	1.89
20-Aug	18.8	68	1.34
21-Aug	21.7	54	4.36
22-Aug	21.5	48	3.31
23-Aug	17.4	58	2.13
24-Aug	15.9	49	2.46
25-Aug	14.9	51	2.05
26-Aug	11.7	82	2.03
27-Aug	13.4	77	3.30
28-Aug	16.5	64	2.21
29-Aug	13.1	73	3.38
30-Aug	9.5	73	1.85
31-Aug	11.1	63	1.20
01-Sep	11.5	57	2.49
02-Sep	13.5	49	5.32
03-Sep	11.1	80	4.59
04-Sep	12.0	89	2.79
05-Sep	14.8	62	3.62
06-Sep	15.6	56	2.12
07-Sep	19.4	46	4.29
08-Sep	19.4	49	2.61
09-Sep	18.9	50	2.95

Table F.3 Daily average air temperature, relative humidity (0.12 m and 0.52 m) and windspeed (0.32 m) measured at for Kernen Farm, for the observation period 1994.

	Daily Average				
	Air Temperature		**Relative Humidity**		**Windspeed**
	0.52 m	0.12 m	0.52 m	0.12 m	0.32 m
Date	(degree C)		(%)		($m\ s^{-1}$)
06-Aug	17.2	17.3	88	87	2.81
07-Aug	13.1	13.1	77	76	2.02
08-Aug	12.9	12.9	81	80	2.32
09-Aug	15.6	15.5	75	75	2.62
10-Aug	19.1	19.0	74	74	1.78
11-Aug	17.8	17.9	87	86	1.46
12-Aug	15.3	15.4	81	80	2.24
13-Aug	13.5	13.5	71	71	1.18
14-Aug	18.7	18.6	61	61	1.58
15-Aug	21.8	22.0	56	56	1.74
16-Aug	17.0	17.0	82	81	2.68
17-Aug	14.8	14.7	82	82	1.40
18-Aug	16.4	16.5	82	82	1.95
19-Aug	18.6	18.7	78	77	1.33
20-Aug	19.9	19.9	68	68	0.97
21-Aug	22.2	22.2	57	57	3.25
22-Aug	21.7	21.7	54	53	2.40
23-Aug	17.9	18.0	63	62	1.56
24-Aug	16.3	16.4	55	55	1.80
25-Aug	15.2	15.2	56	57	1.63
26-Aug	11.6	11.6	91	91	1.66
27-Aug	13.7	13.7	85	84	2.41
28-Aug	17.4	17.5	69	68	1.65
29-Aug	13.3	13.3	79	78	3.00
30-Aug	9.9	10.0	78	77	1.44
31-Aug	11.8	11.8	66	66	0.83
01-Sep	12.1	12.0	61	60	1.84
02-Sep	14.0	13.9	53	53	4.13
03-Sep	11.2	11.2	85	85	3.55
04-Sep	12.5	12.5	93	92	2.20
05-Sep	15.1	15.1	67	67	2.79
06-Sep	16.3	16.4	59	59	1.61
07-Sep	19.8	19.8	49	49	3.31
08-Sep	20.0	20.0	52	52	1.98
09-Sep	19.3	19.3	54	54	2.25